AD-A053 233 OHIO STATE UNIV COLUMBUS DEPT OF GEODETIC SCIENCE F/G 8/5
RECOVERY OF 5 DEGREES MEAN GRAVITY ANOMALIES IN LOCAL AREAS FRO--ETC(U)
SEP 77 D P HAJELA F19628-76-C-0010
UNCLASSIFIED DGS-259 AFGL-TR-77-0272 NL

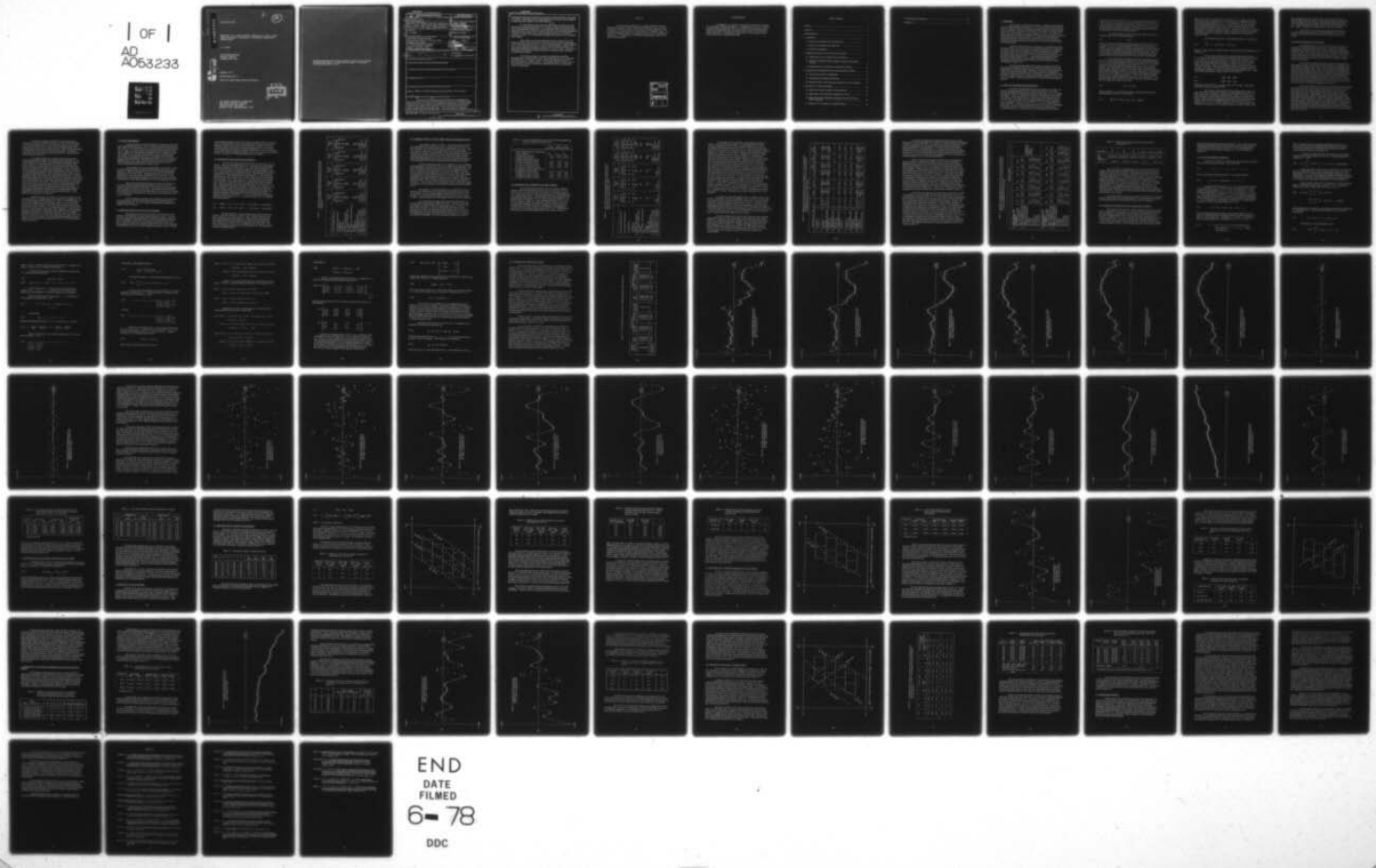

END
DATE FILMED
6-78
DDC

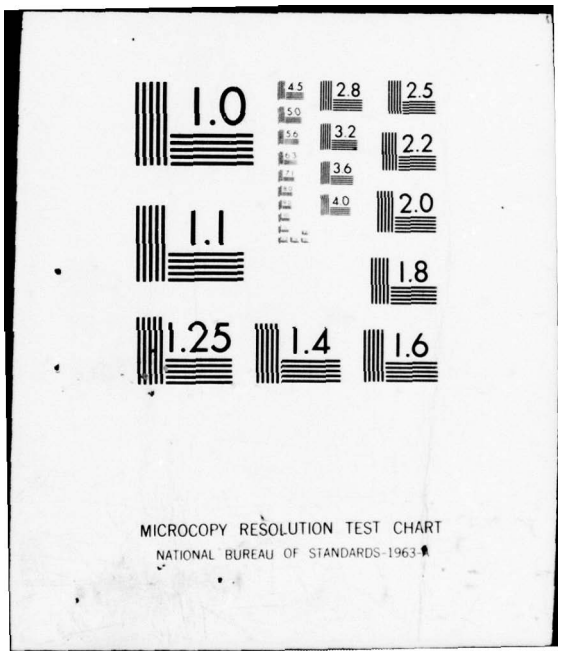
1.0
1.1
1.25
1.4
1.6
1.8
2.0
2.2
2.5
2.8
3.2
3.6
4.0
4.5
5.0
5.6
MICROCOPY RESOLUTION TEST CHART
NATIONAL BUREAU OF STANDARDS-1963-A

AFGL-TR-77-0272

(12)

RECOVERY OF 5° MEAN GRAVITY ANOMALIES IN LOCAL AREAS FROM ATS-6/GEOS-3 SATELLITE TO SATELLITE RANGE-RATE OBSERVATIONS

D. P. Hajela

The Ohio State University
Research Foundation
Columbus, Ohio 43212

September 1977

Scientific Report No. 11

AIR FORCE GEOPHYSICS LABORATORY
AIR FORCE SYSTEMS COMMAND
UNITED STATES AIR FORCE
HANSCOM AFB, MASSACHUSETTS 01731

unclassified

SECURITY CLASSIFICATION OF THIS PAGE (When Data Entered)

REPORT DOCUMENTATION PAGE	READ INSTRUCTIONS BEFORE COMPLETING FORM
1. REPORT NUMBER: AFGL-TR-77-0272	2. GOVT ACCESSION NO. / 3. RECIPIENT'S CATALOG NUMBER
4. TITLE (and Subtitle): RECOVERY OF 5° MEAN GRAVITY ANOMALIES IN LOCAL AREAS FROM ATS-6/GEOS-3 SATELLITE TO SATELLITE RANGE-RATE OBSERVATIONS	5. TYPE OF REPORT & PERIOD COVERED: Scientific Interim Scientific Report No. 11
	6. PERFORMING ORG. REPORT NUMBER: Geodetic Science 259
7. AUTHOR(s): D. P. Hajela	8. CONTRACT OR GRANT NUMBER(s): F19628-76-C-0010
9. PERFORMING ORGANIZATION NAME AND ADDRESS: Department of Geodetic Science, The Ohio State University - 1958 Neil Avenue, Columbus, Ohio 43210	10. PROGRAM ELEMENT, PROJECT, TASK AREA & WORK UNIT NUMBERS: 62101F 7600-0302
11. CONTROLLING OFFICE NAME AND ADDRESS: Air Force Geophysics Laboratory, Hanscom AFB, Mass. 01731, Contract Monitor; Bela Szabo/LW	12. REPORT DATE: Sep[redacted]77
	13. NUMBER OF PAGES: 78 pages
14. MONITORING AGENCY NAME & ADDRESS (if different from Controlling Office): DGS-259, Scientific-11	15. SECURITY CLASS. (of this report): Unclassified
	15a. DECLASSIFICATION/DOWNGRADING SCHEDULE

16. DISTRIBUTION STATEMENT (of this Report)

A-Approved for public release; distribution unlimited

17. DISTRIBUTION STATEMENT (of the abstract entered in Block 20, if different from Report)

18. SUPPLEMENTARY NOTES

19. KEY WORDS (Continue on reverse side if necessary and identify by block number)

geodesy, satellite-to-satellite tracking, gravity anomalies, ATS-6, GEOS-3

20. ABSTRACT (Continue on reverse side if necessary and identify by block number)

The recovery of 5° equal area mean anomalies is investigated from ATS-6/GEOS-3 SST real range-rate data using the least squares collocation method. The observational errors can be very satisfactorily filtered out by using piecewise continuous cubic splines (with continuous first and second derivatives) to fit the range-rate data in the least squares sense. The accelerations are obtained by analytical differentiation of the fitted spline. The accelerations are obtained optimally,

→ over

DD FORM 1 JAN 73 1473 EDITION OF 1 NOV 65 IS OBSOLETE

unclassified

SECURITY CLASSIFICATION OF THIS PAGE (When Data Entered)

matching the smoothness characteristics expected at GEOS-3 altitudes, if the nodes of the spline, where adjacent cubic polynomials meet, are kept every 60 seconds to fit range-rate observations at 10 seconds interval.

It is found that the initial state vectors of ATS-6 and GEOS-3 are best determined by using observations over a 4 to 6 days period to avoid biased values due to occasional faulty observations. The initial state vectors for any other epoch during this period, but not before or after this period, may be obtained by integration. The recovery of anomalies can be examined using observations in one GEOS-3 revolution at a time. Two revolutions having faulty observations could be identified in this manner.

The residual errors in the initial state vector of GEOS-3 of 10 to 20 meters in position, and 1 to 2 cm/sec in velocity were found to cause small linear errors in the radial derivative ($\partial T/\partial r$) of the anomalous potential. These systematic errors may be adjusted for minimum variance of the discordance between $\partial T/\partial r$ values in ascending and descending revolutions at cross-over points. The number of ascending and descending revolutions should be more than four each to obtain an over-determined solution.

The recovery of eight 5° anomalies was attempted using three descending and two ascending revolutions without applying cross-over constraints. The RMS anomaly discrepancy was about 8 mgals with standard deviation of predicted anomalies as about 12 mgals. Tests indicate that these values could be much reduced by using observations from additional revolutions, and applying cross-over constraints.

Foreword

This report was prepared by D. P. Hajela, Research Associate, Department of Geodetic Science, The Ohio State University, under Air Force Contract No. F19628-76-C-0010, The Ohio State University Research Foundation Project No. 710335 (4214 B1), Project Supervisor, Richard H. Rapp. The contract covering this research is administered by the Air Force Geophysics Laboratory, L. G. Hanscom Air Force Base, Massachusetts, with Mr. Bela Szabo, Contract Monitor.

Acknowledgement

I am indebted to Dr. Richard H. Rapp for his guidance and comments at various stages of these investigations. I am grateful to Dr. Urho A. Uotila for his interest and encouragement. Mr. James Marsh of the NASA Goddard Space Flight Center supplied important information relative to the orbital elements of GEOS-3 and ATS-6. The assistance of Miss Laura E. Reiter, and her careful typing of this report, is greatly appreciated.

Table of Contents

1. Introduction

The recovery of mean gravity anomalies, or alternate representations such as surface densities, point masses, etc., from the range rate sum observations in a 'high-low' satellite experiment has been the subject of several investigations, among others in (Schwarz, 1970; Kaula, 1972; Martin, 1972; Hajela, 1974; Kaula et al., 1975; Sjogren et al., 1976; Vonbun et al., 1977). The recovery of gravity parameters in these investigations was based on the 'deterministic' approach of least squares approximation, where we do not fully utilize the statistical information relating to the parameters, particularly the covariance functions between the parameters and the observations (or more usually a related quantity to the observations).

The 'least squares collocation' approach (for a conceptual discussion, see Moritz, 1976, Sec. 4) for the recovery of gravity anomalies from range rate sum observations in high-low satellite to satellite tracking (SST) was suggested by Rummel (1975, Sec. 5) utilizing the cross-covariance function of gravity anomalies with the radial derivative ($\partial T/\partial r$) of the anomalous potential (T), and the autocovariance function of $\partial T/\partial r$. The numerical computation of these functions was made possible by the covariance expressions developed by Tscherning (1976) using an assumed model for the anomaly degree variances (Tscherning and Rapp, 1974).

Rummel, Hajela and Rapp (1976) carried out simulation studies for developing the procedure for the recovery of mean gravity anomalies from SST range-rate data using least squares collocation. The present report applies the results of the previous study (ibid., 1976) to the systematic investigation of problems in utilizing real ATS-6/GEOS-3 observations. These problems will be discussed in outline in Section 1.2 and in greater detail in Sections 2 and 3. The recovery of eight 5° mean gravity anomalies in a local area will be presented in Section 4.

1.1 Recovery of Anomalies from Simulated Data

We briefly recapitulate the discussion in Rummel et al. (1976). We consider the range rate data to be the residual value referred to the earth's normal gravitational field expressed by potential coefficients (P.C.) up to degree and order 12. That is, we subtract from the observed range rate sum (Martin, 1972; Hajela, 1974) at any given time, usually at 10 seconds data interval, the computed value of the range rate sum corresponding to the cartesian position (X, Y, Z) and velocity ($\dot{X}$, $\dot{Y}$, $\dot{Z}$) coordinates of ATS-6 and GEOS-3 satellites. These coordinates, or state vector (X, Y, Z, $\dot{X}$, $\dot{Y}$, $\dot{Z}$), are obtained from an initial state vector at an initial epoch (usually a few hours earlier) by integrating the equations of motions of the satellites in an inertial coordinate system (usually referenced to 0^h of the day) in a force field expressed by the earth's

low-degree normal gravitation (12, 12 P.C.), and also taking into account the lunar and solar gravitation and the solar radiation pressure. (The atmospheric drag is negligible as the altitude of satellites is higher than 800 km.) We will consider the determination of initial state vectors later, but it is obvious that the residual values (observed-computed) of the range rate would be biased if the initial state vectors are not known accurately.

The residual range rate then expresses the range rate of GEOS-3, sensed at ATS-6, due to anomalous potential T

$$T = W - U \tag{1.1}$$

where W expresses the actual gravitational potential of the earth, and U the low-degree (12, 12 P.C.) normal potential, both at the location of GEOS-3 satellite. The line of sight (ATS-6/GEOS-3) residual range rate yields the line of sight residual acceleration by numerical differentiation. The effect of any errors in the raw residual range rate data will be discussed later. However, as the residual accelerations represent the slope of the residual range rate (function), they would be much in error if raw 'noisy' data is used directly.

The projection of this residual acceleration on the radial direction at the GEOS-3 location (denoted by the subscript c) gives the radial derivative $(\partial T/\partial r)_c$ of the anomalous potential, which is used for the recovery of residual gravity anomalies ($\Delta g'$) referred to the low-degree (12, 12 P.C.) normal potential. We will henceforward generally assume the word residual to be implied, unless required for clarity. We will thus refer to the residual line of sight range rate simply as range rate or $\dot{R}$ data. Analogously, we will generally use the word 'accelerations' or $\ddot{R}$ for the residual line of sight accelerations; and assume $\partial T/\partial r$ without the subscript c to refer to the GEOS-3 location. We may refer to residual mean gravity anomalies simply as anomalies. If we denote the angle at GEOS-3 at any given time between the radial direction and the line of sight ATS-6/GEOS-3 by β, then

$$\partial T/\partial r = \ddot{R}/\cos\beta \tag{1.2}$$

and the predicted or recovered anomaly $\hat{\Delta g}'$ is obtained using least squares collocation from a set of n $\partial T/\partial r$ values by:

$$\hat{\Delta g}'(Q) = \underline{C}^{T}(Q)_{\Delta g' r_r}\ (\underline{\underline{C}}_{r_r r_r} + \underline{\underline{D}})^{-1}\ (\underline{\partial T/\partial r}) \tag{1.3}$$

where $C_{\dot{r}\dot{r}}$ is the n x n matrix of autocovariances of n x 1 $\underline{\partial T/\partial r}$ vector with the noise matrix $\underline{\underline{D}}$, usually taken to be a diagonal matrix with the same value for each element on the diagonal; $\underline{C}^{T}(Q)_{\Delta g'\dot{r}}$ is the transposed vector of cross-covariances of predicted anomaly with the $\partial T/\partial r$ values; and Q emphasizes the fact that the location of the anomaly is on the surface of the earth, while the $\partial T/\partial r$ values refer to the GEOS-3 satellite locations. The point auto and cross-covariance elements are computed from global covariance expressions, and the mean anomaly covariance elements are computed by numerical integration of the appropriate point covariances.

The standard deviation $\hat{\sigma}_{\Delta g'}$ of the predicted anomaly is computed by:

$$\hat{\sigma}^{2}_{\Delta g'} = C_0 - \underline{C}^{T}_{\Delta g'\dot{r}} \left(\underline{\underline{C}}_{\dot{r}\dot{r}} + \underline{\underline{D}}\right)^{-1} \underline{C}_{\Delta g'\dot{r}} \tag{1.4}$$

where C_0 is the variance of residual mean 5° anomalies and other notations are as in equation (1.3).

In view of the local nature of the covariance functions in equations (1.3) and (1.4), when referred to a degree 12 reference field (Rummel et al., 1976, p. 15, Table 2.2), it was found (ibid., Sec. 6) that we need to consider $\partial T/\partial r$ values only with sub-satellite points within 7.°5 of the center of the 5° anomaly blocks. It was also found that it is adequate to consider $\partial T/\partial r$ values at 30 seconds data interval. These two considerations will be retained in all tests with real data. The recovery of anomalies with real data will be judged by statistics comparing the magnitudes of the predicted ($\hat{\Delta g'}$) against the expected value, $E(\Delta g')$, and by anomaly discrepancy $\epsilon(\Delta g')$, (see ibid., pp. 20 and 31):

$$\epsilon(\Delta g') = \hat{\Delta g'} - E(\Delta g') \tag{1.5}$$

$$E(\Delta g') = \Delta g_T - \Delta g_{PC} \tag{1.6}$$

where Δg_T is the terrestrial 5° anomaly (Rapp, 1977) and Δg_{PC} is the anomaly implied by the degree 12 reference field.

The elements of the diagonal matrix $\underline{\underline{D}}$ in equations (1.3) and (1.4) could conceivably be considered as the square of the standard deviation of $\partial T/\partial r$ data, which may be obtained by propagation of the variance of $\ddot{R}$, which in turn could be obtained in some manner from the assumed standard deviation of raw $\dot{R}$ data. However, with both simulated and real data, tests on the stability of the solution were performed with different assumed standard deviation of $\partial T/\partial r$ data like 0.5, 1.0, 1.5, 2.0 mgals. Equation (1.4) is not very sensitive to this variation, but in equation (1.3), a standard deviation of 2 mgals or larger would

show a dampened recovery with low R.M.S. (root mean square) value of predicted $\Delta\hat{g}'$. On the other hand, a small value less than 0.5 mgals would show an unstable recovery with large RMS $\Delta\hat{g}'$ (usually larger than RMS value of expected anomalies E ($\Delta g'$)), and also large RMS anomaly discrepancy $\epsilon(\Delta g')$. For details, see Rummel et al. (1976, pp. 34 and 43).

Other details of the formulations and procedures may also be seen in the above report, and are not being repeated here. We will now describe the variations which were required to implement the use of real $\dot{R}$ data.

1.2 Recovery of Anomalies from Real Data

In simulation studies, we considered the initial state vectors of the satellites to have been determined a-priori to an accuracy so that any resulting error (modeling error) in the residual $\dot{R}$ data (due to treating the initial state vectors to be without error) was much less than the observational errors or 'noise'. This a-priori knowledge was necessary, as it was found that the initial state vectors could not be converged (GEODYN, Vol. III, pp. 1.2 - 5; also see below) from the limited time span of 30 to 60 minutes of range rate sum observations.

We presume here that at the satellite altitudes exceeding 800 km, the equations of motion of the satellites can be expressed with negligible error if the earth's gravitational field is described by the full set of potential coefficients of GEM-7 (Wagner et al., 1976). If we also take into consideration the lunar and solar gravitation, and account for the ionospheric and tropospheric refraction and the transponder delays at the satellites, then barring any system bias in the range rate sum observations, the computed values should fit the observed values in the least squares sense, and we may iteratively solve for the initial state vectors of the ATS-6 and GEOS-3 satellites. We will consider the solution to have converged when the corrections to the initial state vectors in two consecutive iterations do not change by more than 2%.

The converged initial state vectors are thus based on the observation type and the time span. They may be strongly biased if the observations were biased in some way, and this possibility would increase if only one type of observation was used for converging the arc, and also if the time span of observations was 'short'. The adequacy of time span depends on the type of observations (and their variance). Conceptually, range computations will be more sensitive to the initial state vector of a satellite as compared to the range rate values, and the range rate sum values of a high-low satellite pair will be still less sensitive to the initial state vectors of the satellites. We should therefore expect the changes in the solution of initial state vectors in successive iterations to vary sharply with the last observation type, and several iterations may be needed for the converged solution even if the time span was comparatively long, like 1 to 3 hours.

The optimum solution would then be to use several types of observations obtaining a weighted least squares solution of the initial state vectors of ATS-6 and GEOS-3. As we did not have access to other types of observations besides the ATS-6/GEOS-3 SSE tracking data (NASA, 1976), the initial state vectors were not solved for by us. These were kindly supplied by Marsh (1976, 1977) and will be discussed in Section 2. The effect of uncertainty in the initial state vectors on the residual $\dot{R}$, $\ddot{R}$ and anomalies will be discussed in Section 4.

In simulation studies, the residual $\dot{R}$ data was numerically differentiated by approximating it by a smooth continuous function, viz. the interpolating natural cubic spline, and then analytically differentiating the spline to obtain $\ddot{R}$. The spline being a set of piecewise continuous cubic polynomials does not exhibit spurious oscillations between the data points, which is a characteristic of higher order polynomials. Also, as the spline has the minimum norm among all interpolating functions (details in Section 2), it is the smoothest function and its first derivative ($\ddot{R}$ in our case) is also a smooth (and continuous) function. The interpolating spline, however, passes through the $\dot{R}$ data points and does not admit any errors in them. The slopes of the interpolating spline would thus be in much error with real $\dot{R}$ data, which have observational errors, as the spline would have spurious 'rise and fall' in trying to fit each data point exactly. We have to thus consider a cubic spline which may fit the data in the least squares sense (Lawson and Hanson, 1974, Chap. 27) so that the fitted spline filters the raw $\dot{R}$ data of the 'noise'. A similar data fitting approach was reported by Muller and Sjogren (1968) in filtering lunar doppler data by fitting piecewise continuous cubic Hermite polynomials, but which did not have a continuous first derivative. Cubic splines were used in their later analyses.

Besides filtering the raw $\dot{R}$ data, we also wish to smooth it in the sense that its slope, $\ddot{R}$, changes smoothly in a physically meaningful way. We know from simulation studies (Rummel et al., 1976, p. 54) that the values of $\partial T/\partial r$ (and $\ddot{R}$) change only gradually within a mgal or so over 30 seconds interval at the GEOS-3 altitude. The spline fitted in the least squares sense should then be further required to be smooth enough so that its first derivative (and $\partial T/\partial r$) should change in the gradual manner indicated. The smoothing is dependent on the spacing of spline nodes, where different cubic polynomials in neighboring intervals meet. If the spline nodes are too far, we will get a dampened representation of $\ddot{R}$ from over-smoothing of the spline; while if the nodes are too near, the slopes of the fitted spline change sharply at the data points (at 10 seconds interval) giving noisy $\ddot{R}$ values. This will be discussed in detail in Section 3.

1.3 Scope of Investigations

The ATS-6/GEOS-3 SSE tracking data was supplied by NASA (1976) in the ATSR format (Bryan et al., 1975). A portion of this data from April 16, 1975 to May 22, 1975 was reformatted in the GEODYN binary format (GEODYN, Vol. III, Appx. C 7) using a preprocessor program kindly supplied by Martin (1975). Agajelu (1977) selected five descending GEOS-3 revolutions 154, 268, 439, 453 and 467, in which the GEOS-3 satellite moved from north-east to south-west, for examining the recovery of 5° anomalies in the Carribean portion of the North Atlantic Ocean between the latitudes 15° to 35° North and longitudes 275° to 295° East. The initial state vectors for both ATS-6 and GEOS-3 satellites were supplied by Marsh (1976) for these five GEOS-3 revolutions during the period April 20 to May 12, 1975.

It was intended to use five ascending GEOS-3 revolutions, in which the GEOS-3 satellite moved over the area of investigation from south-east to north-west. These revolutions were 104, 118, 175, 232 and 246 during the period April 17 to April 27, 1975. The initial state vectors were received (Marsh, 1977) only for the GEOS-3 satellite for three revolutions. It was hoped that the corresponding initial state vectors for ATS-6 could be obtained by integration from the values available for 0^h on April 19 and April 25, 1975.

The present study investigates the above limited real range-rate sum observations for establishing the procedures for the recovery of 5° anomalies using least squares collocation. If the range rate sum observations in all 10 GEOS-3 revolutions could be used, we would have observations from one ascending and one descending revolution for the recovery of each 5° anomaly. As we will later see in Sections 2 and 4, this density of observations was, however, not available.

We will examine the reliability and compatibility of the initial state vectors in Section 2, and their effect on the recovery of anomalies will be investigated in Section 4. We will consider the filtering and smoothing of the residual $\dot{R}$ data in Section 3.

2. Initial State Vectors for ATS-6 and GEOS-3 Satellites

The initial state vectors were provided by Marsh (1976) for both satellites corresponding to five descending revolutions of GEOS-3. We first describe in Section 2.1 the particulars of the observations and time span used for determining these initial state vectors, and the uncertainties ascribed to them. Initial state vectors for three ascending revolutions of GEOS-3 were later provided by Marsh (1977), together with data from which it was hoped that the initial state vectors for two other ascending revolutions of GEOS-3, and the

corresponding elements for ATS-6 (for all five ascending revolutions of GEOS-3), may be obtained by forward or backward integration. We discuss in Section 2.3 attempts to recover these values. We also describe in Section 2.2 the result of trying to filter out some observational and modeling errors in a short time span of range-rate observations by letting the initial state vectors be constrained with suitable weights to change only slightly to see if some errors may be absorbed by them. The results showed that this approach is not workable.

2.1 Initial State Vectors Available for Both Satellites

The five descending revolutions of GEOS-3 were 154, 268, 439, 453 and 467. The epoch of the initial state vectors, the time span of observations and other particulars are given in Table 2.1. The earth's gravitational field was modeled by the full set of potential coefficients of GEM-7 (Wagner et al., 1976). The lunar and solar gravitational effects, including earth tides, and the solar radiation pressure were taken into account. The atmospheric drag was considered zero at the satellite altitude exceeding 800 km. The observations considered were range, including laser ranges, range-rate and average range-rate (GEODYN, Vol. III, 1975, Appx. C.7). The initial state vectors of both ATS-6 and GEOS-3 were adjusted together, keeping observations for a single pass of GEOS-3, as seen from ATS-6, centrally in the time span of observations. The adjustment was done iteratively (GEODYN, Vol. I, 1976, Sec. 2.2) minimizing the sum of squares of residuals of observed minus computed (O - C) values in the force model, till the RMS (root mean square) value in the last iteration converged within 2% of the RMS value in the previous iteration. The RMS position (RMS P_i) standard deviation (S D) and RMS velocity (RMS V_i) standard deviation for each satellite ($i = 1, 2$) was computed from the standard deviations of the position (S_{x_i}, S_{y_i}, S_{z_i}) and velocity ($S_{\dot{x}_i}$, $S_{\dot{y}_i}$, $S_{\dot{z}_i}$) elements at the initial epoch as:

$$(2.1) \qquad \text{RMS } P_i = (S_{x_i}^2 + S_{y_i}^2 + S_{z_i}^2)^{\frac{1}{2}}, \quad i = 1 \text{ for ATS-6, } i = 2 \text{ for GEOS-3}$$

$$(2.2) \qquad \text{RMS } V_i = (S_{\dot{x}_i}^2 + S_{\dot{y}_i}^2 + S_{\dot{z}_i}^2)^{\frac{1}{2}}, \quad i = 1 \text{ for ATS-6, } i = 2 \text{ for GEOS-3}$$

The data interval for range-rate observations in all cases was 10 seconds, except for revolution 467 where it was 1 second during a period of about 7 minutes and 10 seconds otherwise. There was also a break of about 30 seconds at each end of 1 second interval observations in revolution 467. The residuals in this revolution after the convergence of initial state vectors were much larger by a factor of 4 to 6 compared to other revolutions. This revolution was thus not used, and only four revolutions 154, 268, 439 and 453 were used in subsequent work.

Table 2.1. Data Used for Determining Initial State Vectors for ATS-6 and GEOS-3 corresponding to GEOS-3 Revolutions 154, 268, 439, 453 and 467

	Revoln. 154	Revoln. 268	Revoln. 439	Revoln. 453	Revoln. 467
1. Epoch of initial state vector	20 Apr 75 20h 38m 00s	28 Apr 75 20h 50m 00s	11 May 75 00h 02m 00s	11 May 75 23h 38m 40s	12 May 75 23h 32m 00s
2. Time span of observations	Hr. min. sec.	Hr. min. sec.	Hr. min. sec.	Hr. min. sec.	Hr. min. sec.
(a) Begin time	20 38 00	20 54 15	00 02 00	23 38 40	23 32 00
(b) End time	22 59 46	23 31 26	02 14 41	25 59 50	25 45 34
(c) Total time	2 21 46	2 37 11	2 12 41	2 21 10	2 13 34
3. Total no. of observations	650	776	688	640	853
4. No. of obsns. accepted in last iteration	650	659	557	582	726
5. No. of obsns. by measurement type					
(a) Range	193	346	202	238	399
(b) Range-rate	429	313	299	288	271
(c) Average range-rate	28	0	56	56	56
6. RMS Position S. D. of ATS-6	1846.50m	1596.63m	569.78m	18.40m	24.20m
7. RMS Velocity S. D. of ATS-6	42.87cm/sec	11.71cm/sec	4.97cm/sec	0.55cm/sec	0.49cm/sec
8. RMS Position S. D. of GEOS-3	1931.69m	21.22m	43.90m	14.08m	4.32m
9. RMS Velocity S. D. of GEOS-3	564.71cm/sec	2.38cm/sec	4.33cm/sec	1.55cm/sec	0.43cm/sec

2.2 Filtering of Residual $\dot{R}$ Data by Slight Variations to Initial State Vectors

The statistics $RMSP_1$ and $RMSV_1$, expressing the uncertainty in the determination of the initial state vectors, were large (see Table 2.1) for all revolutions, only revolution 453 having a comparatively lower value. This was a cause for concern, for if the initial state vectors were incorrectly determined, it will cause large residuals of range rate (Agajelu, 1976, Sec. 4). A larger value of RMSP and RMSV, however, does not necessarily imply a large discrepancy from the 'true' value of the initial state vector, which is ensured by taking different types of observation for an adequate time span and by the convergence criterion of the determination of the initial state vector.

We will be using the range-rate $\dot{R}$, residual to a (12, 12) potential coefficients field, as the raw data to recover residual gravity anomalies. This data is needed for a limited time span for the recovery of anomalies in a local area. We cannot use this limited data to improve the available initial state vectors in the sense of bringing them closer to the 'true' values. But it may be argued that we could possibly filter the raw $\dot{R}$ values of some observational and modeling errors by letting the initial state vectors take the 'slack' by letting them vary slightly within the standard deviation implied by the statistic RMSP and RMSV. This may still be too large for a case like revolution 154 in Table 2.1. There is also a risk in this approach that the initial state vectors may absorb a part of the signal, while filtering the observational and modeling errors.

Nevertheless, we tested this approach by considering the case of revolution 453, where the a-priori values of the initial state vectors as available in Table 2.1 were assigned standard deviations implied by items 6 to 9 (in Table 2.1), and then allowed to change to fit a span of 30 minutes residual $\dot{R}$ values. Three iterations were tried, and the results are shown in Table 2.2.

It is obvious that the range-rate observations by themselves are not very helpful in tying down the initial state vector. And that, in any case, a 30 minute time span of $\dot{R}$ data is not long enough to do so. A shorter time span would be only worse. We have to thus fix the initial state vectors, obtained from a longer time span and with different data types in Section 2.1, by assigning them very low standard deviations (Hajela, 1974, Section 6.1). The filtering and smoothing of observational and modeling errors would have to be handled subsequently. This will be discussed in Sections 3.1 and 3.2.

Table 2.2. Variation of Initial State Vectors to Filter Residual Range-Rate Data for 30 Minutes in Revolution 453

	1st Iteration	2nd Iteration	3rd Iteration
1. Observations accepted for adjustment			
(a) No. of obsns.	180	17	61
(b) Mean value (cm/sec)	0.72	-50.85	23.07
(c) RMS value (cm/sec)	0.82	67.78	29.28
2. Change to Initial State Vectors			
(a) ATS-6 in position (meters)	0.53	0.40	0.38
(b) ATS-6 in velocity (cm/sec)	0.06	0.05	0.07
(c) GEOS-3 in position (meters)	1.19	12.15	4.88
(d) GEOS-3 in velocity (cm/sec)	0.02	1.85	0.08
3. Uncertainties in Initial State Vectors			
(a) RMSP for ATS-6 (meters)	17.15	17.21	17.19
(b) RMSV for ATS-6 (cm/sec)	0.44	0.48	0.46
(c) RMSP for GEOS-3 (meters)	9.90	12.18	11.65
(d) RMSV for GEOS-3 (cm/sec)	1.05	1.32	1.14

2.3 Initial State Vector Available for only GEOS-3 Satellite

The five ascending revolutions of GEOS-3 (which we wished to consider) with epoch times during April 75 were: 104 (April 17, 07^h), 118 (April 18, 07^h), 175 (April 22, 08^h), 232 (April 26, 08^h) and 246 (April 27, 08^h). Initial state vectors for GEOS-3 for revolutions 175, 232 and 246 were received from Marsh (1977). The particulars for the observations used for determining the initial state vectors for GEOS-3 are given in Table 2.3, on the same lines as in Table 2.1. As the tracking data before April 19, 1975 were not readily available, the initial state vectors for GEOS-3 were not determined for revolutions 104 and 118. Instead, the initial state vectors for both ATS-6 and GEOS-3 satellites solved together were supplied for April 19 ($0^h\ 0^m\ 0^s$), and later also for April 25 ($0^h\ 0^m\ 0^s$). The particulars of observations used for determining these are also given in Table 2.3.

Table 2.3. Data Used for Determining Initial State Vectors for GEOS-3 Revolutions 175, 232, 246 and for ATS-6 and GEOS-3 for Epochs on April 19 and April 25, 1975.

	Revoln. 175	Revoln. 232	Revoln. 246	Epoch 19 Apr 75 0^h	Epoch 25 Apr 75 0^h
1. Epoch of initial state vector	22 Apr 75 06h 40m 00s	26 Apr 75 07h 00m 00s	27 Apr 75 07h 00m 00s	19 Apr 75 00h 00m 00s	25 Apr 75 00h 00m 00s
2. Time span of observations	Hr. min. sec.	Hr. min. sec.	Hr. min. sec.	Hr. min. sec.	Hr. min sec.
(a) Begin time	06 40 00	07 00 00	07 00 00	19 Apr 75 00 00 00	25 Apr 75 00 00 00
(b) End time	08 39 51	10 05 31	09 09 46	24 Apr 75 01 12 04	29 Apr 75 23 59 52
(c) Total time	1 59 51	3 05 31	2 09 46	≈ 5 days	≈ 5 days
3. Total no. of observations	213	667	947	2241	2836
4. No. of obsns. accepted in last iteration	213	546	851	2134	2539
5. No. of obsns. by measurement type					
(a) Range	213	546	851	2070	1668
(b) Range-rate	0	0	0	55	734
(c) Average range-rate	0	0	0	9	137
6. RMS Position S. D. of ATS-6	-	-	-	3.22m	1.52m
7. RMS Velocity S. D. of ATS-6	-	-	-	0.03cm/sec	0.01cm/sec
8. RMS Position S. D. of GEOS-3	2.40m	3.73m	0.67m	0.29m	0.21m
9. RMS Velocity S. D. of GEOS-3	0.79cm/sec	0.37cm/sec	0.10cm/sec	0.02cm/sec	0.02cm/sec

We note that the ATS-6 elements corresponding to the epoch of GEOS-3 revolutions were not available. It was hoped that these could be obtained by integration from the ATS-6 elements available for 19 April 75, or preferably from the nearer epoch 25 April 75. And similarly, the ATS-6 and GEOS-3 elements for revolutions 104 and 118 could be obtained by backward integration from the epoch on 19 April 75 using the GEODYN (1975) program. Before this was done, it was necessary to examine the compatibility of the elements supplied in the last two columns of Table 2.3, which had been rigorously determined from observations of different types over 5 day periods. This was first done for the ATS-6 satellite. The true of date ephemeris for ATS-6 was generated by integrating forwards and backwards in the force field as described in Section 2.1 for the period 19 April 75 to 29 April 75 separately from the elements available in the last two columns of Table 2.3. The position (X, Y, Z) and velocity ($\dot{X}$, $\dot{Y}$, $\dot{Z}$) coordinates were compared from these two ephemeris, and also with the ATS-6 elements available in Table 2.1. The comparisons could be made for the epochs on 19 April 0^h, 20 April for epoch of revolution 154, 22 April for epoch of revolution 175, 25 April 0^h, 26 April for epoch of revolution 232, 27 April for epoch of revolution 246, and 28 April for epoch of revolution 268. Comparisons were also made with ATS-6 elements supplied with SSE tracking data (NASA, 1976) for the epoch on 20 April 0^h. The differences are shown in three rows for each epoch in Table 2.4: (a) first row — integrated elements from April 19, 0^h epoch minus elements available in Tables 2.1 or 2.3; (b) second row — integrated elements from April 25, 0^h epoch minus elements available in Tables 2.1 or 2.3; third row — integrated elements from April 19, 0^h epoch minus integrated elements from April 25, 0^h epoch. When there was no data to complete a row, it was left blank.

It is clear from the entries against row (c) in Table 2.4 that we may be able to integrate the elements reasonably correctly only within the time span of observations used for determining the initial state vector. We may note the large values of the discrepancies (A-B) in rows 1c and 5c. But what is more surprising is that they differ from each other though the time period for backward integration (from 25 April to 19 April 75) of ATS-6 elements on 25 April 75 is the same as the time period for forward integration (from 19 April to 25 April 75) of ATS-6 elements on 19 April 75. We may also note the very large changes in rows 7c and 8c, and also the changes in rows 4c and 5c.

The ATS-6 elements on 19 April 75 and 25 April 75 were converged independently, based on 5-day observations with low RMSP and RMSV values (Table 2.3). But they are not at all compatible with each other outside the time span of observations on which they are based. This is also seen in the large discrepancy in row 2a of Table 2.4. The elements differ widely as they are based on different time spans of observations. The differences are grossly large in row 8b. We recall that the converged elements (C) for ATS-6 in row 8b were obtained for time span of about 2 1/2 hours (see Table 2.1 for revolution 268).

Table 2.4. Differences in Position and Velocity Coordinates for ATS-6 as Integrated from Epochs on 19 April 75 (A) and 25 April 75 (B) in Comparison with Converged Elements (C) for Other Epochs

Epoch (Date, Hr., min., sec.)		ΔX(m)	ΔY(m)	ΔZ(m)	$\Delta\dot{X}$ (cm/sec)	$\Delta\dot{Y}$ (cm/sec)	$\Delta\dot{Z}$ (cm/sec)
1. 19 April 75	a						
0h 0m 0s	b						
	c = A - B	- 315.2	624.3	306.3	4.60	2.22	- 0.46
2. 20 April 75	a = A - C	342.0	201.7	326.1	-1.32	3.48	7.89
0h 0m 0s	b = B - C	723.3	-394.7	22.2	-6.10	1.66	8.38
(C. SSE data, NASA 1976)	c = A - B	- 381.3	596.4	303.9	4.78	1.82	- 0.49
3. 20 April 75	a = A - C	- 122.6	851.0	7,963.6	-0.01	- 25.02	-226.22
20h 38m 00s	b						
(C. GEOS-3 revoln. 154)	c						
4. 22 April 75	a						
06h 40m 00s	b						
(C. GEOS-3 revoln. 175)	c = A - B	669.3	1,077.1	- 158.3	-2.98	- 2.85	- 2.15
5. 25 April 75	a						
0h 0m 0s	b						
	c = A - B	- 692.9	423.8	290.9	5.87	- 0.05	- 0.67
6. 26 April 75	a						
07h 00m 00s	b						
(C. GEOS-3 revoln. 232)	c = A - B	- 486.7	767.6	- 197.6	-0.10	- 2.03	- 1.91
7. 27 April 75	a						
07h 00m 00s	b						
(C. GEOS-3 revoln. 246)	c = A - B	- 427.5	704.9	- 200.9	0.44	- 1.64	- 1.88
8. 28 April 75	a = A - C	-31,973.0	6,866.2	-6,076.3	-0.84	-178.66	-171.18
20h 50m 00s	b = B - C	-30,464.0	5,943.7	-6,340.2	-2.01	-169.32	-172.20
(C. GEOS-3 revoln. 268)	c = A - B	- 1,509.0	922.5	263.9	1.17	- 9.34	1.02

It is therefore not possible to integrate backwards from the initial state vectors of ATS-6 and GEOS-3 on 19 April 75 to obtain elements corresponding to GEOS-3 revolutions 104 and 118 on 17 April and 18 April 75 respectively. We may also integrate the ATS-6 elements forward only within the time span of observations used for converging then, i. e. for epoch of revolution 175 from elements on 19 April 75 and for epochs of revolutions 232 and 246 from elements on 25 April 75. It was found that there was a break in range-rate observations in GEOS-3 revolution 175 over the area of investigation, so we could only process the observations in GEOS-3 revolutions 232 and 246.

We then examined the residuals of range-rate sum in the full force field of Section 2.1, using the initial state vectors of ATS-6 as obtained by integration from 25 April 75, along with the converged initial state vectors of GEOS-3 as available from Table 2.3, for epochs of revolution 232 and 246; 56 and 61 minutes of range-rate sum observations were used respectively for the two revolutions. We would expect the residuals to be random and close to zero, if the initial state vectors were satisfactory. However, this was not so, particularly for revolution 232, and is shown in Table 2.5. As the GEOS-3 elements were already converged as in Table 2.3, only ATS-6 integrated elements could be responsible for unsatisfactory residuals. We then fixed the initial state vector of GEOS-3 by assigning very low standard deviations, and allowed the 56 and 61 minutes of range-rate observations to iteratively improve the ATS-6 elements to fit these observations. The a-priori standard deviation of each ATS-6 element was taken approximately equal to the magnitude of the differences (A-B) in rows 6c and 7c of Table 2.4. A total of up to 9 iterations were tried separately for revolutions 232 and 246, and the results are given in Table 2.5.

We first note that range-rate sum observations, even the time-span of 60 minutes, are not very helpful in tying down the initial state vector. (Also see Eddy and Sutermeister, 1975, Sec. 3.) The elements did not converge even after 9 iterations in revolution 246, and even in the case of revolution 232 there are very sharp fluctuations in the second and fourth iterations. Secondly, the large initial values, shown under iteration 1, of mean and RMS residuals in revolution 232, as compared to revolution 246, points to some systematic errors in range-rate sum observations in revolution 232. Hence, even if the elements converge after seven iterations, and reduce the magnitude of residuals, the systematic error may still remain. This will be discussed again in Section 4.2. For future reference we will refer to the initial state vectors of GEOS-3 in revolution 232 as in Table 2.3 and the corresponding initial state vector of ATS-6 as referring to revolution 232 I with integrated elements of ATS-6, and as revolution 232 A with adjusted elements of ATS-6 after 7 iterations in Table 2.5. The initial state vectors of ATS-6 for revolutions 232 I and 232 A are shown in Table 2.6. The difference between them is as grossly large as for the case in row 8b in Table 2.4.

Table 2.5 Residuals of Range-Rate Sum in Full GEM-7 Field for Revolutions 232 and 246, Using Integrated Elements of ATS-6 from Epoch 25 April 75, 0^h, and Convergence of ATS-6 Elements.

	Iteration Number								
	1	2	3	4	5	6	7	8	9
A. GEOS-3 Revoln. 232 on 26 April 75									
1. No. of obsns. accepted (08h 31m to 09h 27m)	336	335	336	331	329	328	328		
2. Mean of residuals (cm/sec)	-6.07	12.76	-0.39	0.18	0.04	0.02	0.00		
3. RMS of residuals (cm/sec)	6.44	13.38	2.76	2.24	2.15	2.13	2.15		
4. Change in ATS-6 elements from previous iteration in								Elements converged within	
(a) X (km)	6.9	-40.0	0.80	2.37	1.15	0.49	.020	2% after 7	
(b) Y (km)	-4.8	23.8	-0.04	-0.20	-0.22	-0.11	-.013	iterations.	
(c) Z (km)	-1.6	16.9	-0.87	-2.83	-1.21	-0.49	-.007		
(d) $\dot{X}$ (cm/sec)	-32.1	167.2	-2.5	-6.7	-3.5	-1.5	-0.09		
(e) $\dot{Y}$ (cm/sec)	30.7	-151.7	0.6	1.5	1.4	0.7	0.08		
(f) $\dot{Z}$ (cm/sec)	71.1	-493.3	16.0	51.1	23.0	9.6	0.23		
B. GEOS-3 Revoln. 246 on 27 April 75									
1. No. of obsns. accepted (08h 12m to 09h 13m)	358	43	117	358	190	358	358	358	355
2. Mean of residuals (cm/sec)	-0.78	0.43	-0.14	-2.51	4.54	5.70	-11.01	-0.06	0.17
3. RMS of residuals (cm/sec)	1.97	4.18	10.21	5.40	11.79	17.94	25.92	3.53	3.23
4. Change in ATS-6 elements from previous iteration in									
(a) X (km)	-0.04	-2.78	2.27	-7.9	-4.6	2.5	-28.8	.079	2.66
(b) Y (km)	-0.67	0.73	0.55	5.1	8.4	-6.7	22.1	-.018	-1.35
(c) Z (km)	-0.79	0.99	-2.09	2.9	-3.8	4.3	6.2	-.020	-1.65
(d) $\dot{X}$ (cm/sec)	-2.9	2.4	2.8	40.6	30.8	-19.2	157.4	-0.49	-12.7
(e) $\dot{Y}$ (cm/sec)	4.0	-14.9	6.2	-38.1	-57.6	45.7	-161.1	0.23	10.1
(f) $\dot{Z}$ (cm/sec)	-9.9	20.8	-7.2	-99.7	37.7	-59.6	-295.9	0.80	45.9

Table 2.6. Initial State Vectors for ATS-6 for Revolution 232 on 26 April 75 07^h

Revolution	X (m)	Y (m)	Z (m)	$\dot{X}$ (cm/sec)	$\dot{Y}$ (cm/sec)	$\dot{Z}$ (cm/sec)
232 I	-30,047,830	-29,592,060	-433,970	2,156.92	-2,189.72	45.05
232 A	-30,076,114	-29,573,587	-424,089	2,158.12	-2,190.88	41.83
Difference (A - I)	28,284	-18,473	-9,881	-1.20	1.16	3.22

The convergence of the initial state vector by itself is therefore not enough. We have to consider the observation type as well as the time span of observations used for the convergence. The integrated elements of ATS-6 are totally discordant from the converged elements in revolution 232 A, as well as in revolution 268 (Table 2.4). We will later find in Section 4.3 that the converged elements of GEOS-3 in revolution 268 were also grossly different from the integrated elements from the epoch 0^h on 25 April 75. Firstly, this may point to some systematic errors in the data during the time span of about 2 1/2 hours used in Table 2.1 for convergence of revolution 268. Secondly, there is a possibility while converging the elements in a satellite pair, that two widely differing sets of initial state vectors may fit the same range-rate sum and range sum observations. This may be avoided by including sufficient independent range observations to each satellite.

We will also find later in Section 4 that the residual $\dot{R}$ data in revolution 232 and revolution 268 were not usable whether we use the integrated elements or the converged elements in the initial state vectors of the two satellites.

3. Computation of the Radial Derivative of the Anomalous Potential

We consider in this report the residual range-rate ($\dot{R}$) as the raw data, which is range-rate sum observations in satellite to satellite tracking reduced by the computed value corresponding to the gravitational field defined by (12, 12) potential coefficients (Hajela, 1974) with the initial state vectors obtained in Section 2. In Rummel et al. (1976), a natural cubic interpolating spline was used to fit simulated $\dot{R}$ data, which was free of observational and modeling errors. As the $\dot{R}$ data in this report has observational noise, this has to be first filtered out before further processing. We will discuss the use of cubic splines in fitting

noisy data in the least squares sense in Section 3.1. The results of this fitting (filtering and smoothing), and its analytical differentiation to obtain residual acceleration ($\ddot{R}$) will be presented in Section 3.2. The computation of the radial derivative of the anomalous potential ($\partial T/\partial r$) will be described in Section 3.3.

3.1 Use of Cubic Splines for Fitting Data

Let a set of n distinct and monotonically increasing points be defined on the real line on a closed interval $I \equiv [a, b]$, such that:

$$a \leq t_1 < t_2 < \ldots < t_k < t_{k+1} < \ldots t_n \leq b \tag{3.1}$$

and let a real valued continuous function $\dot{R} = f(t)$ assume the values:

$$\dot{R}_k = f(t_k) \quad \text{at the points} \quad t_k\,, \; k = 1, \ldots, n \tag{3.2}$$

We approximate this function f over I by a smooth 'spline' function $S = S(t)$ consisting of a set of piecewise polynomials of degree $2r + 1$ defined respectively in the intervals $I_k \equiv t_k < t \leq t_{k+1}$, such that S is $2r$ times continuously differentiable at each of the 'nodes' (or 'breakpoints', or 'joints') t_k. This spline function is of degree $2r + 1$. We will consider in this report only a cubic spline (function) with $r = 1$, which is twice continuously differentiable at each node and is a set of piecewise cubic polynomials in each interval I_k. If we specify the value of the spline S at the nodes t_k to be the same as the function f, which is being approximated over I, i.e.

$$S_k \equiv S(t_k) = f(t_k) = \dot{R}_k\,, \; k = 1, \ldots, n \tag{3.3}$$

then S is the interpolating cubic spline; and is uniquely defined if we also specify two additional boundary conditions (Ahlberg, Nilson and Walsh, 1967, page 11). The dimension of S_I is therefore $n + 2$, where S_I is the linear space of all cubic splines on I, with nodes at t_k, $k = 1, \ldots, n$; i.e.

$$S_I = \{\, q(t) \in C^2(I) \mid q(t) \text{ is a cubic polynomial on each subinterval } I_k \equiv t_k < t \leq t_{k+1}\,, \text{ defined on the interval } I \,\} \tag{3.4}$$

and $C^2(I)$ denotes all twice continuously differentiable functions on I. S_1 obviously includes the natural interpolating cubic spline used in Rummel et al. (1976), but we are now interested in other splines also with the common condition that they all have nodes at t_k.

A unique representation for the cubic spline, and we may refer to it henceforward simply as spline, in terms of $n+2$ linearly independent members of S_1 is thus:

$$S(t) = \sum_{j=1}^{n+2} c_j \, q_j(t), \quad j = 1, \ldots, n+2, \; c_j \text{ is a real number.} \tag{3.5}$$

If the sample values of the function f at the nodes t_k are not known accurately in equation (3.2), say due to observational errors in $\dot{R}_k$, the approximation of f by a spline using the interpolating condition (3.3) will be unsatisfactory. The errors will be further magnified in subsequent operations on the spline, for example, if the differential operator is of interest, then $S'(t)$ may not recover the signal or the trend ($f'(t)$) from noisy data $\dot{R}_k$.

We may then fit a spline $S^*(t)$ to the function f in the least squares sense, such that the euclidean or the L_2 norm $\| f - S^* \|_2$ is minimized, (Schultz, 1973, Chap. 6; Rice, 1969, Vol. II, Sec. 10.4), i.e.:

$$\| f - S^* \|_2^2 = \sum_{k=1}^{n-1} \int_{t_k}^{t_{k+1}} (f(t) - S^*(t))^2 \, dt \tag{3.6}$$

$$= \sum_{k=1}^{n-1} \int_{t_k}^{t_{k+1}} (\dot{R}_i - S^*(t_i))^2 \, dt = \text{minimum}$$

and the integral may be replaced by a summation for the available observations $\dot{R}_i$ in the interval I_k. We now assume an available vector $\underline{\dot{R}}$ of noisy observations:

$$\dot{R}_i = f(t_i), \quad i = 1, \ldots, m, \; m > n+2 \tag{3.7}$$

Following (3.5) we may represent $S^*(t)$ as:

$$S^*(t) = \sum_{j=1}^{n+2} c_j^* \, q_j(t), \quad j = 1, \ldots, n+2 \tag{3.8}$$

where q_j are $(n + 2)$ cubic polynomials being the bases of S_l in equation (3.4), and $\underline{c}^*$ is the vector of $(n + 2)$ unknown coefficients c_j^*.

We then have to solve for $\underline{c}^*$ under the constraint (3.6) from a set of m linear (observation) equations:

(3.9) $$\underline{\underline{A}}\,\underline{c}^* \simeq \underline{\dot{R}} \quad , \text{ where}$$

(3.10) $$\underline{\underline{A}} = [a_{ij}] \; ; \; a_{ij} = q_j(t_i) \; ; \; i = 1, \ldots, m; \; j = 1, \ldots, n + 2$$

There exist bases for S_l with the property that if the data are ordered, i. e. $t_1 \leq t_2 \leq \ldots \leq t_m$, then the $(m \times (n + 2))$ matrix $\underline{\underline{A}}$ is band limited with a bandwidth of 4 (Lawson and Hanson, 1974, page 223).

We first note that the nodes of the spline, i. e. t_k in equation (3.1) are embedded in the ordered data t_i with:

(3.11) $$t_k = t_i \text{ for } k = 1, \; i = 1 \text{ and for } k = n, \; i = m;$$

$$m > n + 2$$

We then define:

(3.12) $$\Delta t_k = t_{k+1} - t_k \; , \; k = 1, \ldots, n - 1$$

and scale the independent variable t_i to u_i in each interval I_k, such that

(3.13) $$u_i = \frac{t_i - t_k}{\Delta t_k} = \frac{t_i - t_k}{t_{k+1} - t_k} \; ; \; 1 - u_i = \frac{t_{k+1} - t_i}{t_{k+1} - t_k} = \frac{t_{k+1} - t_i}{\Delta t_k}$$

Then for each interval I_k only 4 cubic polynomials out of $q_j(t)$ have non-zero values, i. e. for

(3.14) $$j = k - 1 + \ell \; ; \quad k = 1, \ldots, n - 1 \; ; \quad \ell = 1, \ldots, 4 \; ;$$
$$q_j(t) = p_1(1-u)$$
$$q_{j+1}(t) = p_2(1-u)$$
$$q_{j+2}(t) = p_2(u)$$
$$q_{j+3}(t) = p_1(u)$$

where (ibid., 1974) suggests the choice:

(3.15)
$$p_1(u) = 0.25\,u^3, \text{ and}$$
$$p_2(u) = 1 - 0.75\,(1+u)\cdot(1-u)^2$$

The spline at any point t_i is then evaluated using equation (3.8) as:

(3.16)
$$S^*(t_i) = \sum_{\ell=1}^{4} c^*_{k-1+\ell}\; q_{k-1+\ell}(t_i);\; k = 1, \ldots, n-1$$

It is easy to see from equations (3.13) to (3.15) that S^* is a cubic polynomial in each interval I_k. It can be shown that it is continuous at the nodes also, for in the interval I_k, when:

(3.17)
$$t_i = t_k,\; u_k = 0,\; 1 - u_k = 1,\; q_k(t_k) = p_1(1) = 0.25$$
$$q_{k+1}(t_k) = p_2(1) = 1$$
$$q_{k+2}(t_k) = p_2(0) = 0.25$$
$$q_{k+3}(t_k) = p_1(0) = 0$$

and when

(3.18)
$$t_i = t_{k+1},\; u_{k+1} = 1,\; 1 - u_{k+1} = 0,\; q_k(t_{k+1}) = p_1(0) = 0$$
$$q_{k+1}(t_{k+1}) = p_2(0) = 0.25$$
$$q_{k+2}(t_{k+1}) = p_2(1) = 1$$
$$q_{k+3}(t_{k+1}) = p_1(1) = 0.25$$

Then if we use the notation $S^*_k(t_{k+1})$ for the value of spline in the interval I_k at the node t_{k+1}, and similarly use the notation $S^*_{k+1}(t_{k+1})$ for the value of spline in the interval I_{k+1} at the same node t_{k+1}, then the continuity of S^* is ensured by the condition:

(3.19)
$$S^*_k(t_{k+1}) = S^*_{k+1}(t_{k+1})$$

which is true, as from equations (3.16) to (3.18):

$$(3.20)\quad S_k^*(t_{k+1}) = c_k^* \cdot p_1(0) + c_{k+1}^* \cdot p_2(0) + c_{k+2}^* \cdot p_2(1) + c_{k+3}^* \cdot p_1(1)$$

$$= 0.25\, c_{k+1}^* + c_{k+2}^* + 0.25\, c_{k+3}^*$$

$$S_{k+1}^*(t_{k+1}) = c_{k+1}^* \cdot p_1(1) + c_{k+2}^* \cdot p_2(1) + c_{k+3}^* \cdot p_2(0) + c_{k+4}^* \cdot p_1(0)$$

$$= 0.25\, c_{k+1}^* + c_{k+2}^* + 0.25\, c_{k+3}^*$$

Similarly, we may show that the first and second derivatives of the spline, $S^{*\prime}$ and $S^{*\prime\prime}$, are also continuous at the nodes. From equation (3.15):

$$(3.21)\quad p_1'(u) = 0.75\, u^2;\ p_1'(0) = 0,\ p_1'(1) = 0.75$$

$$p_2'(u) = 0.75\,(1 + 2u - 3u^2);\ p_2'(0) = 0.75,\ p_2'(1) = 0,\ \text{and}$$

$$(3.22)\quad p_1''(u) = 1.5u;\ p_1''(0) = 0,\ p_1''(1) = 1.5$$

$$p_2''(u) = 1.5\,(1 - 3u);\ p_2''(0) = 1.5,\ p_2''(1) = -3$$

Using notations similar to that in equation (3.19) and (3.20), and using equations (3.21) and (3.22), it follows that:

$$(3.23)\quad S_k^{*\prime}(t_{k+1}) = c_k^* \cdot p_1'(0) + c_{k+1}^* \cdot p_2'(0) + c_{k+2}^* \cdot p_2'(1) + c_{k+3}^* \cdot p_1'(1)$$

$$= 0.75\, c_{k+1}^* + 0.75\, c_{k+3}^*$$

$$S_{k+1}^{*\prime}(t_{k+1}) = c_{k+1}^* \cdot p_1'(1) + c_{k+2}^* \cdot p_2'(1) + c_{k+3}^* \cdot p_2'(0) + c_{k+4}^* \cdot p_1'(0)$$

$$= 0.75\, c_{k+1}^* + 0.75\, c_{k+3}^*\ ,\ \text{and}$$

$$(3.24)\quad S_k^{*\prime\prime}(t_{k+1}) = c_k^* \cdot p_1''(0) + c_{k+1}^* \cdot p_2''(0) + c_{k+2}^* \cdot p_2''(1) + c_{k+3}^* \cdot p_1''(1)$$

$$= 1.5\, c_{k+1}^* - 3\, c_{k+2}^* + 1.5\, c_{k+3}^*$$

$$S_{k+1}^{*\prime\prime}(t_{k+1}) = c_{k+1}^* \cdot p_1''(1) + c_{k+2}^* \cdot p_2''(1) + c_{k+3}^* \cdot p_2''(0) + c_{k+4}^* \cdot p_1''(0)$$

$$= 1.5\, c_{k+1}^* - 3\, c_{k+2}^* + 1.5\, c_{k+3}^*$$

which leads to:

$$S_k^{*\prime}(t_{k+1}) = S_{k+1}^{*\prime}(t_{k+1}) \quad , \text{ and} \tag{3.25}$$

$$S_k^{*\prime\prime}(t_{k+1}) = S_{k+1}^{*\prime\prime}(t_{k+1})$$

Finally, it can be shown that the polynomials q_k in equations (3.17) and (3.18) do satisfy the condition (Spath, 1974, page 58):

$$\det \begin{bmatrix} q_k(t_k) & q_{k+1}(t_k) & q_{k+2}(t_k) & q_{k+3}(t_k) \\ q_k(t_{k+1}) & q_{k+1}(t_{k+1}) & q_{k+2}(t_{k+1}) & q_{k+3}(t_{k+1}) \\ q_k'(t_k) & q_{k+1}'(t_k) & q_{k+2}'(t_k) & q_{k+3}'(t_k) \\ q_k'(t_{k+1}) & q_{k+1}'(t_{k+1}) & q_{k+2}'(t_{k+1}) & q_{k+3}'(t_{k+1}) \end{bmatrix} \neq 0 \tag{3.26}$$

$$k = 1, \ldots, n-1$$

because using equations (3.17), (3.18) and (3.21), equation (3.26) takes the following form:

$$\det \begin{bmatrix} p_1(1) & p_2(1) & p_2(0) & p_1(0) \\ p_1(0) & p_2(0) & p_2(1) & p_1(1) \\ p_1'(1) & p_2'(1) & p_2'(0) & p_1'(0) \\ p_1'(0) & p_2'(0) & p_2'(1) & p_1'(1) \end{bmatrix}$$

$$= \det \begin{bmatrix} 0.25 & 1 & 0.25 & 0 \\ 0 & 0.25 & 1 & 0.25 \\ 0.75 & 0 & 0.75 & 0 \\ 0 & 0.75 & 0 & 0.75 \end{bmatrix} \neq 0$$

Equation (3.16) using equations (3.12) to (3.15) is therefore a valid representation of the cubic spline (3.8). We now return to the solution of $(n+2)$ vector $\underline{c}^*$ from m linear equations (3.9) under the constraint (3.6). This was done by an algorithm given in Lawson and Hanson (1974, Chap. 27). It is known that there exists a $(m \times m)$ orthogonal (Householder's) matrix $\underline{\underline{Q}}$ such that if it multiplies from the left the augmented $(m \times (n+3))$ matrix $[\underline{\underline{A}} : \underline{\dot{R}}]$ of equation (3.9), the augmented matrix is decomposed into a $((n+2) \times (n+2))$ upper triangular matrix $\underline{\underline{R}}$ in the following form:

(3.27) $$ {}_m\underline{\underline{Q}}_m \; [\, {}_m\underline{\underline{A}}_{n+2} : {}_m\dot{\underline{R}}_1 \,] = \begin{bmatrix} {}_{n+2}\underline{\underline{R}}_{n+2} & : & {}_{n+2}\underline{d}_1 \\ {}_1\underline{0}_{n+2} & : & {}_1\ell_1 \\ {}_{m-n-3}\underline{0}_{n+2} & : & {}_{m-n-3}\underline{0}_1 \end{bmatrix} $$

and the upper triangular matrix $\underline{\underline{R}}$ retains the same bandwidth 4 as the matrix $\underline{\underline{A}}$. Further, the solution of (n + 2) linear equations:

(3.28) $$ {}_{n+2}\underline{\underline{R}}_{n+2} \;\; {}_{n+2}\underline{c}^*_1 = {}_{n+2}\underline{d}_1 $$

is the same as that of equation (3.9) under the constraint (3.6), and the euclidean or L_2 norm of the residual vector $\underline{r}$ is given by ℓ of equation (3.27), i.e.,

(3.29) $$ \| \underline{r} \|_2 = \| \dot{\underline{R}} - \underline{\underline{A}} \, \underline{c}^* \|_2 = \ell $$

The solution of $\underline{c}^*$ in equation (3.28) is straightforward by back substitution as R is upper triangular. We therefore transform the observation equations (3.9) directly by the QR decomposition into equations (3.28), and the formation of normal equations and the inversion of normals matrix is avoided. Further, as there are only five non-zero elements in the augmented matrices $[\underline{\underline{A}} : \dot{\underline{R}}]$ and $[\underline{\underline{R}} : \underline{d}]$ in equation (3.27), we only need an array (m x 5) in the storage. The Lawson-Hanson algorithm (ibid, 1974) processes the observations sequentially in this array according to equation (3.27), with all observations in the interval I_k being processed at a time.

Specifically, the matrix $\underline{\underline{Q}}$ is a product of (n + 3) orthogonal (m x m) Householder's transformation matrices $\underline{\underline{Q}}_j$:

(3.30) $$ \underline{\underline{Q}} = \underline{\underline{Q}}_{n+3} \; \underline{\underline{Q}}_{n+2} \cdots \underline{\underline{Q}}_{j+1} \; \underline{\underline{Q}}_j \cdots \underline{\underline{Q}}_2 \; \underline{\underline{Q}}_1 $$

which reduce the column vectors $\underline{v}_j$; j = 1, ..., n + 3 of the augmented matrix $[\underline{\underline{A}} : \dot{\underline{R}}]$ to 0 below the diagonal. The matrix $\underline{\underline{Q}}_j$ are computed by:

(3.31) $$ \underline{\underline{Q}}_j = \underline{\underline{I}}_m - 2 \; \underline{v}_j \; \underline{v}_j^T / (\underline{v}_j^T \; \underline{v}_j) $$

where $\underline{\underline{I}}_m$ is the (m x m) unit matrix and vector $\underline{v}_j^T$ is the transpose of vector $\underline{v}_j$.

3.2 Filtering and Smoothing of Raw $\dot{R}$ Data

The spline in equation (3.16) filters the given raw data $\underline{\dot{R}}$ in the least squares sense. It also smooths the raw data depending on the spacing of nodes in equation (3.12), or analogously depending on the number of nodes in equation (3.1). For a given number of data points m, if the number of nodes n = m - 2, we get the interpolating spline. But as n is reduced, i.e. the spacing of nodes is increased, we get a smoother representation of the data. It is important to choose a suitable spacing of the nodes, particularly if $S^{*\prime}(t)$ is of interest, as the slope of the fitted spline is sensitive to the smoothing of the data. Inadequate smoothing will give large and 'noisy' slope values, while over-smoothing will dampen them out. We now describe these experiments with different spacing of nodes in respect to residual range-rate ($\dot{R}$) data. The spacing of nodes was kept uniformly as 30, 40, 60, 80 or 100 seconds.

We first consider the range-rate sum observations in revolutions 154 and 453 described in Section 2.1. We deduct from these the computed value of range-rate sum in the gravitational field of (12, 12) potential coefficients out of GEM-7 (Wagner et al., 1976), with the initial state vectors kept fixed at the values given in Table 2.1. We consider these residual range-rate $\dot{R}$ values as the raw data. We fit splines in the least squares sense to this raw data at 10 seconds interval using equation (3.16) over a 20 minute period, i. e. 121 raw data points. The 20 minute period was chosen to straddle the observations over the area of investigations centrally. With 121 raw data points, and with the condition in equation (3.11), the spacing of nodes at any of the values 30, 40, 60, 80 or 100 seconds ensured that the spline nodes were always coincident with the location of some data points.

We give in Table 3.1 for each nodal spacing the RMS values in cm/sec of raw data, smoothed data, residuals after spline fit (= smoothed - raw data) and also the total number of residuals out of 121 points, which had an absolute value larger than an arbitrary value of 0.1 cm/sec.

A plot of raw and smooth data corresponding to nodal spacing of 40, 60 and 80 seconds is shown in Figures 3.1 to 3.3 for revolution 154, and in Figures 3.4 to 3.6 for revolution 453. From Table 3.1, as well as Figures 3.1 to 3.6, we note greater smoothing of data with increased spacing of nodes. We note that the outlying data points have a lesser effect on the shape of the spline as the spacing of spline nodes is increased. This may be seen particularly for a large positive data point in the center of Figures 3.1 to 3.3, and for a negative data point to the left in Figures 3.4 to 3.6. The least squares nature of fit is seen clearly in Figures 3.7 and 3.8, showing the plot of residuals after spline fit at nodal spacing of 60 seconds for revolutions 154 and 453 respectively. The RMS value of residuals (filtering) does not show large changes in Table 3.1, but the slopes (smoothing) of the fitted splines get smoother (Figures 3.1 to 3.6).

Table 3.1 Least Squares Spline Fit to Raw $\dot{R}$ Data Showing RMS Values in cm/sec

Spacing of Nodes (sec.) (1)	Revolution 154				Revolution 453			
	Raw Data (2)	Smoothed Data (3)	Residuals (4) = (3) - (2)	# of Large Residuals	Raw Data (6)	Smoothed Data (7)	Residuals (8) = (7) - (6)	# of Large Residuals
30	0.2321	0.2211	0.0708	11	0.4389	0.4347	0.0604	13
40	0.2321	0.2201	0.0738	13	0.4389	0.4339	0.0659	11
60	0.2321	0.2167	0.0833	16	0.4389	0.4333	0.0695	14
80	0.2321	0.2151	0.0874	17	0.4389	0.4328	0.0725	17
100	0.2321	0.2144	0.0891	22	0.4389	0.4324	0.0750	20
Mean value in all cases	-0.0943	-0.0943	0.0000		0.4096	0.4096	0.000	

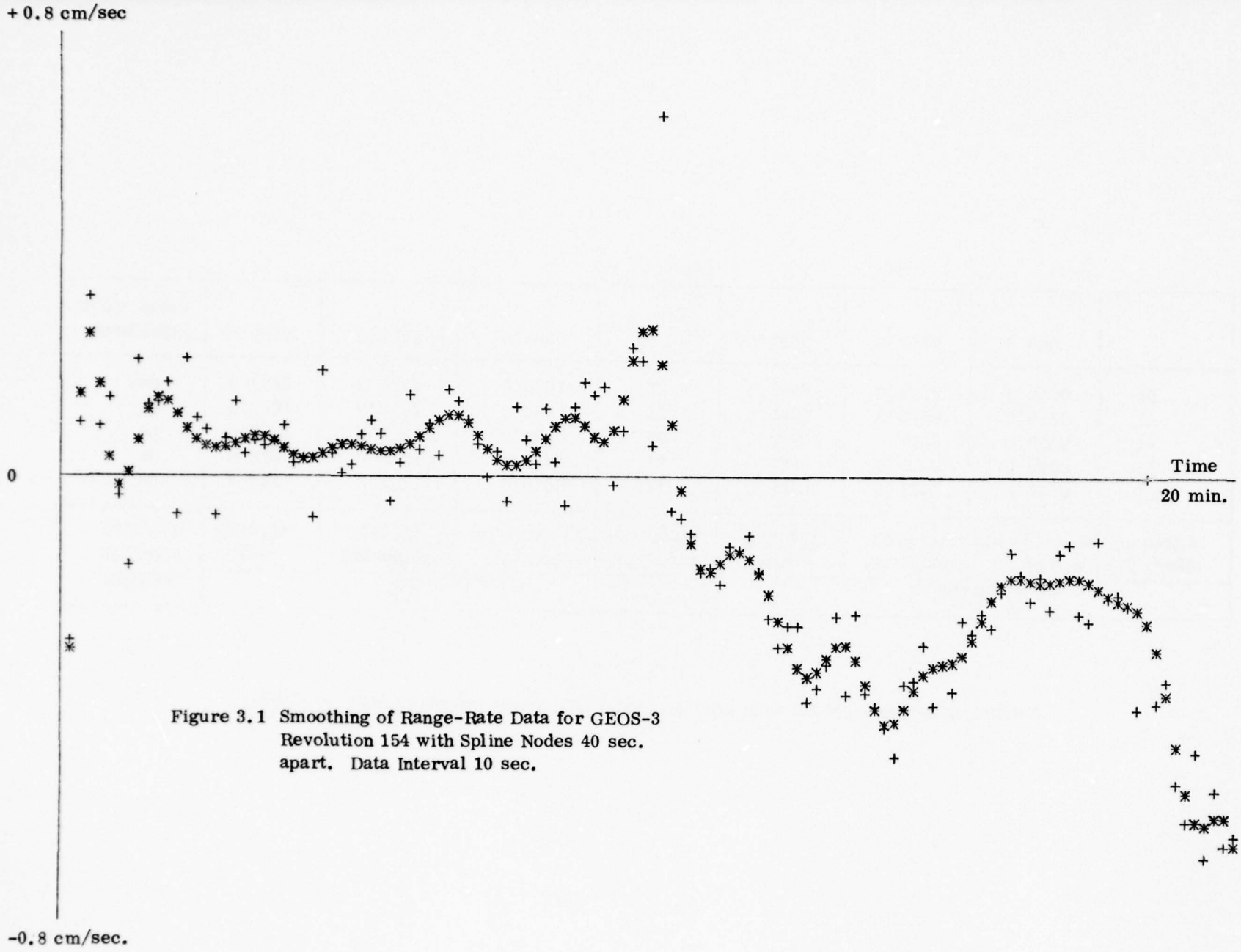

Figure 3.1 Smoothing of Range-Rate Data for GEOS-3 Revolution 154 with Spline Nodes 40 sec. apart. Data Interval 10 sec.

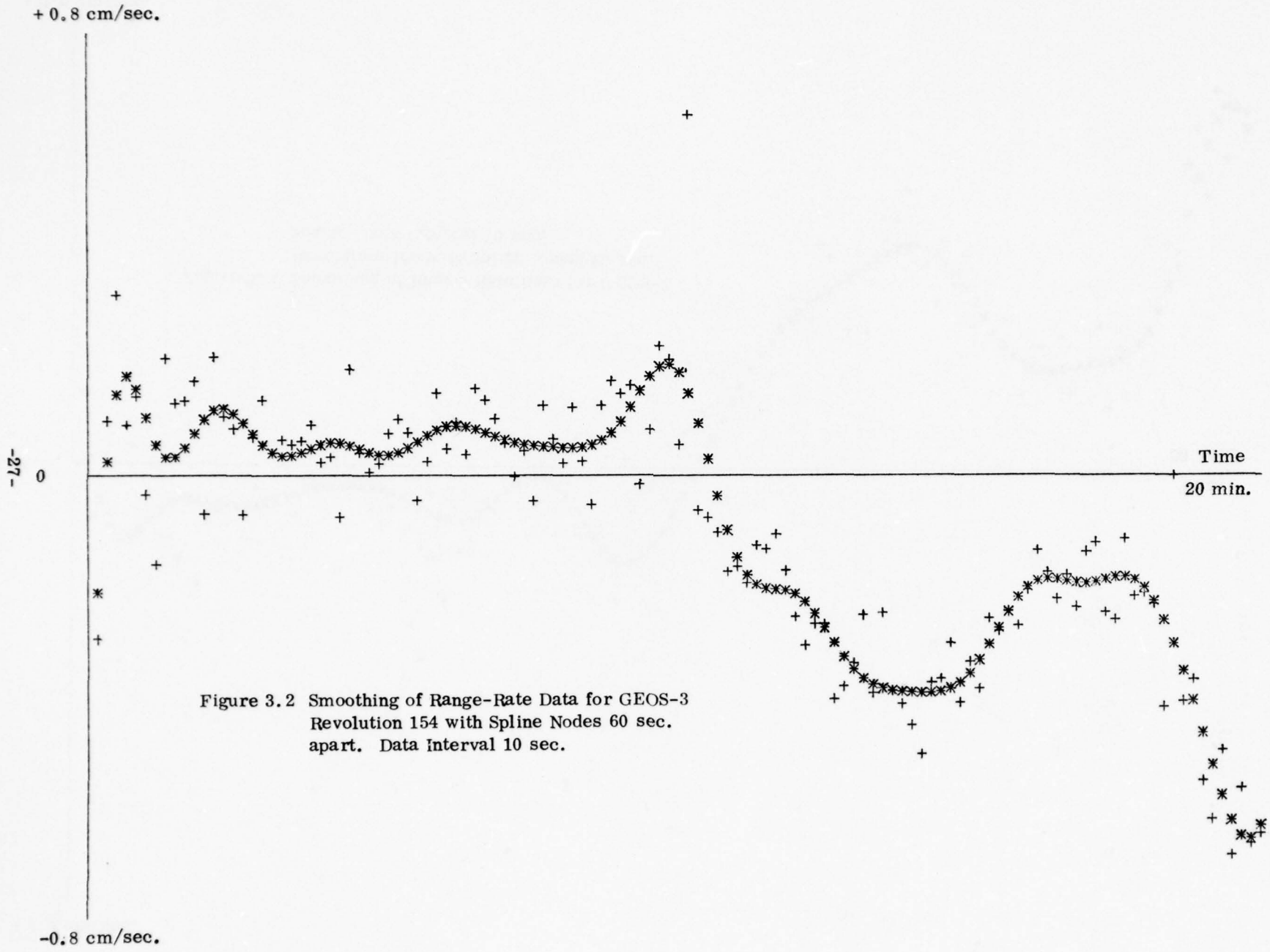

Figure 3.2 Smoothing of Range-Rate Data for GEOS-3 Revolution 154 with Spline Nodes 60 sec. apart. Data Interval 10 sec.

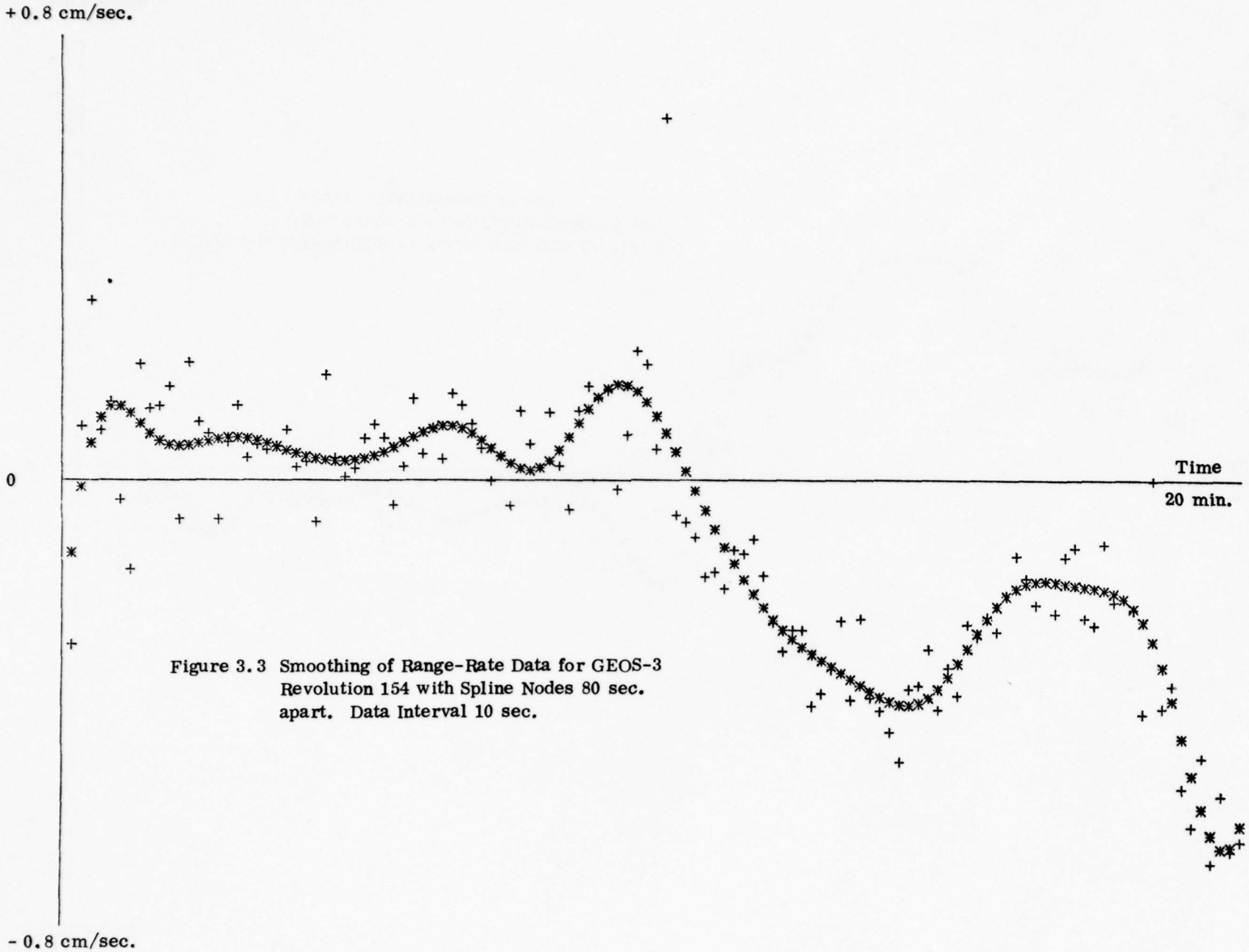

Figure 3.3 Smoothing of Range-Rate Data for GEOS-3 Revolution 154 with Spline Nodes 80 sec. apart. Data Interval 10 sec.

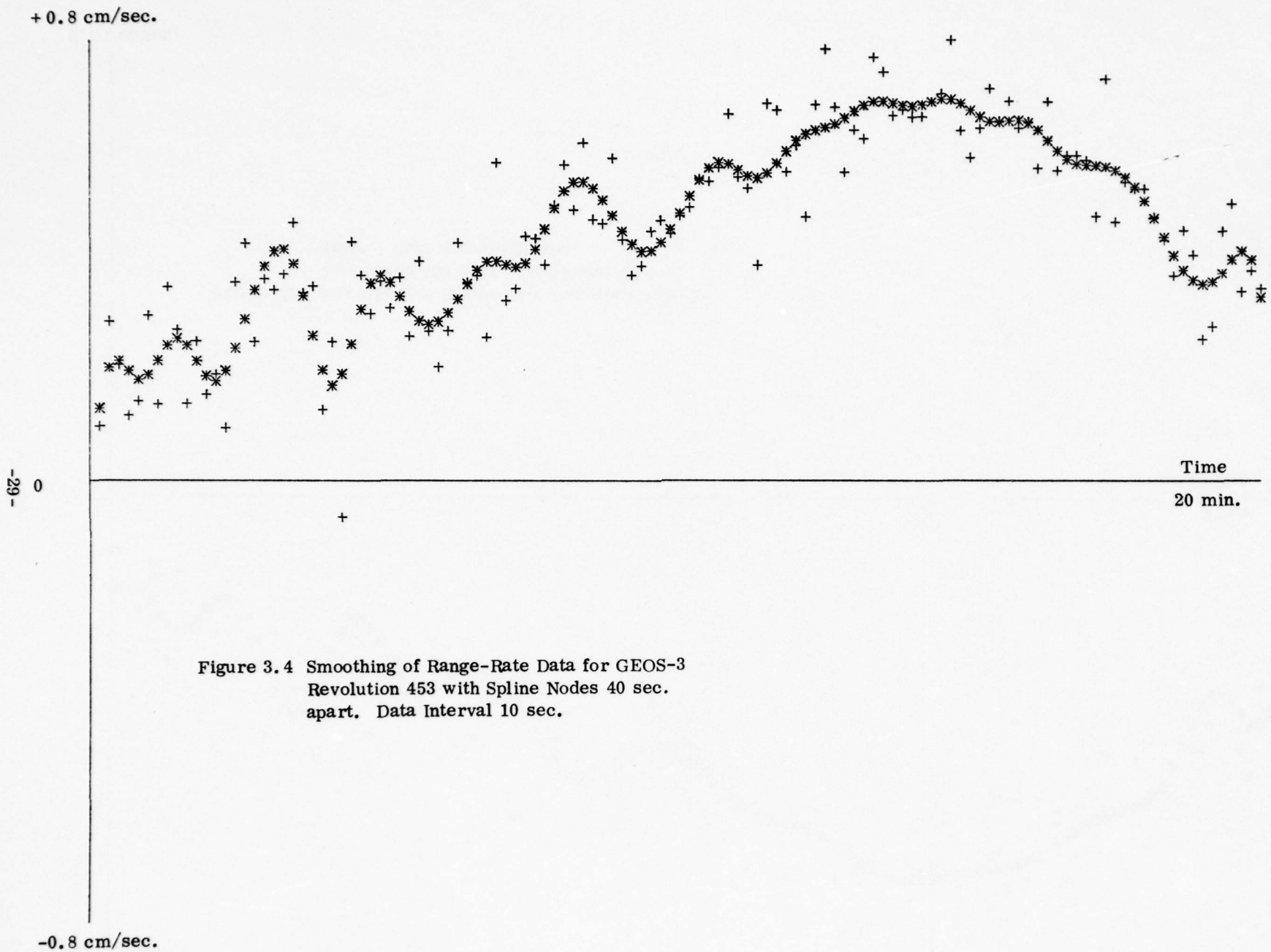

Figure 3.4 Smoothing of Range-Rate Data for GEOS-3 Revolution 453 with Spline Nodes 40 sec. apart. Data Interval 10 sec.

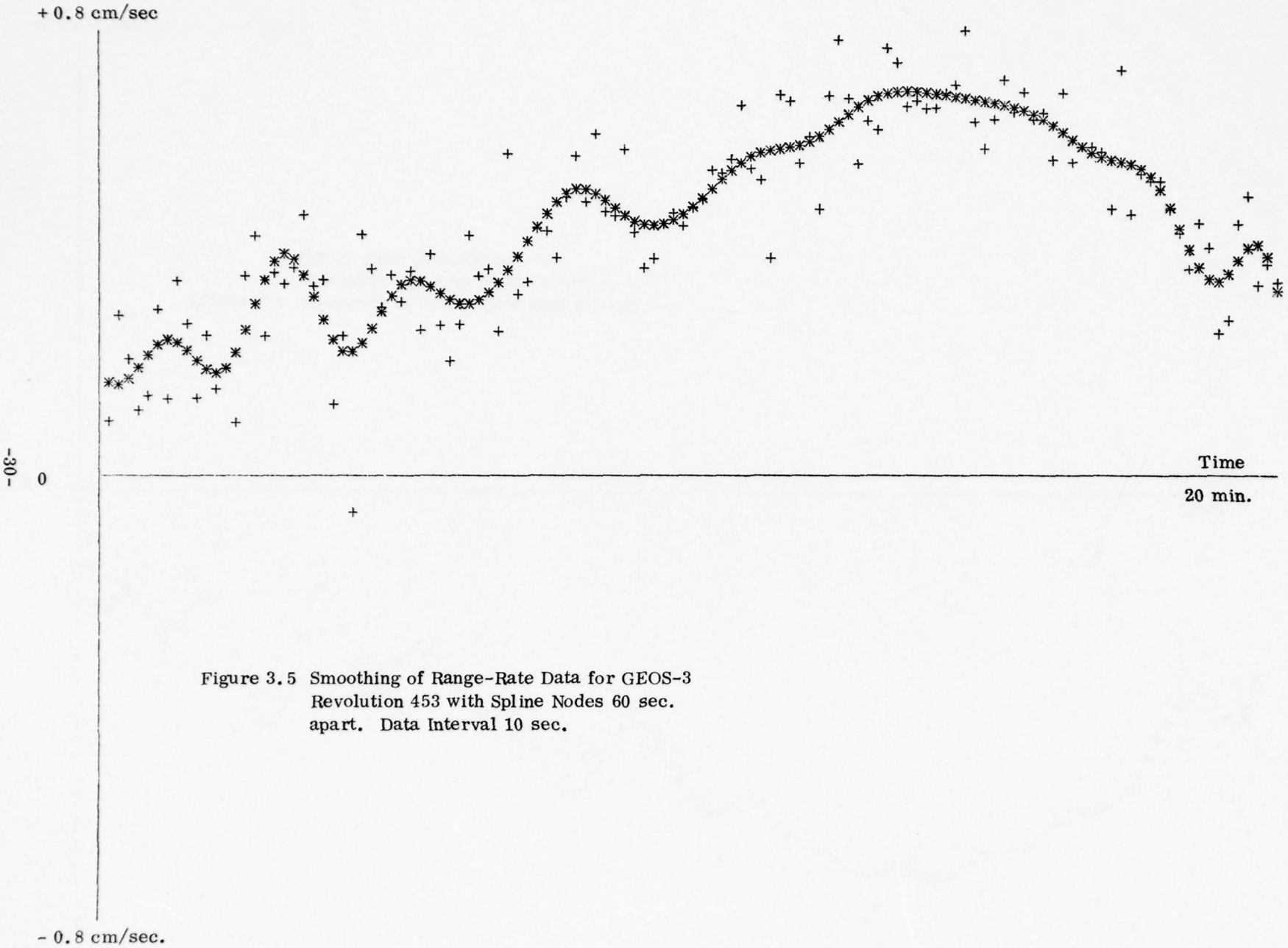

Figure 3.5 Smoothing of Range-Rate Data for GEOS-3 Revolution 453 with Spline Nodes 60 sec. apart. Data Interval 10 sec.

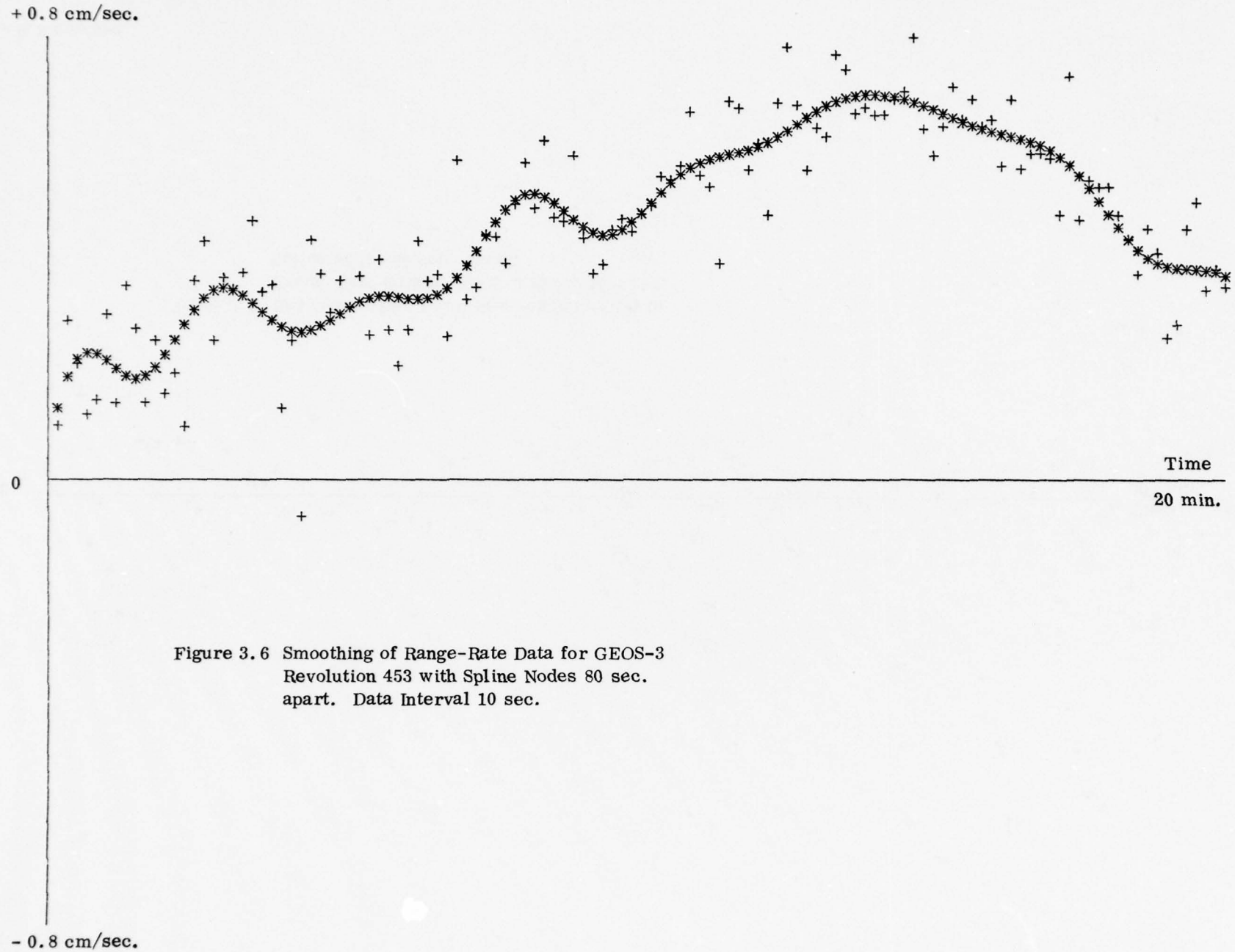

Figure 3.6 Smoothing of Range-Rate Data for GEOS-3 Revolution 453 with Spline Nodes 80 sec. apart. Data Interval 10 sec.

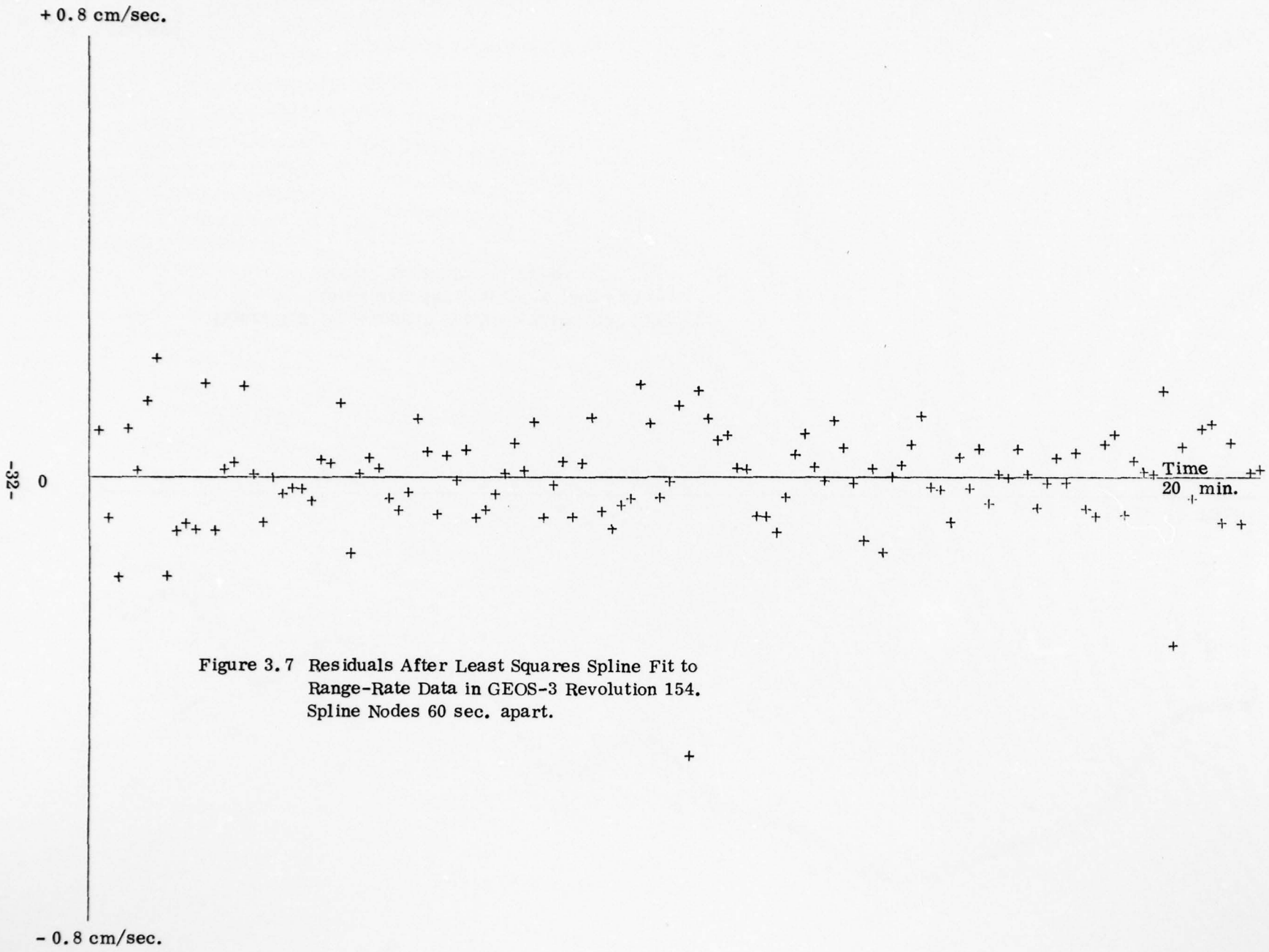

Figure 3.7 Residuals After Least Squares Spline Fit to Range-Rate Data in GEOS-3 Revolution 154. Spline Nodes 60 sec. apart.

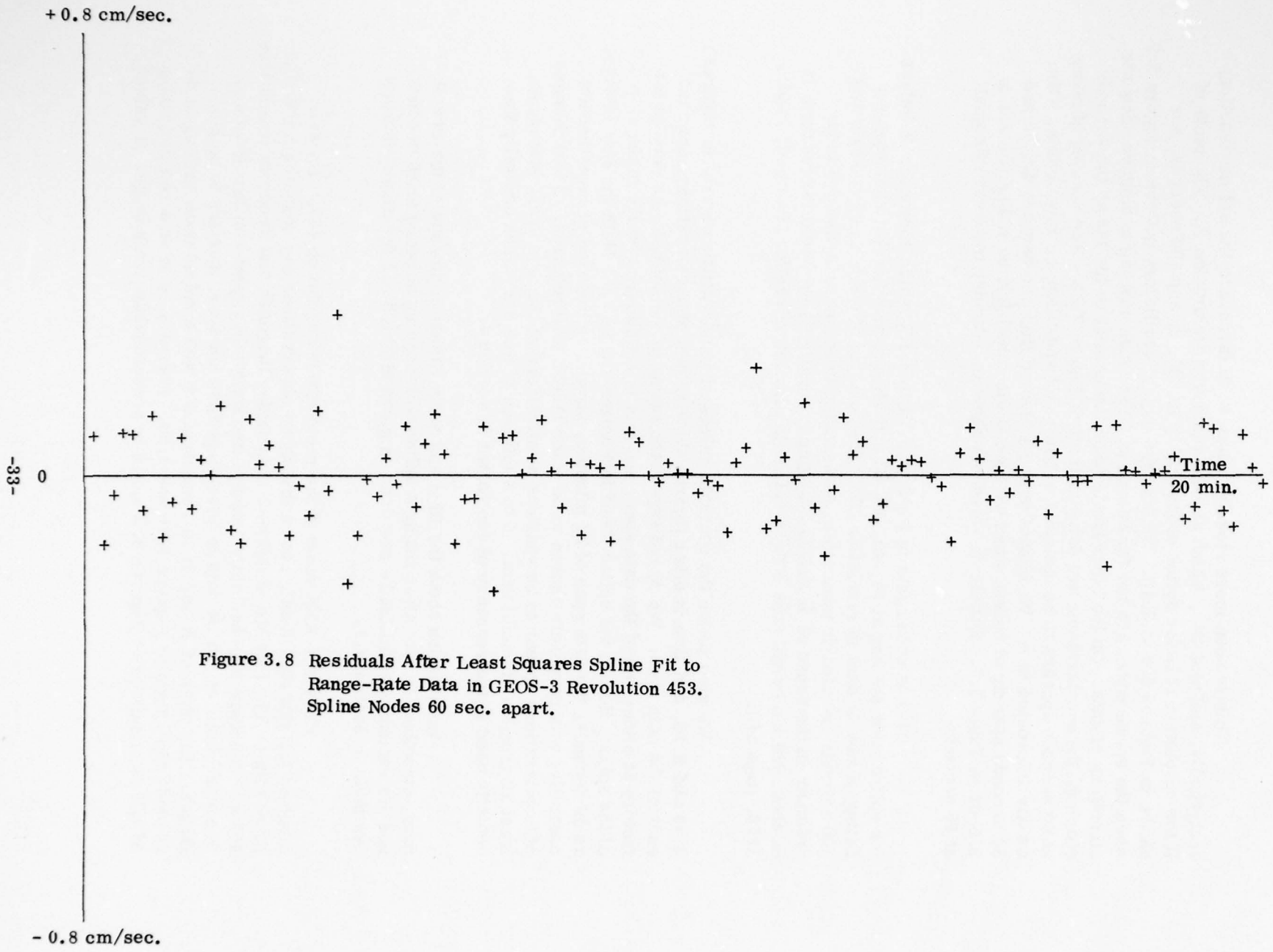

Figure 3.8 Residuals After Least Squares Spline Fit to Range-Rate Data in GEOS-3 Revolution 453. Spline Nodes 60 sec. apart.

This is seen more clearly, when we differentiate the spline (function) analytically, and plot $S^{*'}$, which are the residual acceleration $\ddot{R}$. The plots of $\ddot{R}$ for revolution 154, for spline nodes at 30, 40, 60, 80 and 100 seconds, are shown in Figures 3.9 to 3.13. We note the 'noisy' oscillatory pattern in Figure 3.9 when the spline nodes are not far enough at 30 seconds spacing to achieve adequate smoothing of data. On the other hand, when the nodes are too far at 100 seconds spacing, the accelerations are dampened off in Figure 3.13. The spacing of nodes at 60 seconds appears to be optimum to filter and smoothen the raw $\dot{R}$ data, when we are interested in $\ddot{R}$. We cannot notice a clear difference between 40, 60 and 80 seconds spacing of nodes, when we look at smoothed $\dot{R}$ data in Figures 3.1 to 3.6 or in Table 3.1. But the $\ddot{R}$ values do show an optimum recovery of signal at 60 seconds.

This is seen again in Figures 3.14 to 3.18, which shown the $\ddot{R}$ values for spline node spacing at 30, 40, 60, 80 and 100 seconds for the least squares fitting of raw $\dot{R}$ data in revolution 453. The spacing of nodes at 30 seconds and 100 seconds are clearly unsuitable, and spacing of 60 seconds appears to be optimum in the sense of $\ddot{R}$ values changing gradually as we would expect them to at about 850 km height (see $\partial T/\partial r$ values in simulation studies (Rummel, et al., 1976, page 54)).

We also notice the spurious values of accelerations clearly in Figures 3.11 and 3.16, and also in other figures showing plot of accelerations, near the ends of the data span. We do not expect the fitting of the spline to be very satisfactory at either end of the data span, and this is seen more clearly in the slopes of the spline, than in the spline itself in Figures 3.1 to 3.6. With the data interval as 10 seconds, the data span of 20 minutes, straddling the area of investigation centrally, was purposely chosen to be much larger than required. 2 to 4 minutes of accelerations appear to be spurious at either end of the data span, leaving at least 12 minutes of useful data. 6 to 8 minutes of this data taken centrally was actually used in the recovery of anomalies in Section 4.

Information about the RMS and mean values in cm/sec of the raw $\dot{R}$ data, smoothed $\dot{R}$ data after fitting a spline with spacing of nodes at 60 seconds, and the residuals (smoothed - raw data) is given in Table 3.2 for all revolutions available in Section 2.1.

The large RMS value of the residuals in revolution 467, almost as large as the raw data itself, shows that these observations are unusable for further processing. The location of GEOS-3 in latitude, longitude and height in revolutions 467 and 268 were matched quite closely, and we would expect similar $\dot{R}$ values. The RMS value of raw $\dot{R}$ data in revolution 268, however, appears to be much larger. The plots of $\dot{R}$ and $\ddot{R}$ in revolution 268 with a spline node spacing of 60 seconds are shown in Figures 3.19 and 3.20. Figure 3.19 is on a reduced scale of 1/3 as compared to Figures 3.1 to 3.6 to accommodate much larger $\dot{R}$ values.

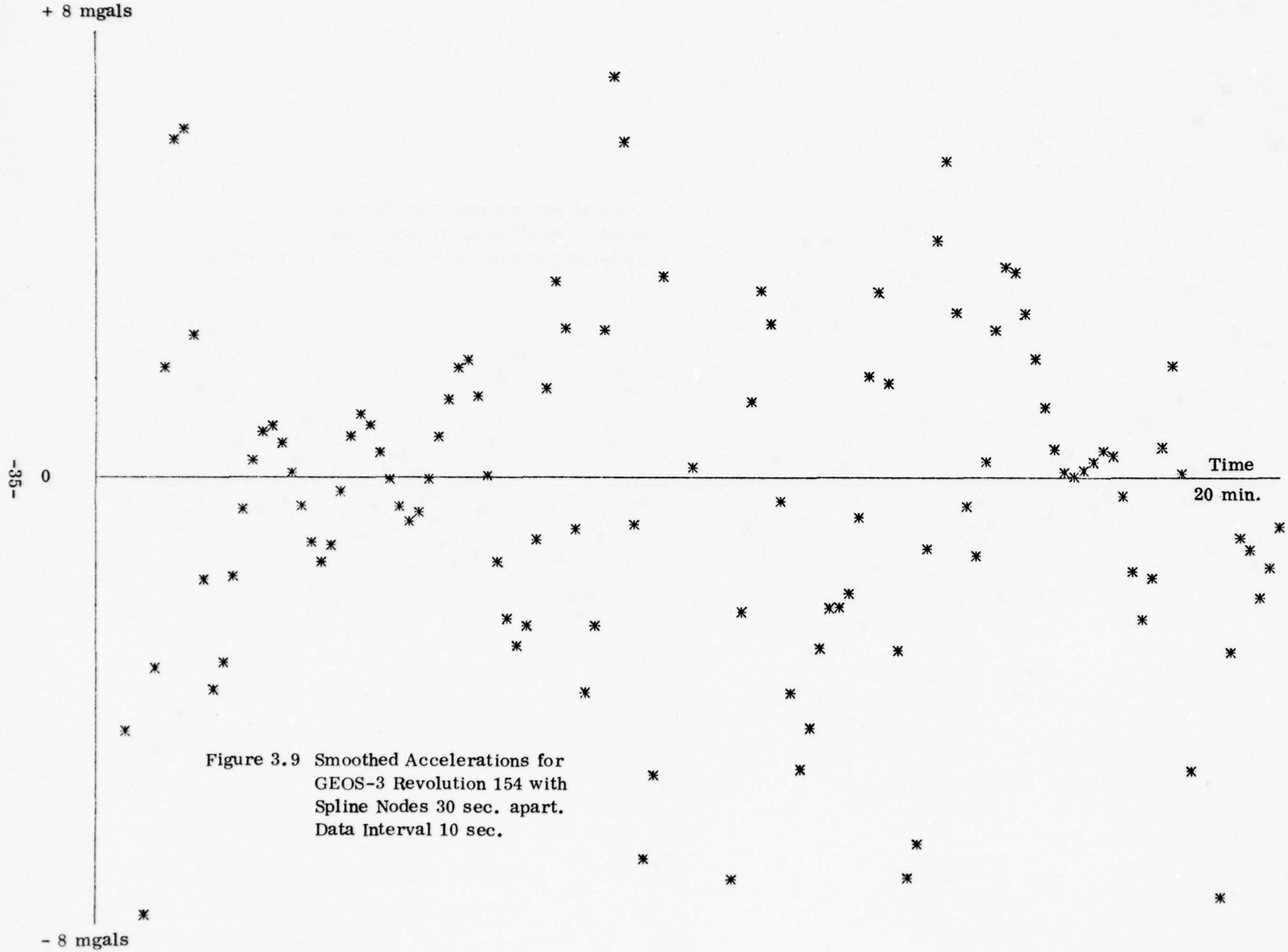

Figure 3.9 Smoothed Accelerations for GEOS-3 Revolution 154 with Spline Nodes 30 sec. apart. Data Interval 10 sec.

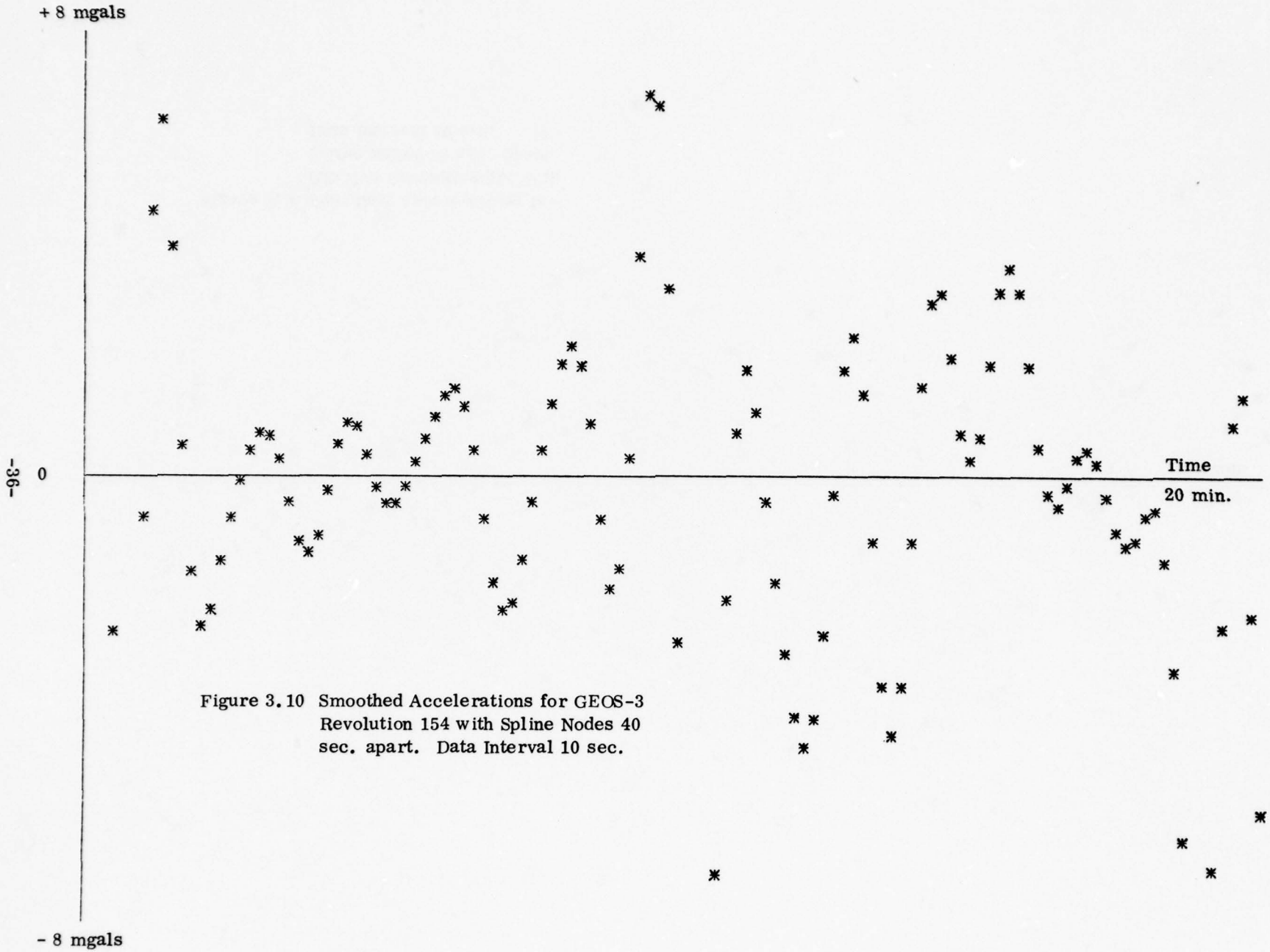

Figure 3.10 Smoothed Accelerations for GEOS-3 Revolution 154 with Spline Nodes 40 sec. apart. Data Interval 10 sec.

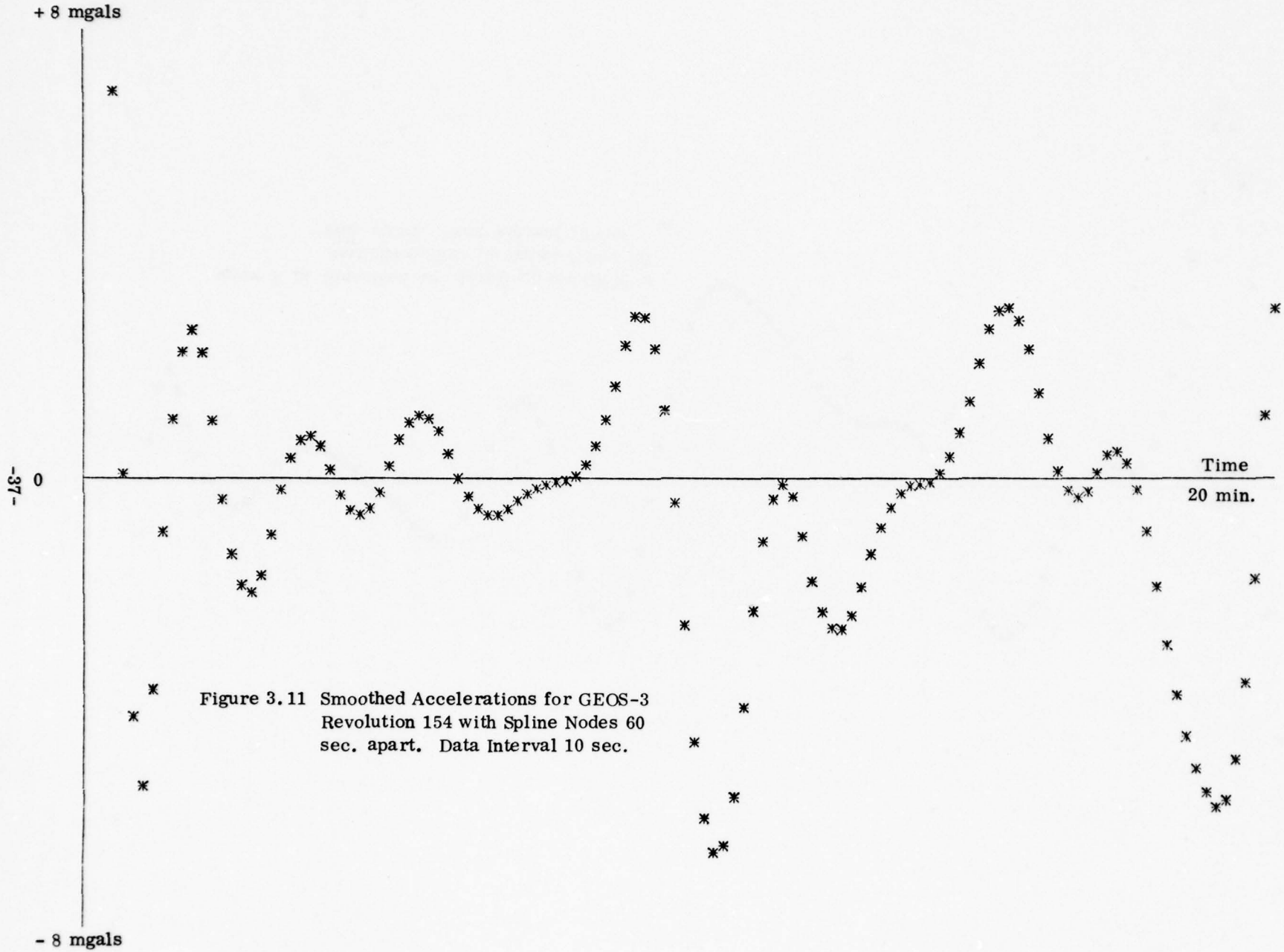

Figure 3.11 Smoothed Accelerations for GEOS-3 Revolution 154 with Spline Nodes 60 sec. apart. Data Interval 10 sec.

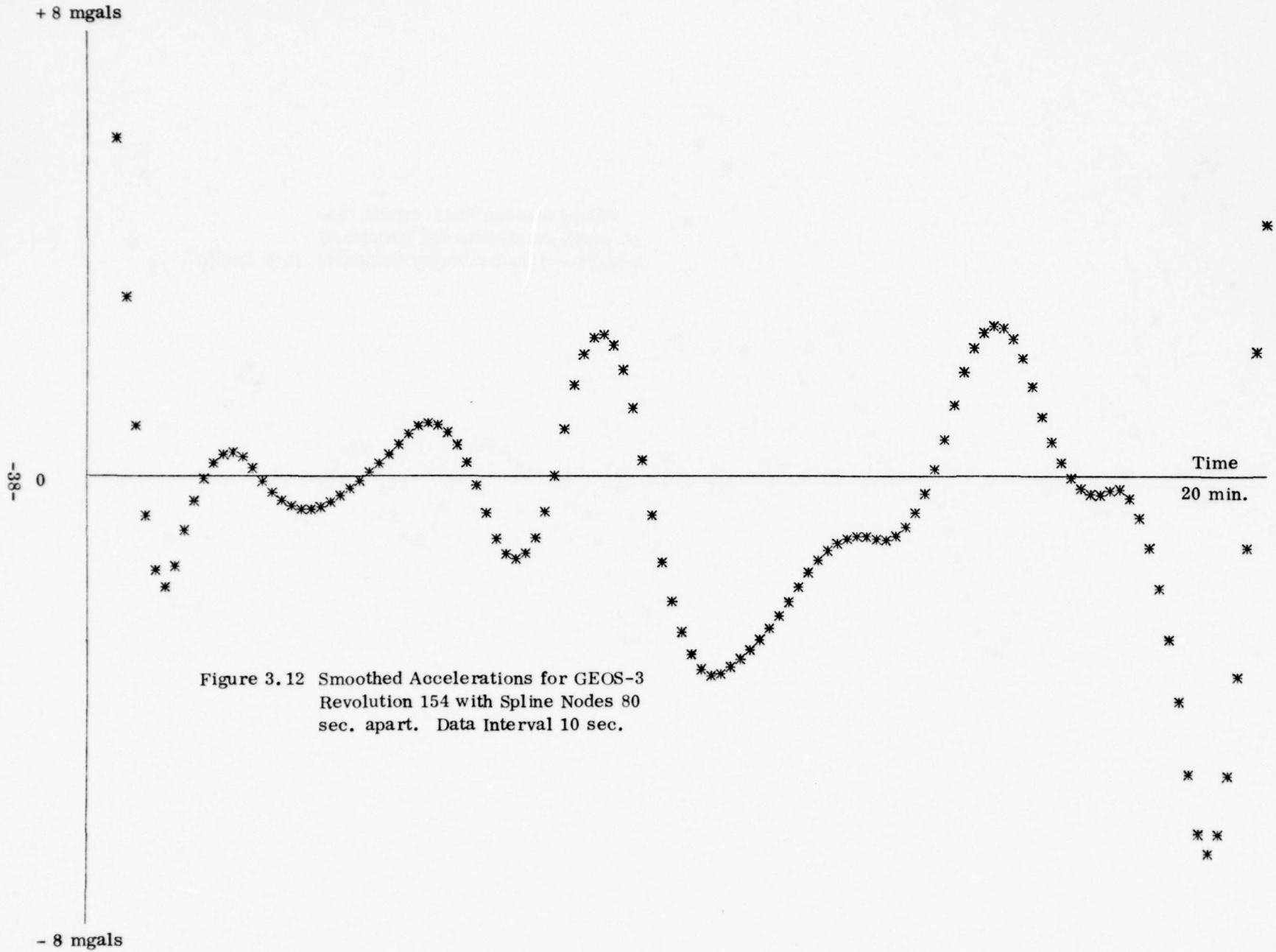

Figure 3.12 Smoothed Accelerations for GEOS-3 Revolution 154 with Spline Nodes 80 sec. apart. Data Interval 10 sec.

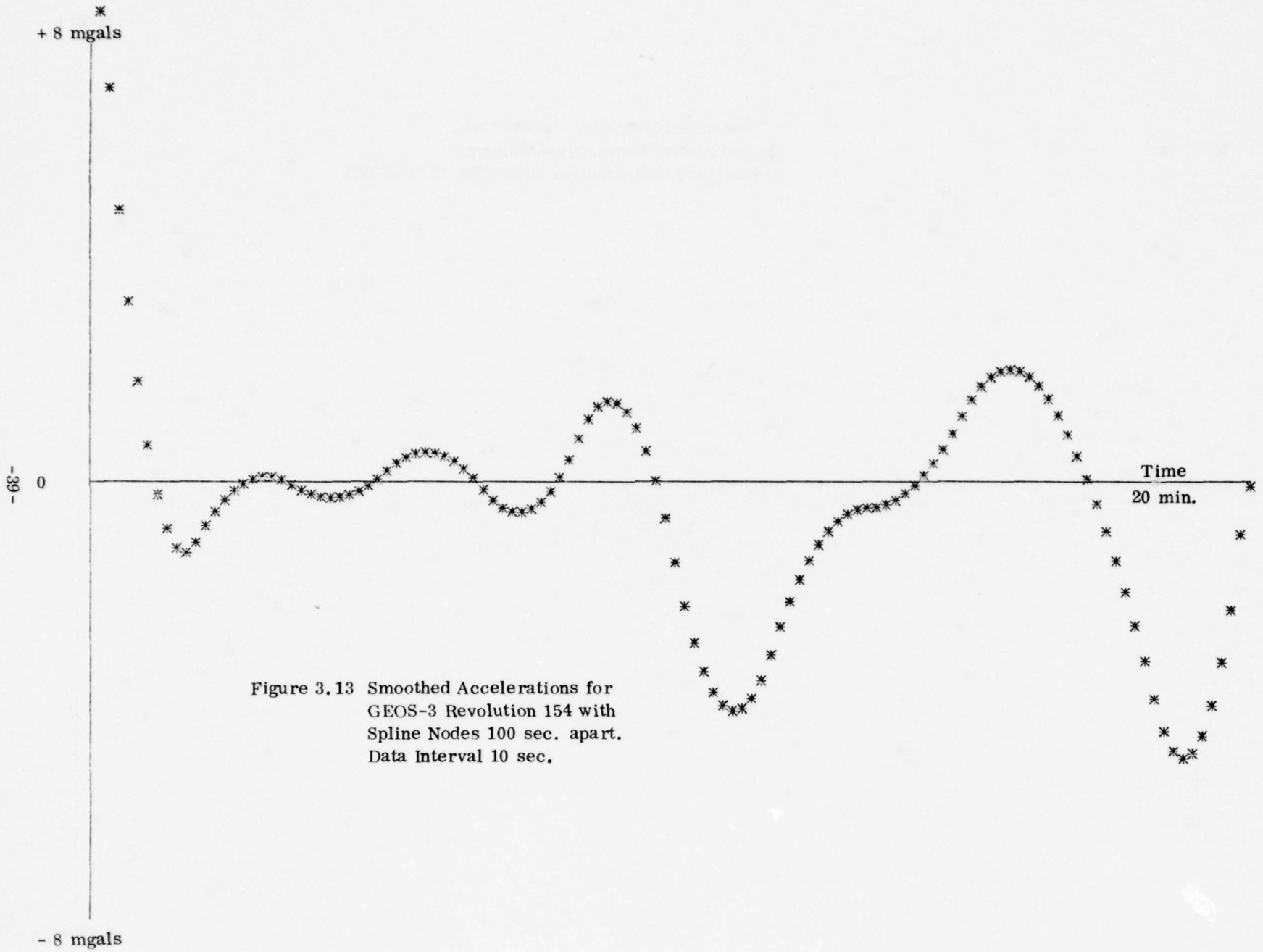

Figure 3.13 Smoothed Accelerations for GEOS-3 Revolution 154 with Spline Nodes 100 sec. apart. Data Interval 10 sec.

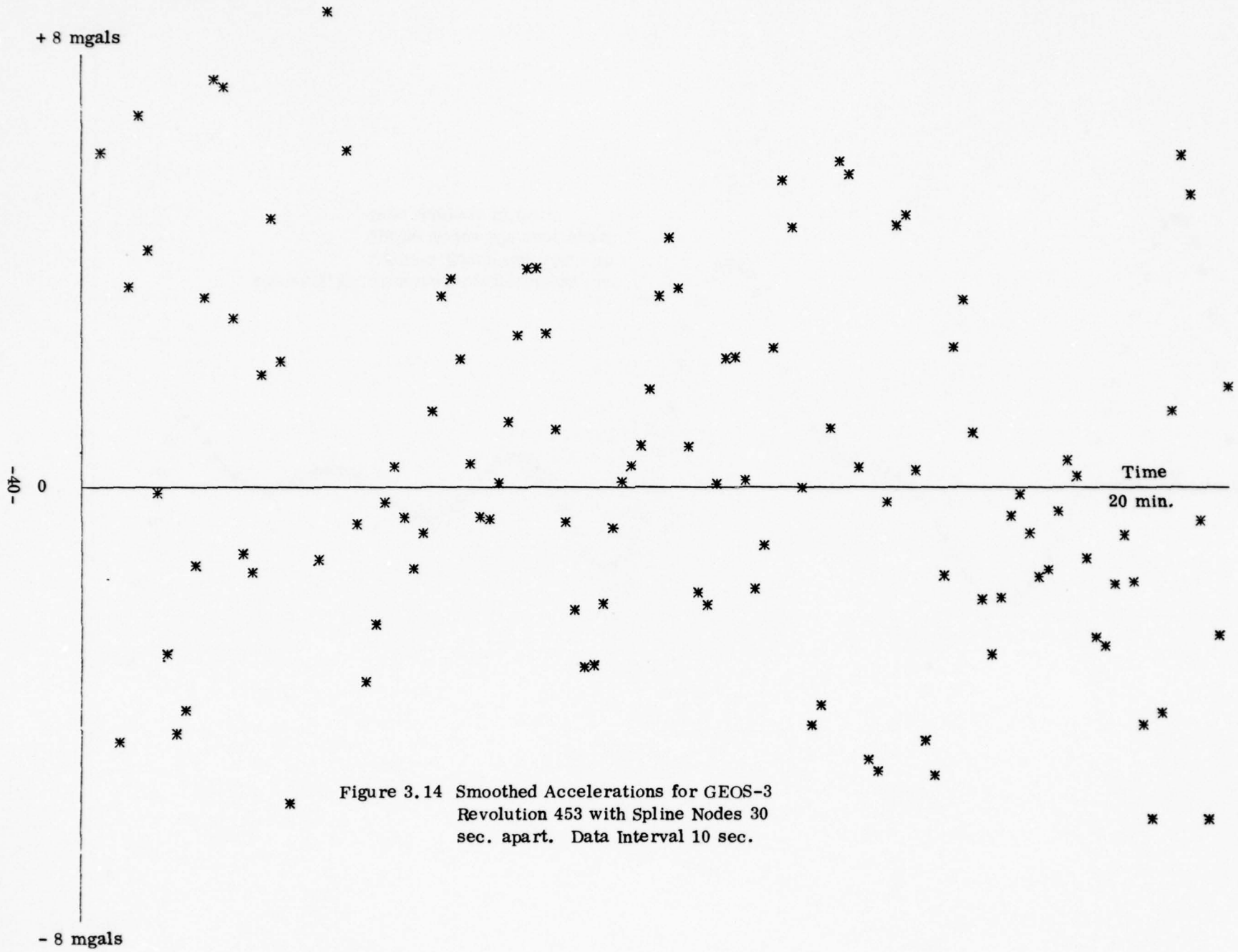

Figure 3.14 Smoothed Accelerations for GEOS-3 Revolution 453 with Spline Nodes 30 sec. apart. Data Interval 10 sec.

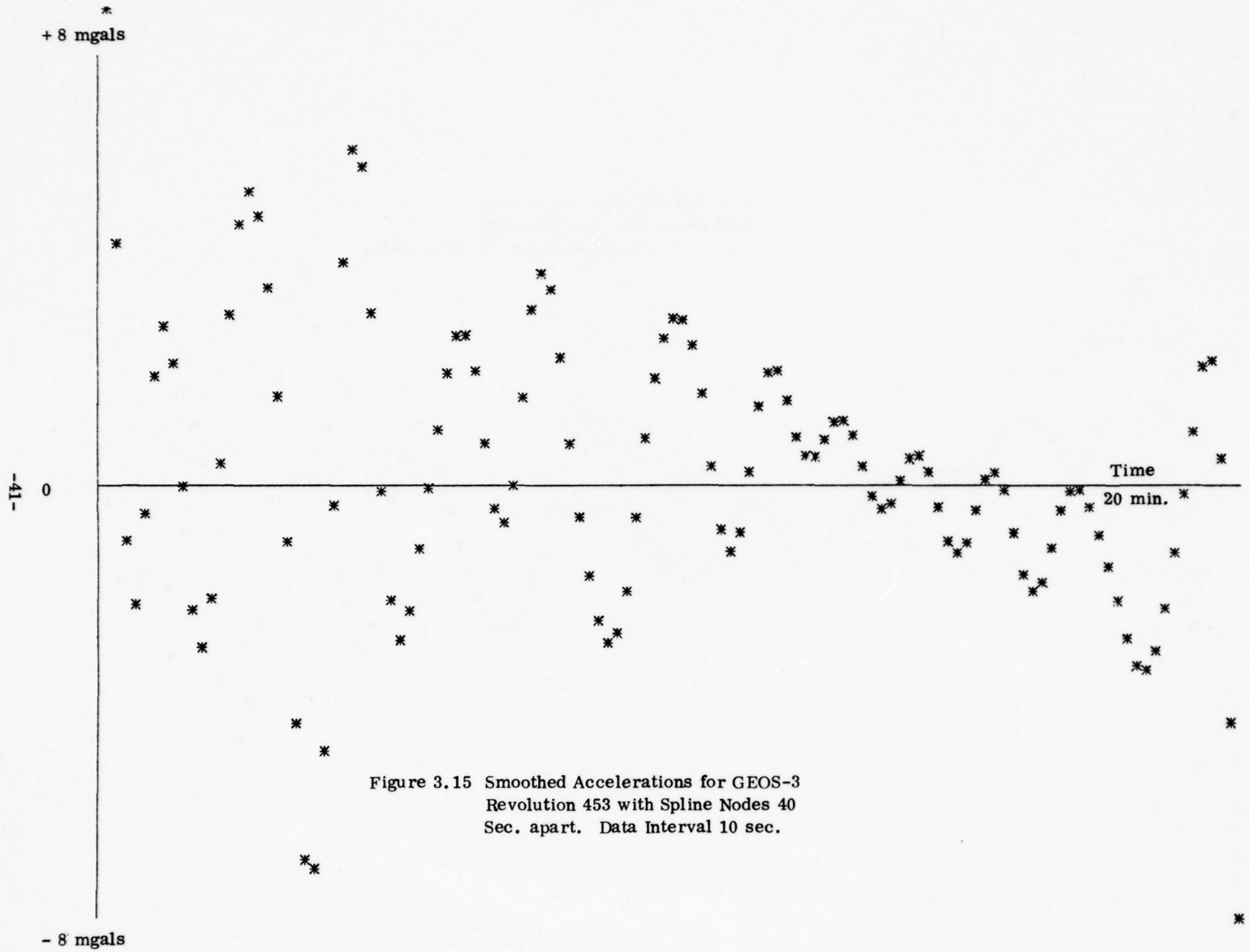

Figure 3.15 Smoothed Accelerations for GEOS-3 Revolution 453 with Spline Nodes 40 Sec. apart. Data Interval 10 sec.

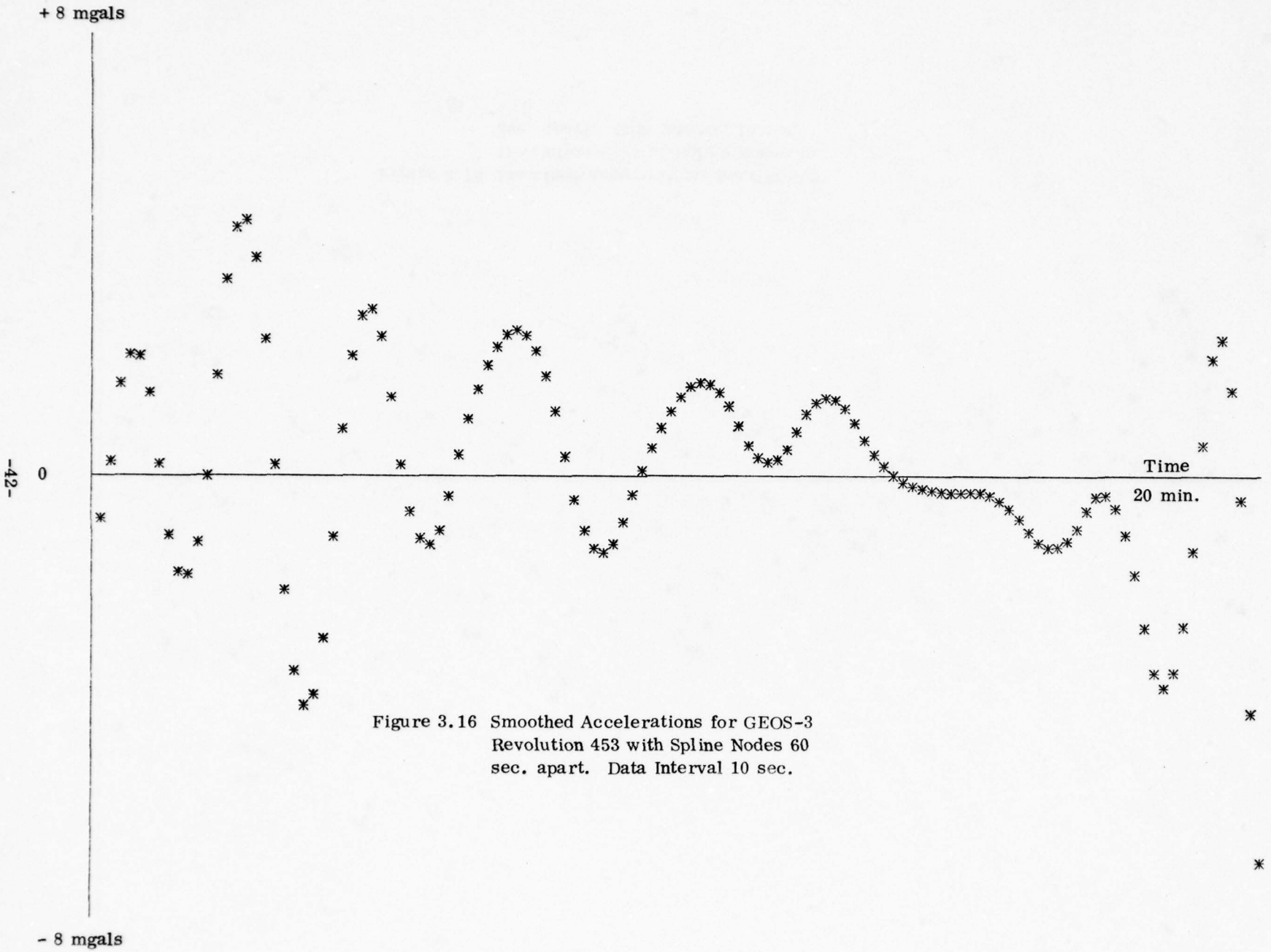

Figure 3.16 Smoothed Accelerations for GEOS-3 Revolution 453 with Spline Nodes 60 sec. apart. Data Interval 10 sec.

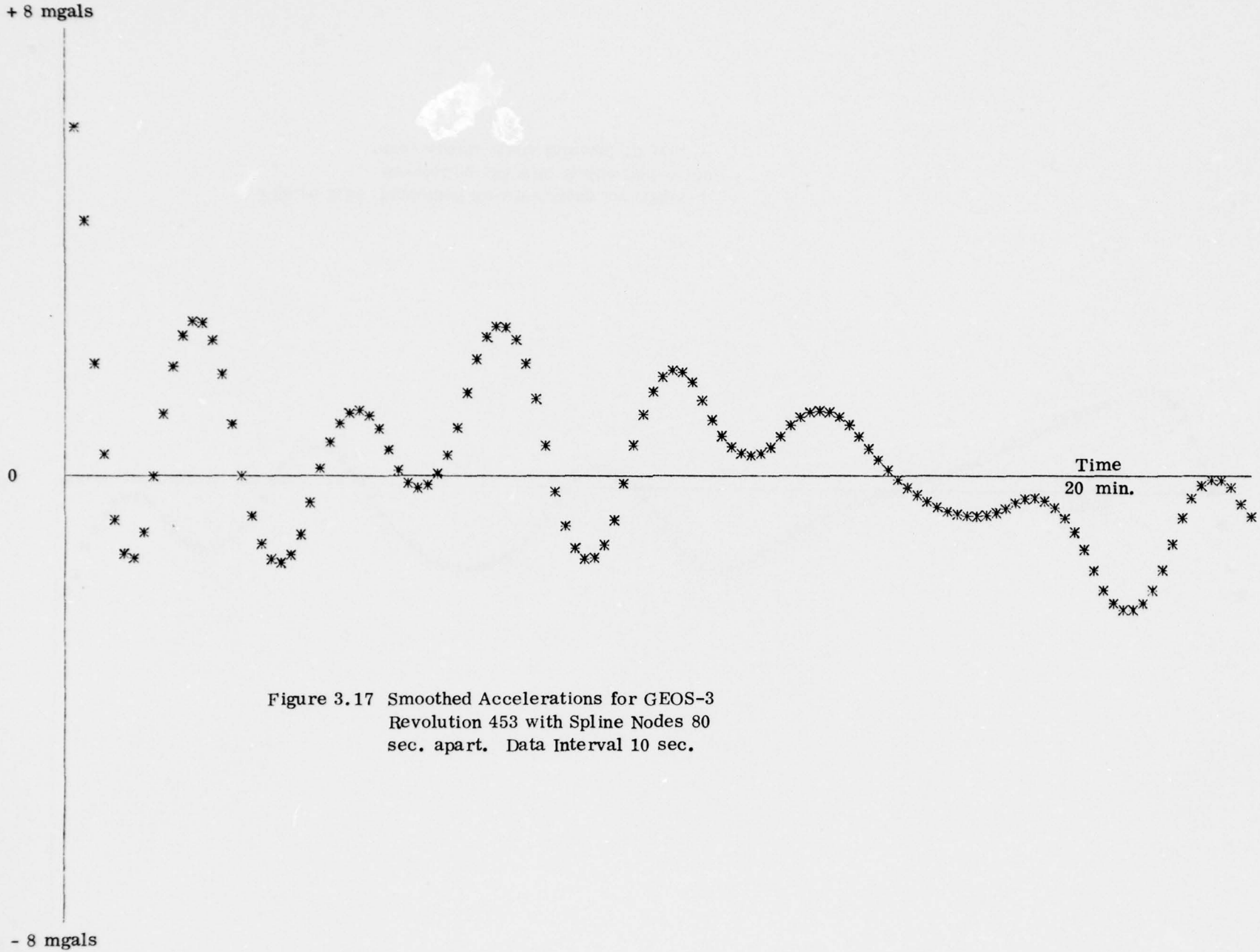

Figure 3.17 Smoothed Accelerations for GEOS-3 Revolution 453 with Spline Nodes 80 sec. apart. Data Interval 10 sec.

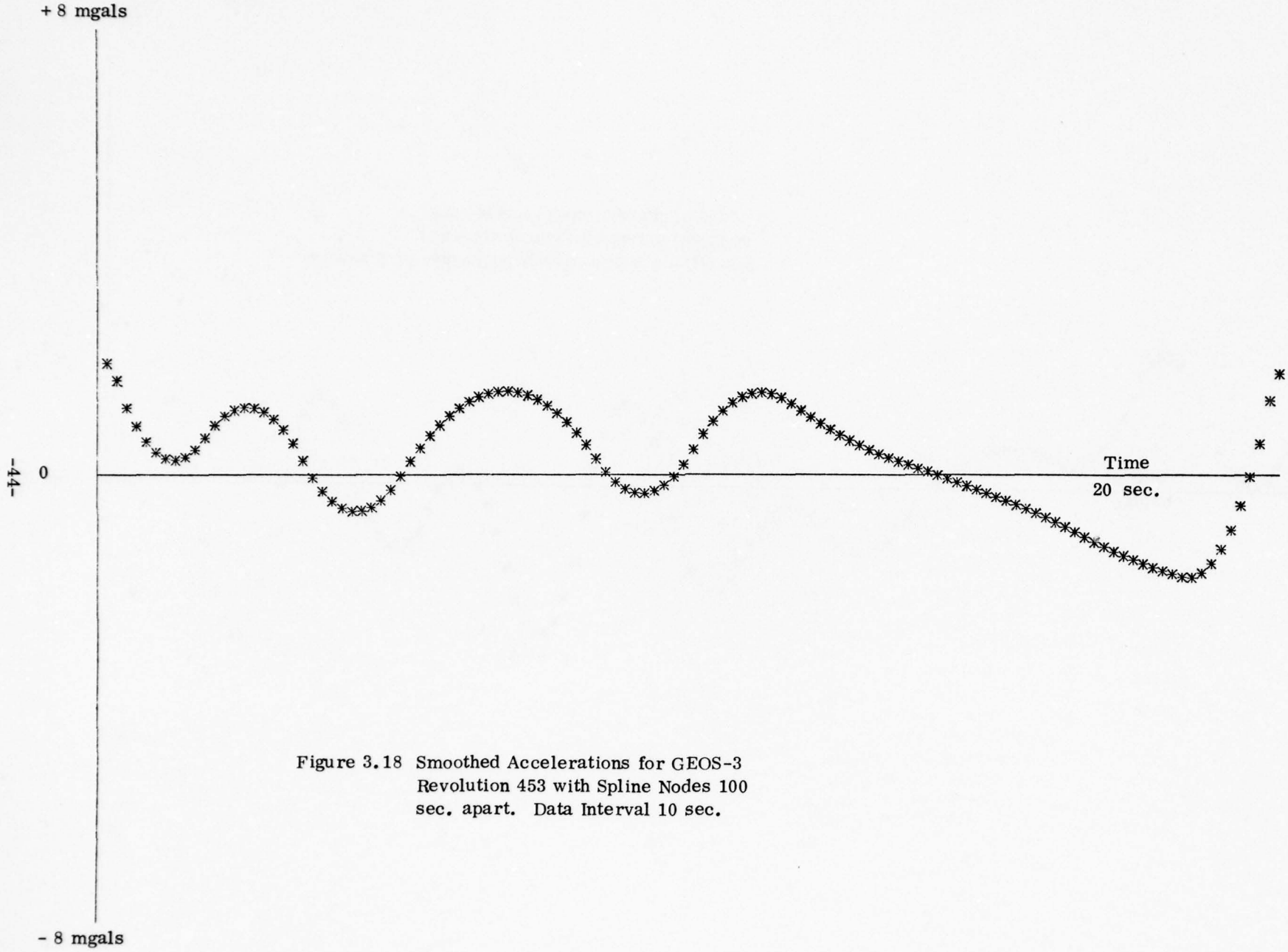

Figure 3.18 Smoothed Accelerations for GEOS-3 Revolution 453 with Spline Nodes 100 sec. apart. Data Interval 10 sec.

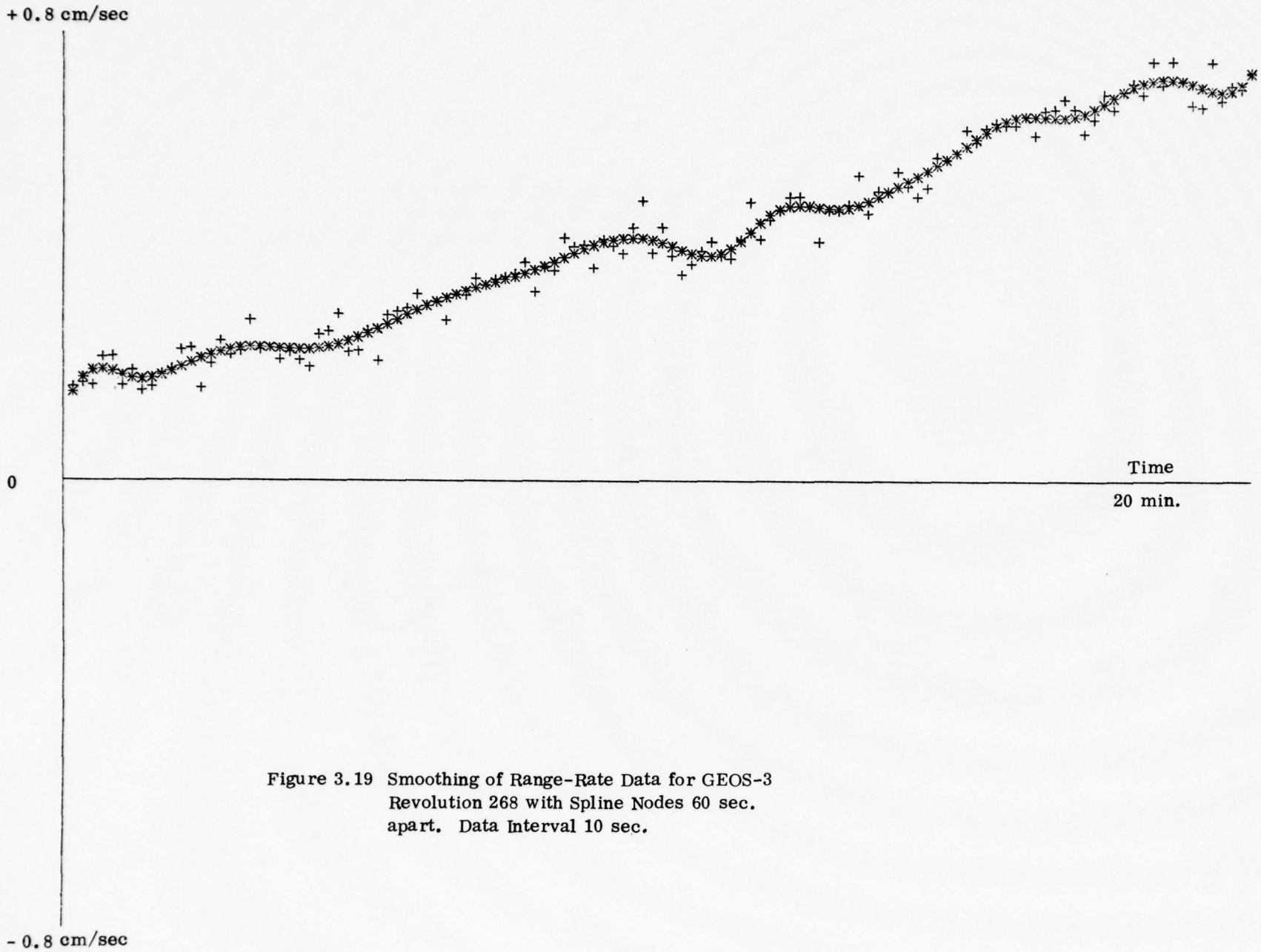

Figure 3.19 Smoothing of Range-Rate Data for GEOS-3 Revolution 268 with Spline Nodes 60 sec. apart. Data Interval 10 sec.

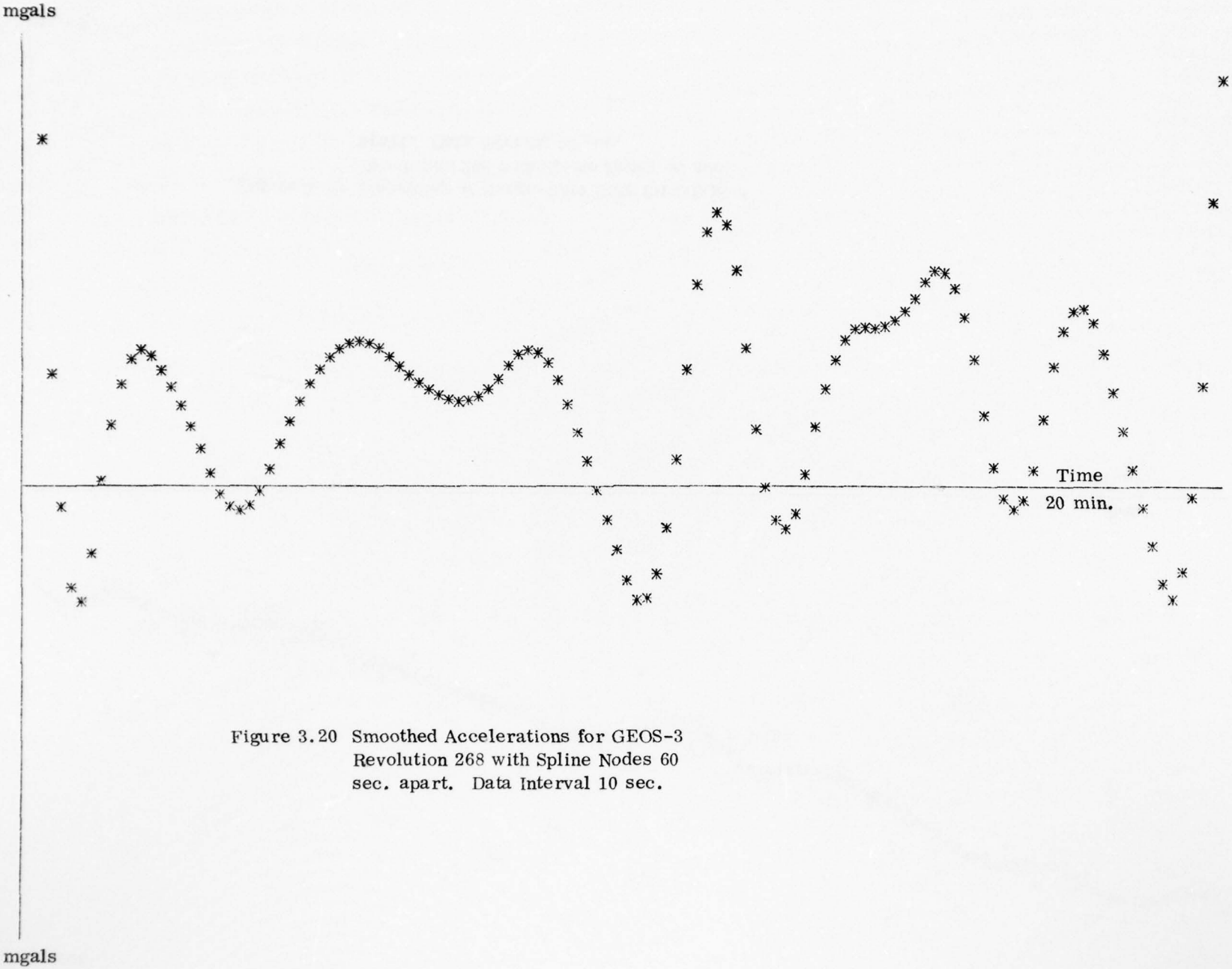

Figure 3.20 Smoothed Accelerations for GEOS-3 Revolution 268 with Spline Nodes 60 sec. apart. Data Interval 10 sec.

Table 3.2. Least Squares Spline Fit with Spline Nodes 60 Seconds Apart to Raw $\dot{R}$ Data at 10 Seconds Interval to GEOS-3 Revolutions 154, 268, 439, 453 and 467.

GEOS-3 Rev.#	Raw $\dot{R}$ Data R.M.S.	Mean	Smoothed $\dot{R}$ Data R.M.S.	Mean	Residuals After Spline Fit R.M.S.	Mean
154	0.2321	-0.0943	0.2167	-0.0943	0.0833	0.0000
268	1.2643	1.1730	1.2626	1.1730	0.0648	0.0000
439	0.1286	-0.0049	0.0933	-0.0049	0.0885	0.0000
453	0.4389	0.4096	0.4333	0.4096	0.0695	0.0000
467	0.6512	0.4345	0.4772	0.4345	0.4431	0.0000

Units are cm/sec.

Figure 3.20 is on the same scale as Figures 3.9 to 3.18. When we compare the accelerations in revolution 268 (Figure 3.20) with accelerations in revolutions 154 and 453 (Figures 3.11 and 3.16), the accelerations $\ddot{R}$ in revolution 268 appear reasonable. But there does appear to be some systematic error in $\dot{R}$ in revolution 268 from Figure 4.19, when we compare it with Figures 3.2 and 3.4. We will comment on this again in Section 4.1.

3.3 Radial Derivative of the Anomalous Potential at GEOS-3 Locations

The radial derivative $(\partial T/\partial r)_c$ of the anomalous potential at a particular location (φ, λ, h) of the GEOS-3 satellite is obtained from the residual acceleration $(\ddot{R})_{\varphi,\lambda,h}$ by equation (1.2) reproduced here specifically:

$$(\partial T/\partial r)_{\varphi,\lambda,h} = (\ddot{R})_{\varphi,\lambda,h}/\cos\beta \tag{3.32}$$

where β is the angle (Rummel et al., 1976, page 19) between the radial direction to GEOS-3 and the direction GEOS-3 to ATS-6. Whenever GEOS-3 happens to be directly below the ATS-6, $(\varphi \approx 0°, \lambda \approx 266°)$ $\partial T/\partial r$ would equal $\ddot{R}$, but at other locations of GEOS-3 the $\partial T/\partial r$ values will be magnified sec β times the $\ddot{R}$ values. We show this for revolutions 154 and 453 in Table 3.3 at one minute intervals out of the GEOS-3 locations actually used for the recovery of anomalies in Section 4.

Table 3.3. $\partial T/\partial r$ and $\ddot{R}$ Values for GEOS-3 Revolutions 154 and 453

Revolution 154					Revolution 453				
φ°	λ°	$\ddot{R}$ mgals	sec β	$\partial T/\partial r$ mgals	φ°	λ°	$\ddot{R}$ mgals	sec β	$\partial T/\partial r$ mgals
34	300	-0.30	-1.71	0.51	39	293	-1.03	-1.71	1.75
31	297	-0.26	-1.57	0.41	36	290	1.42	-1.56	-2.21
28	295	0.21	-1.45	-0.30	33	287	2.05	-1.44	-2.95
25	293	2.57	-1.36	-3.49	30	285	-1.19	-1.34	1.59
21	291	-5.45	-1.28	6.97	26	283	0.45	-1.26	-0.57
18	289	-1.02	-1.22	1.24	23	281	1.49	-1.20	-1.79
15	287	-2.15	-1.17	2.51	20	279	0.22	-1.14	-0.25
12	285	-0.80	-1.12	0.90	17	277	1.27	-1.10	-1.40
					14	275	0.15	-1.07	-0.16

We find that the magnification by sec β in practice is not of great concern for the area of investigation in this report. However, when β exceeds, say, 60° ($|\sec \beta| > 2$), we may lessen the effect of this magnification by smoothing the $\dot{R}$ data with spline nodes at 80 seconds apart in that area, instead of 60 seconds. For this report, we used spline nodes at uniform spacing, but the algorithm in Section 3.1 can accommodate uneven spacing of the nodes in view of the scaling of the data in each interval according to equation (3.13). The spline nodes may thus be fixed at 60 seconds apart for data up to 60° around the subsatellite point of ATS-6, and 80 seconds apart after that. The 80 seconds spacing may serve an adequate balance between dampening of $\ddot{R}$ because of larger spacing, and the magnification of $\partial T/\partial r$ because of larger β.

Rice (1969, Vol. II, Chap. 10) discusses algorithms for the non-linear problem of solving both for the spline coefficients, as well as for the spacing of nodes by treating them as variable nodes. De Boor (1977) has a package of programs which may be modified for this purpose. This approach was, however, not tried in this report, as the treatment of noisy $\dot{R}$ data by fixed spline nodes appeared to be adequate for the current investigations.

4. Recovery of 5° Gravity Anomalies

With the $\partial T/\partial r$ values from Section 3, the recovery of residual gravity anomalies ($\Delta g'$) was attempted by least squares collocation according to the procedures described in Rummel et al. (1976). Eight 5° anomalies were chosen which were covered by GEOS-3 revolutions described in Section 2. We first present in Section 4.1 the results of tests with GEOS-3 revolutions in Section 2.1, where reliable values of initial state vectors were available for both satellites. Next,

we describe in Section 4.2 the tests with revolutions discussed in Section 2.3 where the ATS-6 elements were not known reliably, but were obtained by integration from another epoch. We continue this inquiry in Section 4.3 where the initial state vectors are obtained by integration for both ATS-6 and GEOS-3 satellites instead of using converged elements. The combined results using all reliable observations are presented in Section 4.4.

4.1 Initial State Vectors Available for Both Satellites

The GEOS-3 revolutions available from Section 2.1 were 154, 268, 439, and 453. The location of GEOS-3 at 30 seconds interval in these revolutions is shown in Figure 4.1. The location of the eight 5° anomalies chosen for recovery are also shown. The terrestrial value of these anomalies $\underline{\Delta g}$, and their standard deviations, were taken from Rapp (1977, pages 55, 56) and the same numbering system was retained. The expected value of the residual anomalies $\underline{E(\Delta g')}$ were obtained by subtracting from $\underline{\Delta g}$ the anomalies $\underline{\Delta g_{PC}}$ implied by (12, 12) potential coefficients in the GEM 7 set. (For details, see Rummel et al. (1976, pages 20, 21).) The values of the eight 5° anomalies are given in Table 4.1.

Table 4.1. Particulars of Eight 5° Residual Anomalies

Anom. #	φ_N°	φ_S°	λ_E°	λ_W°	Δg mgals	s.d. mgals	Δg_{PC} mgals	$\Delta g'$ mgals
402	35	30	289	283	-34.1	2.4	-22.3	-11.8
403	35	30	295	289	-26.8	2.5	-25.1	- 1.7
465	30	25	287	281	-15.4	2.8	-23.6	8.2
466	30	25	293	287	-29.8	2.8	-30.2	0.4
531	25	20	285	279	7.3	2.6	- 9.9	17.2
532	25	20	290	285	-44.9	2.9	-14.7	-30.2
599	20	15	282	277	5.8	1.4	5.0	0.8
600	20	15	287	282	- 5.5	1.3	- 2.6	- 2.9

The recovered values of anomalies, $\underline{\hat{\Delta g}'}$, was compared with the expected value of the anomalies by examining the anomaly discrepancies $\underline{\epsilon(\Delta g')}$ and the correlation coefficient ρ, which were computed as:

$$\epsilon(\Delta g_i') = \hat{\Delta g}_i' - E(\Delta g_i') \tag{4.1}$$

$$\rho = \left(\sum_{i=1}^{n} \hat{\Delta g}_i' \, E(\Delta g_i')/n \right) \Big/ \left(\left(\sum_{i=1}^{n} \hat{\Delta g}_i'^2/n \right)^{\frac{1}{2}} \left(\sum_{i=1}^{n} E(\Delta g_i')^2/n \right)^{\frac{1}{2}} \right) \tag{4.2}$$

where n is the number of anomalies.

The $\partial T/\partial r$ values used in the recovery of anomalies were 30 seconds apart, and all available data up to $7^{\circ}.5$ from the center of the anomaly block was considered. Different solutions were tried, considering the $\partial T/\partial r$ values to have a standard deviation of 0.5, 1.0, 1.5, 2.0, 2.0 or 5.0 mgals. (For details, see Rummel et al. (1976, Sec. 6).) We first report the results with all $\partial T/\partial r$ values having a standard deviation of 1.5 mgals. The reasons for this choice will be explained later.

The statistics for the recovered anomalies is shown in Table 4.2 using $\partial T/\partial r$ values in GEOS-3 revolutions 154, 268, 439 and 453. Three different solutions were tried with $\partial T/\partial r$ values being computed for the cases when the spline nodes for fitting the $\dot{R}$ data were 40, 60 or 80 seconds apart.

Table 4.2. Statistics for Recovered Anomalies Using GEOS-3 Revolutions 154, 268, 439, 453

Spline Node Spacing (sec.)	RMS Expec. Anom. $E(\Delta g')$ (mgals)	RMS Predic. Anom. $\hat{\Delta g}'$ (mgals)	RMS Anom. Discr. $\epsilon(\Delta g')$ (mgals)	Correln. coeff. ρ (eqn. 4.2)
40	13.3	10.5	13.5	0.38
60	13.3	10.6	13.6	0.38
80	13.3	10.0	14.0	0.31

The results showed a poor recovery of anomalies. We recall from discussion in the end of Section 3.2 that there was reason to suspect the $\dot{R}$ data in revolution 268. The recovery of anomalies was therefore attempted from only three revolutions, 154, 439 and 453, though we notice from Figure 4.1 that the data then becomes sparse over the four eastern anomalies, when we omit revolution 268. The statistics for the recovered anomalies is shown for

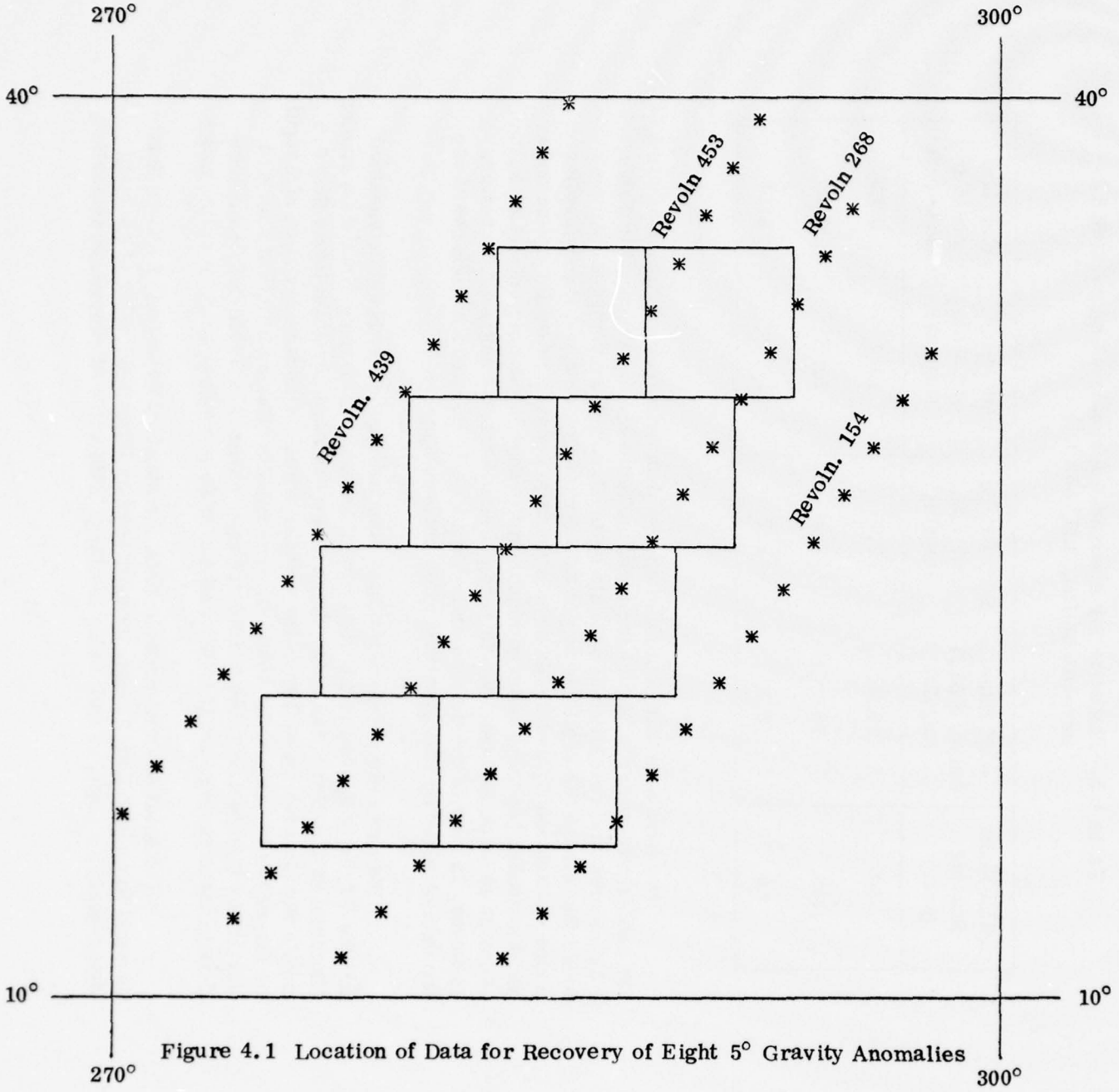

Figure 4.1 Location of Data for Recovery of Eight 5° Gravity Anomalies

three solutions for $\partial T/\partial r$ values being computed for spline node spacing for fitting the $\dot{R}$ data as 40, 60 or 80 seconds. The standard deviation of $\partial T/\partial r$ values was assumed to be 1.5 mgals.

Table 4.3. Statistics for Recovered Anomalies Using GEOS-3 Revolutions 154, 439, 453

Spline Node Spacing (sec.)	RMS Expec. Anom. $E(\Delta g')$ (mgals)	RMS Predic. Anom. $\Delta\hat{g}'$ (mgals)	RMS Anom. Discr. $\epsilon(\Delta g')$ (mgals)	Correln. coeff. ρ (eqn. 4.2)
40	13.3	7.7	10.4	0.63
60	13.3	7.8	10.7	0.60
80	13.3	7.7	11.3	0.53

We first note that in spite of sparse data over four eastern anomalies, the anomaly recovery is in fact improved in Table 4.3 as compared to Table 4.2, which shows that revolution 268 should be taken out of the solution. We also found that though the solutions do get worse with data obtained through spline nodes at 80 seconds, and the same was found in separate tests for spline nodes at 30 seconds, but there is no noticeable difference in the solutions using spline nodes at 40 or 60 seconds, the 40 seconds solution appearing slightly better. However, in view of the discussion in Section 3.2, we would henceforward use the data obtained by fitting splines at 60 seconds spacing.

We now examine what optimum standard deviation should be assumed for the $\partial T/\partial r$ data used in the recovery of anomalies. During simulation studies (Rummel et al., Sec 6.1), it was found that a standard deviation lower than 0.5 mgals would cause instability in the solution while a standard deviation of 2 mgals or larger would dampen the solution. The results of using different standard deviations is shown in Table 4.4 for the case covered in Table 4.3, i.e. using data in three revolutions 154, 439 and 453 at 60 seconds spacing of spline nodes.

The solutions are unstable when the standard deviation of $\partial T/\partial r$ data is equal to or less than 1 mgal, as evidenced by large RMS value of anomaly discrepancy, $\epsilon(\Delta g')$, as well as by the large RMS value of recovered anomalies,

Table 4.4. Statistics for Recovered Anomalies for Different Assumed Standard Deviation of $\partial T/\partial r$. GEOS-3 Revolutions 154, 439, 453. Spacing of Spline Nodes 60 seconds

Assumed s.d. of $\partial T/\partial r$ data (mgals)	RMS $(\Delta\hat{g}')$ mgals	RMS $\epsilon(\Delta g')$ mgals	ρ
0.5	17.6	15.1	0.56
1.0	10.5	10.9	0.60
1.5	7.8	10.7	0.60
2.0	6.2	10.9	0.59
3.0	4.1	11.5	0.57
5.0	2.1	12.3	0.54

$(\Delta\hat{g}')$. The RMS value 17.6 mgals of recovered anomalies in Table 4.4 for the standard deviation of 0.5 mgals, for example, is much larger than the RMS value of 13.3 mgals for the expected anomalies. We also note from Table 4.4 that the solutions are dampened off when the standard deviation is 2 mgals or larger, as evidenced by smaller RMS values of the recovered anomalies. The solution appears to be optimum, when the standard deviation of $\partial T/\partial r$ data is assumed to be 1.5 mgals. Hence, the statistics of recovered anomalies will be reported for the standard deviation of 1.5 mgals, as was already done in Tables 4.2 to 4.4.

To ensure our conclusion (after Table 4.3) that the data in revolution 268 had some systematic error and was thus responsible for the poor recovery seen in Table 4.2, we tried two other solutions shown in Table 4.5. In the first case (first row in Table 4.5), we note from Figure 4.1 that as revolution 439 was not directly located over the 8 anomalies, it could only marginally improve their recovery (second row in Table 4.3), as compared to using revolutions 154 and 453 only. Secondly, if the effect of revolution 439 is indeed marginal, and if the data in revolution 268 is erroneous, the results of using revolutions 268 and 439 should be much poorer. This was actually found to be so, as may be seen in the second row of Table 4.5. Both solutions in Table 4.5 assumed the standard deviation of $\partial T/\partial r$ as 1.5 mgals, and the spacing of spline nodes was 60 seconds.

Table 4.5. Statistics for Recovered Anomalies Using Only 2 GEOS-3 Revolutions out of Revolutions 154, 268, 439, 453

Revolutions Used (see Fig. 4.1)	RMS E $(\Delta g')$ mgals	RMS $\Delta\hat{g}'$ mgals	RMS ϵ $(\Delta g')$ mgals	ρ
154 and 453	13.3	8.3	11.4	0.53
268 and 439	13.3	9.5	15.6	0.10

We have to, therefore, take the data in revolution 268 out of the solution. (This will be discussed again in Section 4.3.) We would, of course, prefer the solution using three revolutions 154, 439 and 453, as shown in the second row of Table 4.3 over the solution using two revolutions 154 and 453, as shown in the first row of Table 4.5. But, as revolution 439 lies outside the eight anomalies to one side, it contributes to the recovery only marginally. It is therefore remarkable that we do get a recovery with only two revolutions 154 and 453. The location of data points at 30 seconds interval used in these two revolutions with respect to eight anomalies is shown in Figure 4.2. In spite of the data being so sparse, the solution in the first row of Table 4.5 shows that the procedures are satisfactory. The improvement in the solution shown in the second row of Table 4.3 with the addition of revolution 439 is a pointer that the recovery of anomalies would show improvement, as we add to the data set from more revolutions located over the anomalies.

4.2 Initial State Vector Obtained by Integration for ATS-6 Satellite

As we have already considered the data in all revolutions available in Section 2.1, we can only consider additional data from the revolutions in Section 2.3, where the initial state vector was available only for GEOS-3, while that for ATS-6 had to be obtained by integration from an earlier epoch. We recall from the discussion at the end of Section 2.3 that we had data available for consideration for three revolutions, which we called 232 A, 232 I and 246 I. The initial ATS-6 elements were obtained from integration from the epoch 0^h on 25 April 75 for revolutions 246 I and 232 I, and were the adjusted values in revolution 232 A for 56 minutes of range-rate data. The initial state vector for GEOS-3 was kept fixed as the a priori value in Table 2.3. The RMS and the mean value of the raw residual range-rate $\dot{R}$ data, the smoothed $\dot{R}$ data after fitting a spline with nodes 60 seconds apart, and the residuals remaining after the spline fit, are shown in Table 4.6 for the three revolutions.

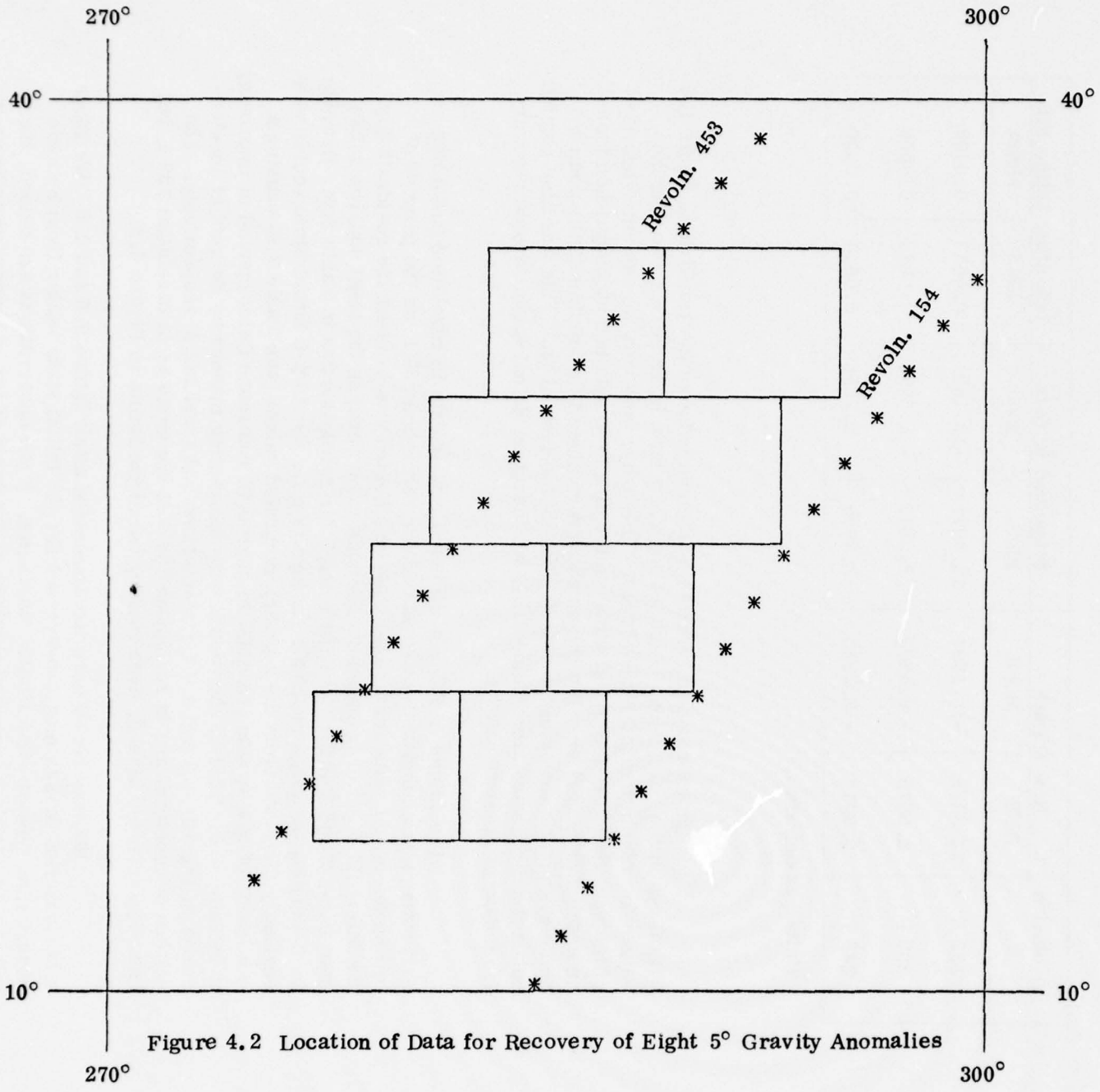

Figure 4.2 Location of Data for Recovery of Eight 5° Gravity Anomalies

Table 4.6. Least Squares Spline Fit to Raw $\dot{R}$ Data in GEOS-3 Revolutions 232 A, 232 I and 246 I

Revolution #	Raw $\dot{R}$ Data		Smoothed $\dot{R}$ Data		Res. after Spline Fit	
	RMS	Mean	RMS	Mean	RMS	Mean
232 A	13.3072	-13.1831	13.3071	-13.1831	0.0643	0.0000
232 I	8.5816	- 8.5790	8.5813	- 8.5790	0.0643	0.0000
246 I	2.3917	- 2.2856	2.3909	- 2.2856	0.0640	0.0000

Units are cm/sec.

When we compare the RMS and mean value of the raw data in Table 4.6 with those in the revolutions from Section 2.1 shown in Table 3.2, we find the values for revolution 246 I to be large. This may, however, be explained because of the uncertainty in the initial state vector of ATS-6 obtained by integration from an epoch 2 days earlier. But the much larger values in revolution 232 I point to some systematic error in the raw $\dot{R}$ data in this revolution. This was also pointed out in the discussion after Table 2.5. We therefore do not expect a good recovery from data in revolution 232 I.

The values in Table 4.6 for the raw $\dot{R}$ data in revolution 232 A are surprising when compared to the values for revolution 232 I, as the purpose of letting the initial state vector of ATS-6 be adjusted was to make the residuals for the full GEM-7 set of potential coefficients to be small in the least squares sense (see items 2 and 3 under iteration 1 and 7 for revolution 232 in Table 2.5). However, in dispersing the large residuals (in iteration 1), the ATS-6 initial state vector was seriously distorted from the a priori integrated values (see Table 2.6) causing a worsening of raw $\dot{R}$ data (residual to degree 12 reference field) instead of improving it in Table 4.6. This is shown in a very interesting manner by the plot of accelerations in Figures 4.3 and 4.4 for revolutions 232 I and 232 A respectively. The pattern of accelerations in revolution 232 A is the same as in revolution 232 I, but has been severely biased, even running out of the limits in Figure 4.4.

We may recall here the discussion after Tables 2.5 and 2.6. We incur a serious risk in obtaining convergence for the initial state vector from a single observation type or for a limited time span. If the observations are biased, the converged initial state vector obtained on the basis of fitting these observations in the least squares sense would be much in error. We therefore do not expect any recovery at all from data in revolution 232 A.

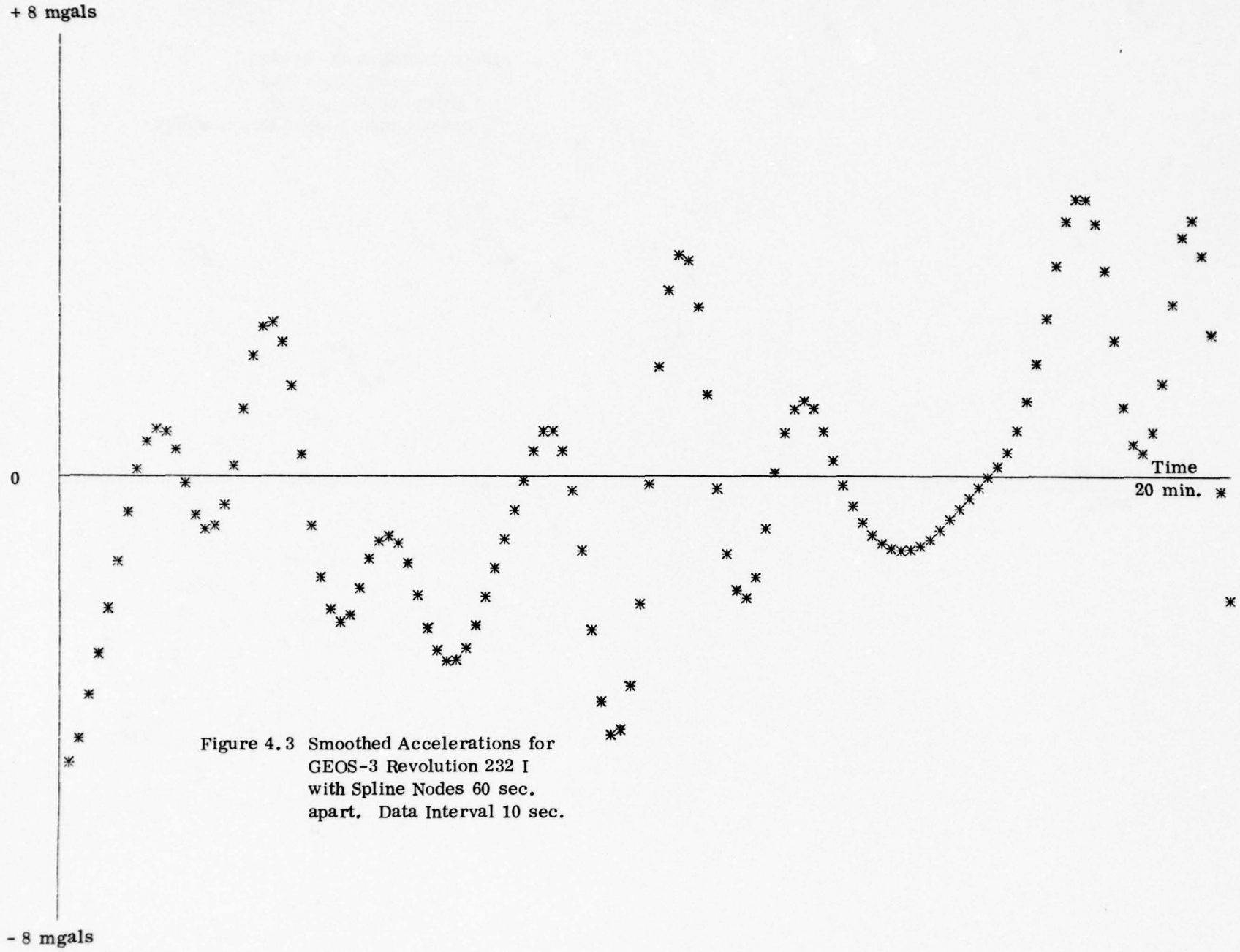

Figure 4.3 Smoothed Accelerations for GEOS-3 Revolution 232 I with Spline Nodes 60 sec. apart. Data Interval 10 sec.

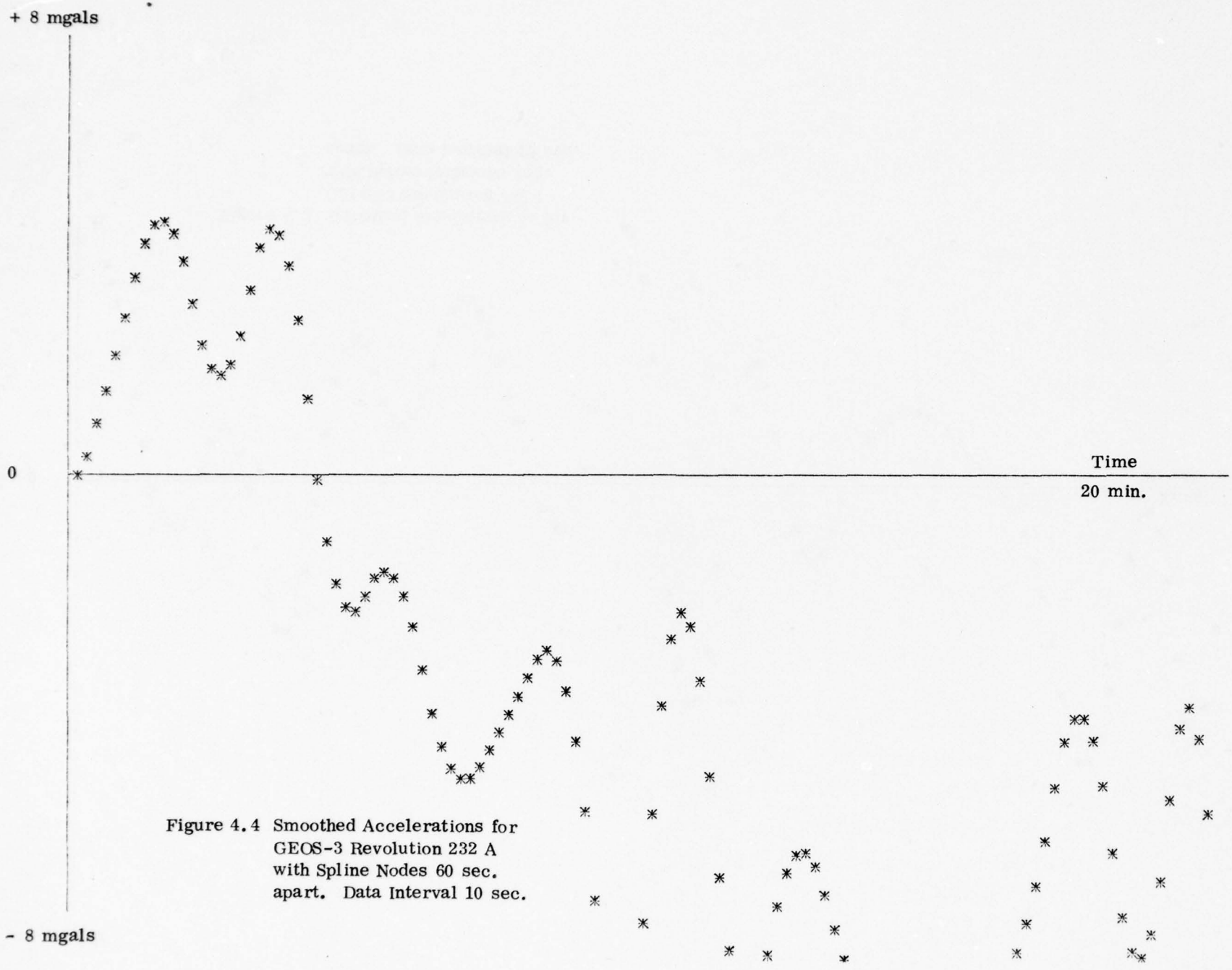

Figure 4.4 Smoothed Accelerations for GEOS-3 Revolution 232 A with Spline Nodes 60 sec. apart. Data Interval 10 sec.

The statistics for the recovery of 6 anomalies using data for only one revolution 232 A, 232 I and 246 I at a time is shown in Table 4.7. The spline nodes were 60 seconds apart and the standard deviation of $\partial T/\partial r$ was assumed as 1.5 mgals. The north-east and the south-west anomalies were not considered, as there would be no data within 7°.5 from the center of these anomaly blocks. This is seen in Figure 4.5 from the location with respect to eight anomalies of the $\partial T/\partial r$ data points at 30 seconds interval used in revolutions 232 and 246.

Table 4.7. Statistics for 6 Recovered Anomalies Using One GEOS-3 Revolution at a Time Out of Revolutions 232 A, 232 I, 246 I

Revolutions Used (see Figure 4.5)	RMS E ($\Delta g'$) mgals	RMS ($\Delta \hat{g}'$) mgals	RMS ϵ ($\Delta g'$) mgals	ρ
232 A	15.4	26.8	31.9	-0.08
232 I	15.4	6.0	18.0	-0.29
246 I	15.4	15.2	14.3	0.56

The data in revolution 232 is unusable, whether the initial state vector of ATS-6 was obtained by integration (232 I) or was then adjusted (232 A) to fit the 56 minutes of range-rate sum observations. However, it appears that the data in revolution 246 I is usable and may help improve the solution obtained earlier with 3 revolutions 154, 439, and 453 in Table 4.3. The statistics for the recovery of eight 5° anomalies are shown in Table 4.8 with 2, 3 and 4 revolutions. The spline nodes in all cases were 60 seconds apart and the standard deviation of $\partial T/\partial r$ data was taken as 1.5 mgals.

Table 4.8. Statistics for Recovered Anomalies Using GEOS-3 Revolutions 154, 439, 453 and 246 I

Revolutions Used	RMS E ($\Delta g'$) mgals	RMS ($\Delta \hat{g}'$) mgals	RMS ϵ ($\Delta g'$) mgals	ρ
154, 453	13.3	8.3	11.4	0.53
154, 453, 439	13.3	7.8	10.7	0.60
154, 453, 439, 246 I	13.3	13.2	10.2	0.70

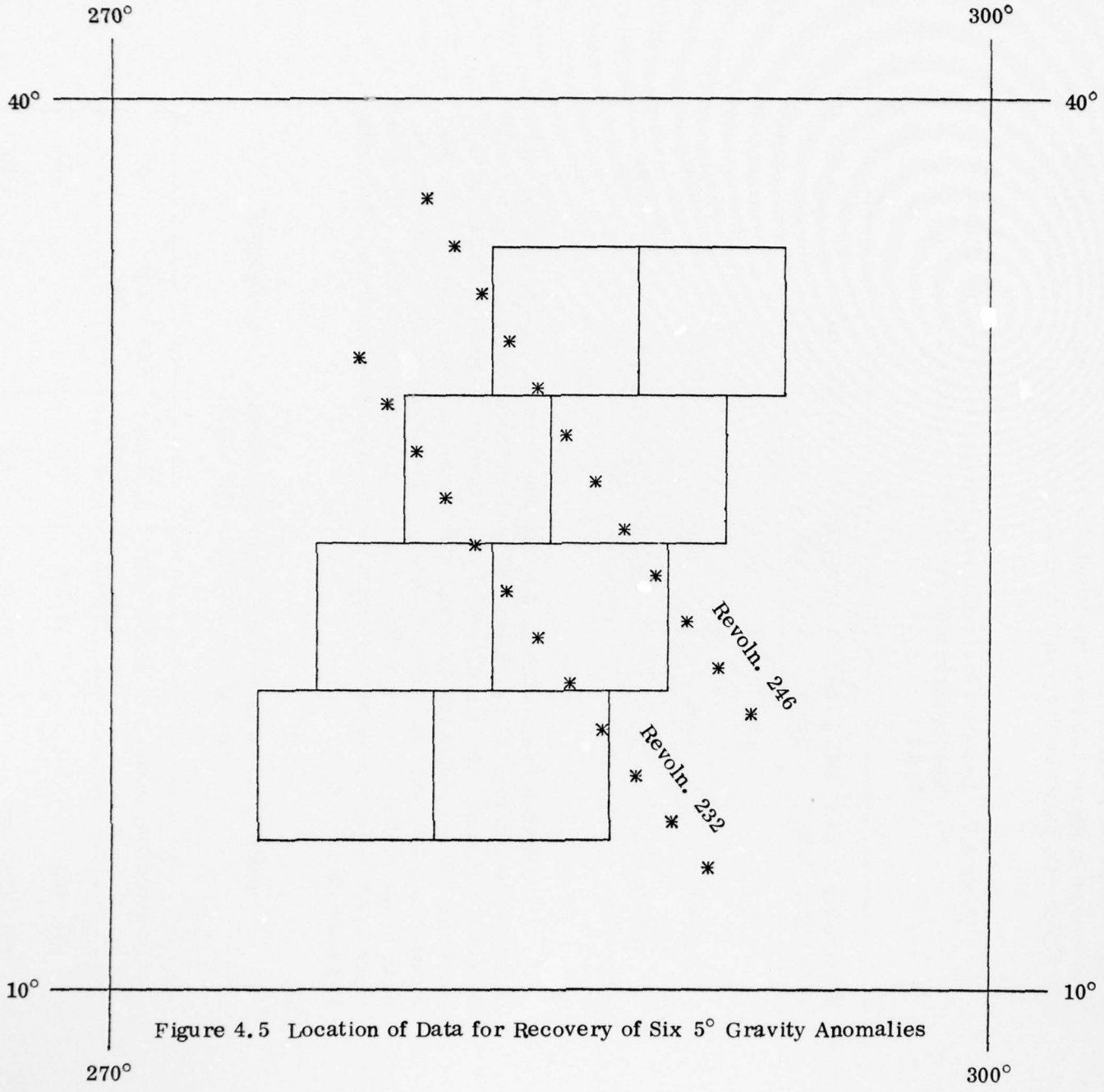

Figure 4.5 Location of Data for Recovery of Six 5° Gravity Anomalies

We find continuing improvement in the solutions, as data from more revolutions is added, by a reduction in the anomaly discrepancy $\epsilon(\Delta\acute{g})$ and increase in the correlation coefficient ρ (equations 4.1 and 4.2). But what is more remarkable is that the data in revolution 246 I is usable inspite of the ATS-6 elements having been integrated from an epoch two days earlier (Table 2.3) and thus causing large residual range-rate (Table 4.6). The modeling error in $\dot{R}$ due to uncertainty in ATS-6 initial state vector was apparently 'differenced out' during numerical differentiation and did not significantly bias the $\ddot{R}$ (and $\partial T/\partial r$) values. However, if this contention is true, we should be able to integrate from well determined (by multiple observation types and long time span) initial state vectors at 0^h on April 25, 1975 (Table 2.3) not only for the ATS-6 satellite but also for the GEOS-3 satellite. We would then be able to examine the difference in integrated and previously converged elements of GEOS-3 (on the lines of Table 2.4 for ATS-6) and check out the values of $\dot{R}$, $\ddot{R}$ and recovered anomalies not only for revolutions 232 and 268 where the data is suspected of having systematic errors, but also for revolution 246 where the range rate sum observations have already yielded satisfactory results.

4.3 Initial State Vectors Obtained by Integration for Both ATS-6 and GEOS-3 Satellites

The differences in the initial state vector for GEOS-3 satellite as obtained from integration from the epoch 0^h on April 25, 1975 minus the converged initial state vector values in Tables 2.1 and 2.3 is shown in Table 4.9. The integration was, of course, carried out only for the period (April 25 to April 29, 1975) during which the observations were used for determining the initial state vector at 0^h on April 25, 1975 (last column in Table 2.3). This was discussed after Table 2.4 where we concluded that the integrated elements could only be compatible during the period on which they were converged.

Table 4.9. Differences in Position and Velocity Coordinates for GEOS-3 as Integrated From Epoch 0^h on April 25, 1975 Minus Converged Elements for Other Epochs

Epoch (Date, Hr., min., sec.)	X (m)	Y (m)	Z (m)	$\dot{X}$ (cm/sec)	$\dot{Y}$ (cm/sec)	$\dot{Z}$ (cm/sec)
1. 26 April 75 07h 00m 00s (GEOS-3 revoln. 232)	-17.2	50.3	-22.4	2.28	-6.39	-2.00
2. 27 April 75 07h 00m 00s (GEOS-3 revoln. 246)	- 7.4	-1.7	18.0	- 0.15	2.56	-0.71
3. 28 April 75 20h 50m 00s (GEOS-3 revoln. 268)	30.3	573.8	201.4	-23.25	16.44	40.36

The differences are small for revolution 246, though substantially what may be expected in converged elements, being 10 to 20 m in position elements and 1 to 2 cm/sec in velocity elements. The differences are much larger for revolution 232, 20 to 50 m in position elements and 2 to 6 cm/sec in velocity elements. There are, however, grossly large differences in the integrated and converged elements of GEOS-3 for revolution 268. We had also noticed very large differences for this revolution for the integrated and converged ATS-6 elements (row 8b in Table 2.4). Some observations in the 2 1/2 hour time span used for converging revolution 268 in Table 2.1 are likely to have systematic bias. Also, it is conceivable that when the time span is comparatively shorter (2 1/2 hours vs. 5 days), a very different set of initial state vectors for a pair of satellites may fit the data. The initial state vectors based on the longer time span would be more reliable.

We will refer to the data in these revolutions as 232 II, 246 II and 268 II to indicate that the initial state vectors of both satellites have been obtained by integration from the epoch 0^h on April 25, 1975. The particulars of $\dot{R}$ data in these revolutions are given in Table 4.10.

Table 4.10. Least Square Spline Fit to Raw $\dot{R}$ Data in GEOS-3 Revolutions 232 II, 246 II, 268 II

Revolution	Raw $\dot{R}$ Data		Smoothed $\dot{R}$ Data		Res. after Spline Fit	
#	RMS	Mean	RMS	Mean	RMS	Mean
232 II	5.1172	-5.1050	5.1168	-5.1050	0.0643	0.0000
246 II	4.3777	-4.3495	4.3772	-4.3495	0.0640	0.0000
268 II	1.2855	-1.1834	1.2839	-1.1834	0.0648	0.0000

Units are cm/sec.

The magnitude of $\dot{R}$ is reduced as compared to revolution 232 I while slightly enlarged as compared to revolution 246 I. The latter should be expected as the integrated elements of GEOS-3 from a 2 day earlier epoch in revolution 246 II have greater uncertainty and thus large residual $\dot{R}$. (Compare with Table 4.6).

The RMS values of $\dot{R}$ in revolution 268 II are about the same as for revolution 268 (Table 3.2), but the mean values have an opposite sign. The plot of $\dot{R}$ in revolution 268 II is shown in Figure 4.6. It is on the same scale and uses the same data as in Figure 3.19 and is remarkably similar, except for its slope

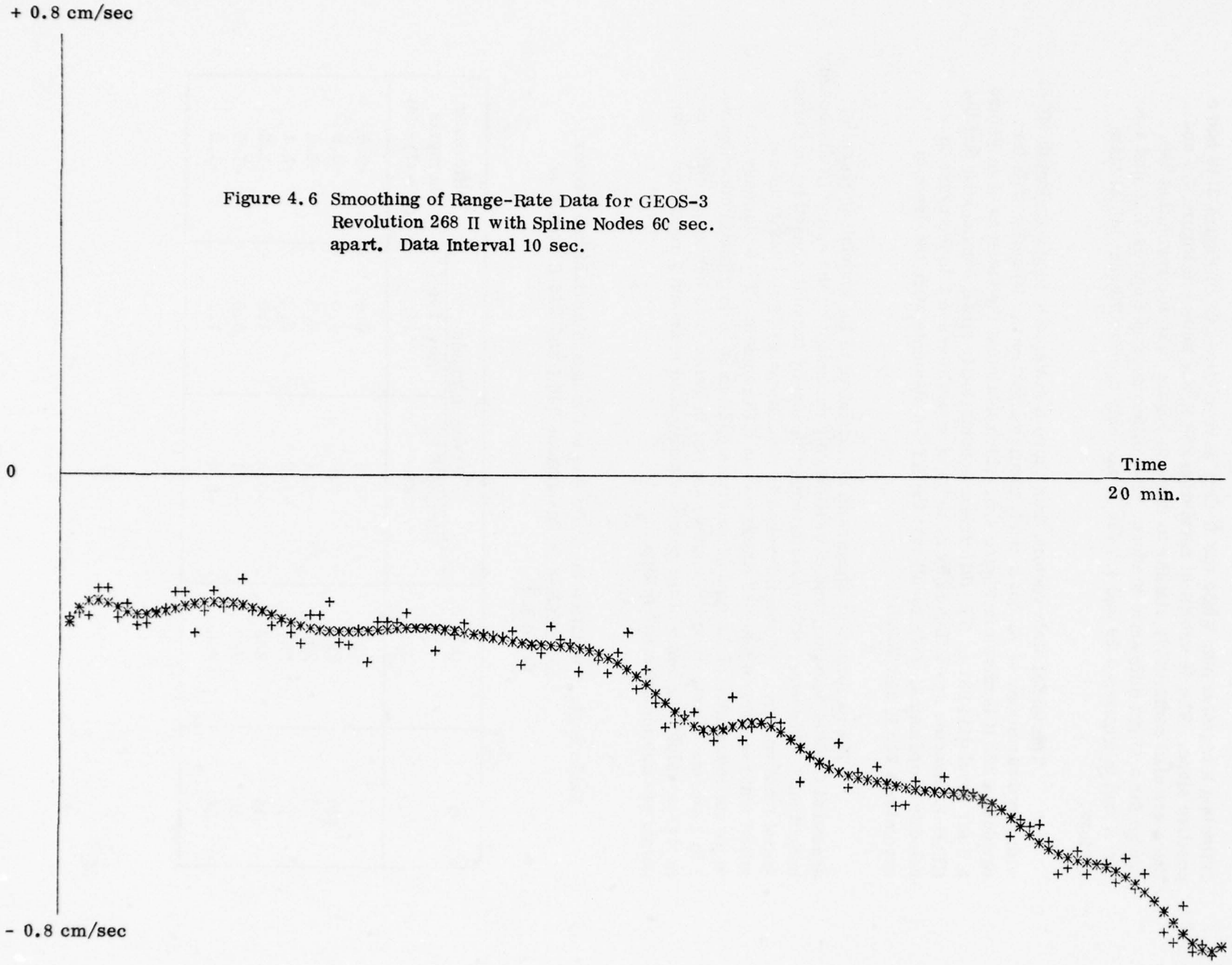

Figure 4.6 Smoothing of Range-Rate Data for GEOS-3 Revolution 268 II with Spline Nodes 60 sec. apart. Data Interval 10 sec.

reflecting a negative bias while the $\dot{R}$ data in revolution 268 in Figure 3.19 had a positive slope. The $\dot{R}$ values in revolution 268 II are shown in Figure 4.7 and these are also remarkably similar to those in Figure 3.20 for revolution 268, except for a slight difference in slope. The differences in Figures 3.19 and 4.6 for $\dot{R}$ and in Figures 3.20 and 4.7 for $\ddot{R}$ are only due to different initial state vectors.

The initial state vectors thus cause a systematic long wavelength effect with large variations in $\dot{R}$, but a much smaller effect on $\ddot{R}$. The plot of $\ddot{R}$ for revolution 232 II is shown in Figure 4.8, which is almost the same as $\ddot{R}$ in Figure 4.3 for revolution 232 I. The difference is remarkably small considering that the GEOS-3 elements are different by 20 to 50 m in position and 2 to 6 cm/sec in velocity coordinates. (We recall that the ATS-6 elements were the same in revolutions 232 II and 232 I.)

The pattern of $\ddot{R}$ appears to be indicative of the anomalous potential sensed at GEOS-3 location, and is qualitatively dependent on the spline fit discussed in Section 3. However, it is quantitatively affected by the bias caused by incorrect initial state vectors. As the difference in revolutions 246 I and 246 II in the initial state vectors of GEOS-3 (there was no difference in ATS-6 elements) is more representative of the type of uncertainty (10 to 20 m in position coordinates, 1 to 2 cm/sec in velocity coordinates), we list in Table 4.11 the actual differences in $\partial T/\partial r$ values for some of the points actually used in anomaly recovery. The points are one minute apart in time.

Table 4.11. Variation in $\partial T/\partial r$ due to Change in Initial State Vector for GEOS-3 in Revolutions 246 I and 246 II (row 2 in Table 4.9)

φ°	λ°	$\partial T/\partial r$ in mgals		Difference in mgals
		Rev. 246 II	Rev. 246 I	
(1)	(2)	(3)	(4)	(5) = (3) - (4)
17	293	5.6	6.4	-0.8
20	291	3.9	4.8	-0.9
23	289	4.8	5.8	-1.0
27	287	1.2	2.3	-1.1
30	284	-0.3	1.0	-1.3
33	282	-1.4	0.0	-1.4
36	280	-0.4	1.1	-1.5

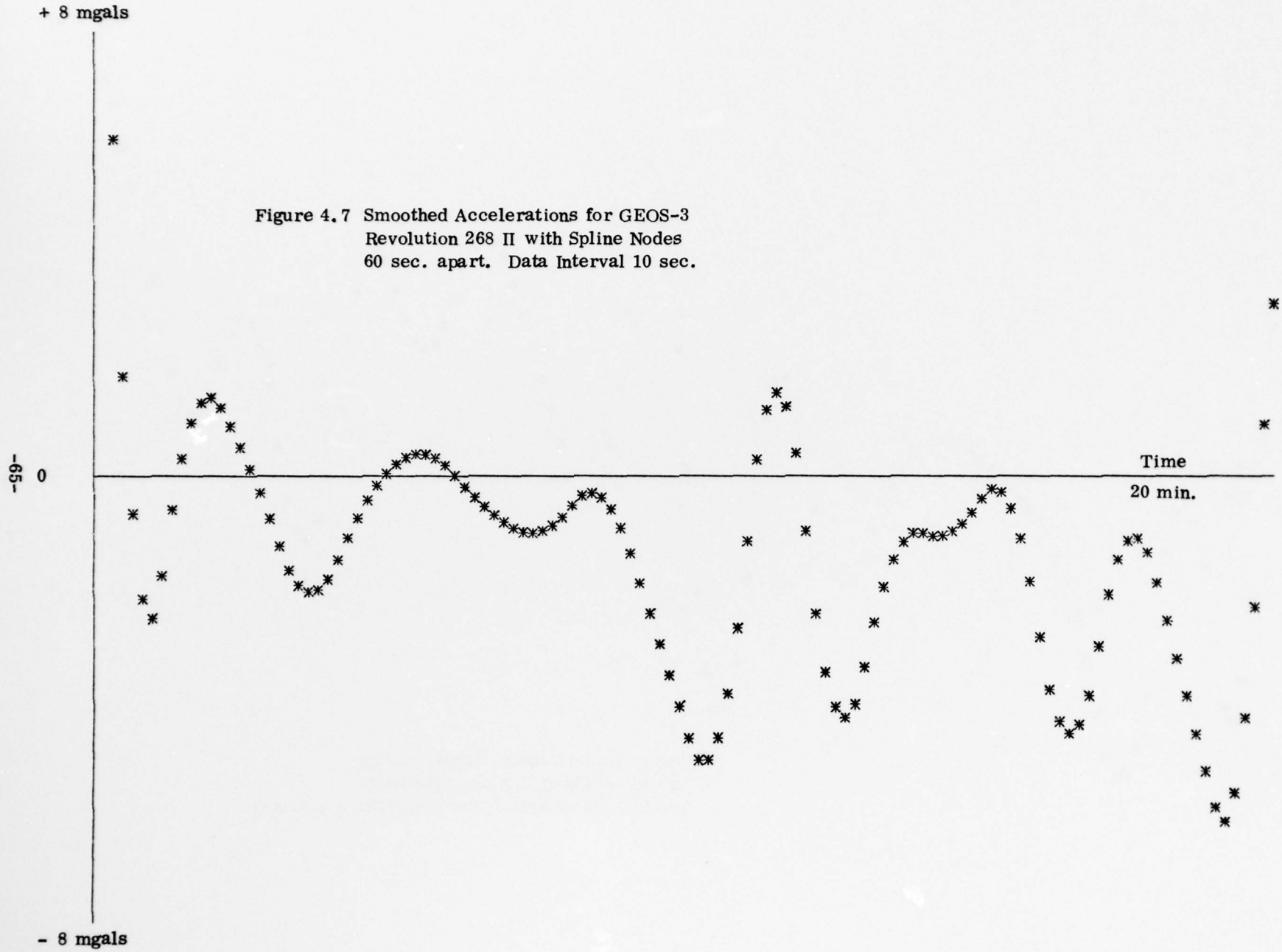

Figure 4.7 Smoothed Accelerations for GEOS-3 Revolution 268 II with Spline Nodes 60 sec. apart. Data Interval 10 sec.

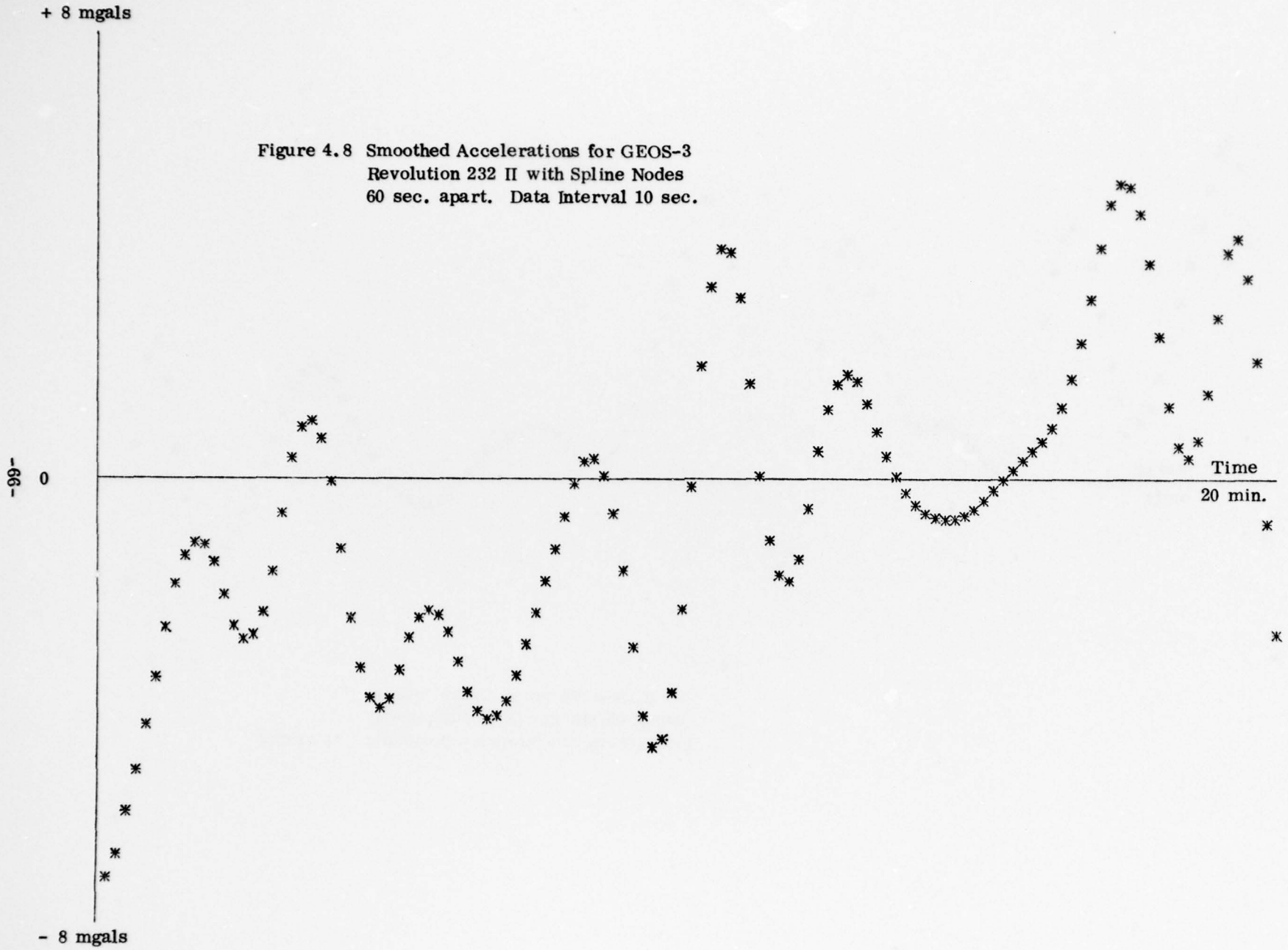

Figure 4.8 Smoothed Accelerations for GEOS-3 Revolution 232 II with Spline Nodes 60 sec. apart. Data Interval 10 sec.

We note a linear bias in $\partial T/\partial r$ values due to changes in initial state vector. The differences in $\partial T/\partial r$ are magnified by about 6 times in the differences in the recovered anomalies using revolutions 246 I and 246 II. This maximum difference is in the anomalies directly below the GEOS-3 locations and gets reduced in neighboring anomalies. Accordingly, the largest difference which may be expected in recovered anomalies due to uncertainties in initial state vectors is about one-half of the standard deviation of the anomalies, which was about 12 mgals.

The statistics for the six 5° anomalies recovered by data in revolutions 232 II and 246 II, one revolution at a time, is given in Table 4.12. These values are comparable to entries in Table 4.7. The statistics for eight 5° anomalies recovered by revolutions 268 and 268 II are also given in Table 4.12.

Table 4.12. Statistics for Recovered Anomalies Using One GEOS-3 Revolution at a Time out of Revolutions 232 II, 246 II, 268 II

Revolutions Used	RMS E ($\Delta\acute{g}$) mgals	RMS ($\Delta\hat{\acute{g}}$) mgals	RMS ϵ ($\Delta\acute{g}$) mgals	ρ
232 II	15.4	7.7	18.2	-0.14
246 II	15.4	11.6	12.8	0.58
268 II	13.3	12.0	14.9	0.31
268	13.3	9.5	16.1	0.03

We note that the recovery is equally poor in revolutions 232 I and 232 II. The recovery in revolution 268 II is slightly better than in revolution 268. Apparently, there are some systematic errors in the range-rate sum observations in revolutions 232 and 268, and this data has to be excluded from the solutions.

The recovery in revolution 246 II happens to be slightly better than for revolution 246 I. But it is preferable anyway, to use the initial state vectors for both satellites analogously, i.e. integrated from the values at epoch 0^h on April 25, 1975, which was done for revolution 246 II.

Now that we have established that the initial state vectors may be obtained from integration, we would like to see if we may obtain $\dot{R}$ data for any other revolution covering the eight 5° anomalies, starting from the epochs at 0^h on April 19 and 0^h on April 25, 1975 (last two columns of Table 2.3) until April 29, 1975. The only range-rate sum observations over the anomalies during this period, besides revolutions already considered (154, 175, 232, 246, 268), were in GEOS-3 descending revolution 254 (April 27, 1975 22^h) and ascending revolution 260 (April 28, 1975 08^h). However, the location of revolution 254 closely followed the location of revolution 453, and would thus not provide any additional information. The $\dot{R}$ data was, however, obtained from revolution 260, and we may call it revolution 260 II, as the initial state vectors for both ATS-6 and GEOS-3 satellites were obtained by integration from epoch 0^h on April 25, 1975. The solution with the additional data in revolution 260 II will be reported in Section 4.4.

4.4 Recovery of 5° Anomalies — Combined Solution

We have finally the $\dot{R}$ data available for revolutions 154, 439, 453, 246 II and 260 II. The location of GEOS-3 satellite at 30 seconds time interval in these revolutions used for the recovery of eight 5° anomalies is shown in Figure 4.9. The $\partial T/\partial r$ values in the locations where the ascending and descending GEOS-3 revolutions cross each other are given in Table 4.13.

Though the locations (φ, λ, h) of the crossover points were not corresponding exactly, but the data could perhaps be adjusted in a linear manner in all ascending and descending revolutions so that the discordance at the crossover points is a minimum in the least squares sense. The justification for the linear adjustment of data in each arc lies in the fact that the errors in the initial state vectors cause a linear bias in the $\partial T/\partial r$ values (see Table 4.11). The adjustment was not done in the present study, as we should first perhaps use $\dot{R}$ data from at least 2 more revolutions — one ascending revolution in a location corresponding to revolution 232 (Figure 4.5) and one descending revolution in a location corresponding to revolution 268 (Figure 4.1). Preferably, we should consider data from another two ascending revolutions, one each in the north-east and south-west corners, so that each anomaly is covered by at least one ascending and one descending revolution.

We now give in Table 4.14 the values of the anomaly discrepancies, $\epsilon(\Delta\acute{g})$, for each of the eight 5° anomalies as they change from a solution using data for only 2 revolutions (154 and 453), and as data from revolutions 439, 246 II and 260 II is added for one revolution at a time. The RMS value of the predicted anomalies (RMS $\Delta\hat{\acute{g}}$) and the anomaly discrepancies (RMS $(\epsilon\,\Delta\acute{g})$), and the correlation coefficient (ρ) is also given for ease of reference. We recall that the RMS value of the expected anomalies was 13.3 mgals.

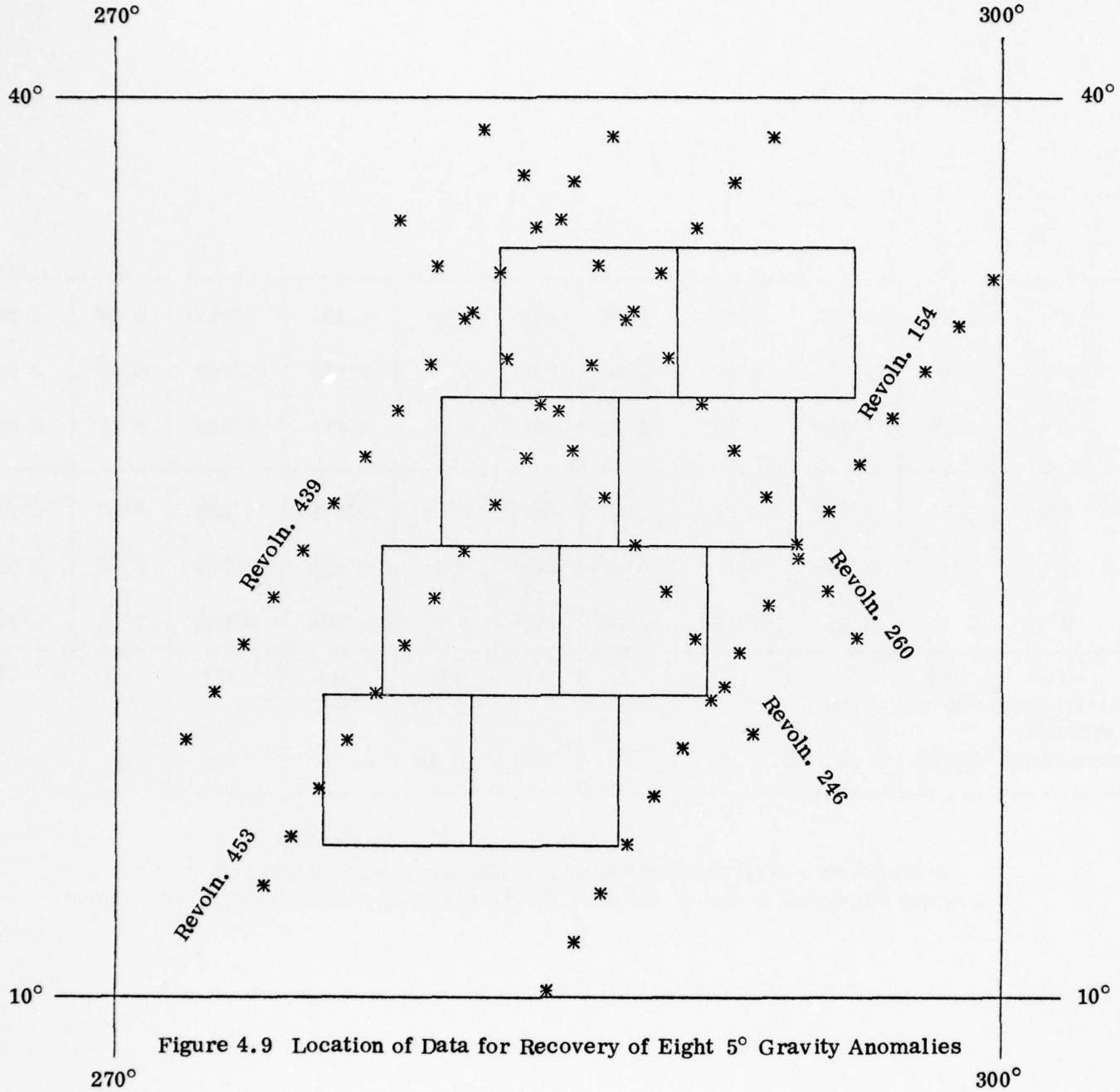

Figure 4.9 Location of Data for Recovery of Eight 5° Gravity Anomalies

Table 4.13. Comparative $\partial T/\partial r$ Values at Crossover Points of Ascending GEOS-3 Revolutions 246 II and 260 II with Descending GEOS-3 Revolutions 154, 453 and 439

Rev. (1)	φ° (2)	λ° (3)	h km. (4)	$\partial T/\partial r$ mgals (5)	Rev. (6)	φ° (7)	λ° (8)	h km. (9)	$\partial T/\partial r$ mgals (10)	Difference in mgals (11)=(5)-(10) (11)
246 II	20.3	290.6	843.7	3.9	154	20.4	290.4	847.2	7.4	-3.5
246 II	29.2	284.7	845.6	-0.8	453	29.0	284.6	850.7	1.7	-2.5
246 II	32.8	282.1	846.6	-1.4	439	33.1	282.2	851.5	2.3	-3.7
260 II	24.5	293.4	844.5	1.8	154	24.6	293.1	847.9	-3.5	5.3
260 II	32.9	287.5	846.6	1.5	453	32.6	287.2	851.4	-2.9	4.4
260 II	36.4	284.7	847.6	-0.8	439	36.2	284.6	852.2	-2.2	1.4

Table 4.14. Improvement in Anomaly Recovery with $\dot{R}$ Data in Additional GEOS-3 Revolutions

Anom. # (see T.4.1)	Latitud. Extent	Longitud. Extent	$\epsilon(\Delta\dot{g})$ in mgals with $\dot{R}$ Data in Revolns. 154 + 453	+ 439	+ 246 II	+ 260 II
402	30-35	283-289	21.2	18.2	18.6	14.7
403	30-35	289-295	10.8	10.5	10.4	4.3
465	25-30	281-287	-9.6	-7.5	-9.7	-9.3
466	25-30	287-293	5.2	5.2	0.3	-2.3
531	20-25	279-285	-10.2	-11.6	-14.3	-14.3
532	20-25	285-290	14.7	14.7	0.8	0.6
599	15-20	277-282	4.1	4.7	4.7	4.7
600	15-20	282-287	-3.4	-3.4	-3.7	-3.7
RMS Anom. Discr. ($\epsilon(\Delta\dot{g})$) mgals			11.4	10.7	9.9	8.4
RMS Pred. Anom. ($\Delta\hat{\dot{g}}$) mgals			8.3	7.8	11.6	11.0
Correln. Coeff. (ρ)			0.53	0.60	0.69	0.78
Mean of std. dev. of pred. anom. mgals			12.8	12.7	12.4	12.1

We note from Table 4.14 and Figure 4.9 that the data in any revolution primarily affects the anomaly directly below it. Hence, as already mentioned, we should have $\dot{R}$ data from at least two (preferably four) additional revolutions to further improve the anomaly recovery in the last column of Table 4.14. We should also attempt to adjust the $\partial T/\partial r$ data linearly in all revolutions for a minimum variance of non-agreement over the cross-over points before the final solution to cater for systematic biases in $\partial T/\partial r$ data due to inaccurate initial state vectors.

Finally, the predicted anomalies with the five revolutions in Figure 4.9 used in the present study (without any cross-over constraints), along with standard deviations, are shown in Table 4.15. The number of $\partial T/\partial r$ points within $3^\circ.5$ ($\psi = 3^\circ.5$) of the center of each anomaly block are also given, as these primarily affect the anomaly recovery. All $\partial T/\partial r$ values lying within $7^\circ.5$ ($\psi = 7^\circ.5$) of the center of each anomaly block were, however, used; their number is also given. The time interval of $\partial T/\partial r$ values was 30 seconds and they were assumed to have a standard deviation of 1.5 mgals to ensure stability of the solution (see Table 4.4 and relevant discussion). The splines to filter and smooth the raw $\dot{R}$ data had their nodes 60 seconds apart, and used $\dot{R}$ data at 10 seconds interval.

Table 4.15. Anomaly Recovery of Eight 5° Anomalies Using $\dot{R}$ Data From Five GEOS-3 Revolutions 154, 439, 453, 246 II, 260 II (see Fig. 4.9)

Anomaly #	Latitud. Extent	Longitud. Extent	Expec. Anom. mgals	# of Data Points ψ=3°.5	ψ=7°.5	Predic. Anom. mgals	Stnd. Dev. mgals	Anom. Discr. mgals
402	30-35	283-289	-11.8	9	30	2.9	11.3	14.7
403	30-35	289-295	- 1.7	3	25	2.6	12.4	4.3
465	25-30	281-287	8.2	7	27	-1.1	11.3	- 9.3
466	25-30	287-293	0.4	5	28	-1.9	11.6	- 2.3
531	20-25	279-285	17.2	4	18	2.9	11.9	-14.3
532	20-25	285-290	-30.2	4	25	-29.6	12.4	0.6
599	15-20	277-282	0.8	3	11	5.5	12.7	4.7
600	15-20	282-287	- 2.9	1	16	-6.6	13.5	- 3.7
RMS Value (mgals)			13.3			11.0		8.4
Correlation coefficient between predicted and expected anomalies = 0.78								

A solution was also tried with the above data but with standard deviation of $\partial T/\partial r$ data as 1.0 mgal, but the solution was worse. The RMS value of predicted anomalies was 15.7 mgals, and the RMS value of anomaly discrepancies was 10.7 mgals, with correlation coefficient as 0.74 mgals. Additional data from revolution 268 II (row 3 of Table 4.12) also made the solution worse. The solution in Table 4.15 is therefore the optimum one with the data from five revolutions shown in Figure 4.9.

5. Summary and Conclusions

There are two main considerations in the use of real range-rate sum observations, from which we subtract the computed value of the range-rate sum based on a certain model to obtain line of sight residual range-rate between the 'high-low' satellite pair. First are the modeling errors most significantly contributed by the assumed initial state vectors of the satellites, and second are the random observational errors of the raw data, after it has been corrected for physical and instrumental effects like ionospheric and tropospheric refraction, transponder delays, etc. The observations may sometimes also exhibit system biases, which may be accounted for if 'small' and linear, but which otherwise may make the observations unusable.

The initial state vectors are 'determined' on the basis that if the earth's gravitational field at the satellite altitude may be described with neglibible error by a full set (e.g. GEM-7) of potential coefficients (and if we consider other force fields like solar radiation pressure, etc.), then the computed values should fit the observations in the least squares sense with the only parameters being the initial state vectors. However, in practice, this depends on the observation type and its reliability and the time span of observations. Range-rate sum observations are not sensitive enough to the determination of the initial state vectors, and if they are used on a 'single pass' basis — the time duration of the 'visibility' from ATS-6 in one revolution of GEOS-3 —, the initial state vectors even if 'converged' may be seriously biased.

As we are interested in the range-rate sum observation type for the recovery of gravity anomalies, we require a two stage process, the first stage being the determination of unbiased initial state vectors in which we employ other observation types particularly range observations, including laser ranges, in addition to range-rate sum observations. It is usually possible with this multiple observation type to get converged initial state vectors on a single pass basis. However, if the observations include sufficient 'paired' observations like range-rate sum or range sum, one may obtain a 'wrong' pair of initial state vectors which may or may not introduce a bias in range rate residuals. It appears to be a much better procedure to use converged initial state vectors for a much longer time span like 4 to 6 days (Table 2.3). Firstly, any biased observations in one or two revolutions would not significantly bias the initial state vectors. This will result in greater reliability in terms of the standard deviations of the initial state vectors, which otherwise on a single pass basis even with multiple observations may reach very large values of a kilometer in position and several meters/sec in velocity (Table 2.1), making it impossible to judge their reliability. Secondly, on a long time span of 4 to 6 days, it would become possible to use even range-rate sum observations from multiple passes to obtain convergence, which even if it requires several iterations, has the practical advantage of not requiring access to other observation types.

We find that there is no cause for concern for obtaining initial state vectors for other epochs by integration, but these epochs must be within the time span used for obtaining the converged elements (Table 2.4). Any modeling error due to incorrect initial state vector appears to show up as a linear bias in the residual range-rate $\dot{R}$ and the residual accelerations $\ddot{R}$. This may have a large effect on $\dot{R}$, but gets differenced out while computing $\ddot{R}$, with very small linear bias on accelerations (Table 4.11) for the usual uncertainty of 10 to 20 meters in position and 1 to 2 cm/sec in velocity of GEOS-3 initial state vector.

It is not possible to filter any residual modeling errors and the observational errors by letting the initial state vectors take the 'slack' by letting them vary within the standard deviations (computed for them in the first stage), while computing residual range-rate $\dot{R}$. The $\dot{R}$ function can, however, be filtered of

observational 'noise' by approximating it in the least squares sense by a piecewise continuous cubic spline, with continuous first and second derivatives. It is remarkable that bases exist for this spline in terms of two simple cubic polynomials, such that a linear combination with only four non-zero coefficients is required to represent the spline between consecutive nodes, where the adjacent piecewise continuous cubics meet. This results in a simple computationally stable algorithm described in Section 3.1.

A unique approximating spline gets defined once the spline nodes are selected. As the spacing between nodes is increased, the slopes of the spline, $\ddot{R}$ in our case, get smoother. The optimum representation of $\ddot{R}$, in the sense that the variation in neighboring points at 10 to 30 seconds interval is what may be expected at the satellite altitude, occurs with spline nodes 60 seconds apart when the raw $\dot{R}$ data is 10 seconds apart. A smaller spacing of spline nodes causes $\ddot{R}$ to vary too sharply, while a larger spacing causes $\ddot{R}$ to be dampened. The observational noise in the revolutions used in this study was found to vary from 0.06 to 0.09 cm/sec, while in one revolution, which was not used, it was as large as 0.44 cm/sec (Table 3.2).

The spline should be fitted to include raw $\dot{R}$ data 2 to 4 minutes at each end beyond the data span needed for recovery of anomalies, so that the spurious accelerations at the ends of data span may be discarded. The $\partial T/\partial r$ values are magnified from $\ddot{R}$ values by secant times the angle at GEOS-3 between the radial directions and line of sight ATS-6/GEOS-3. When this angle exceeds 60°, it may be advisable to make the spline nodes 80 seconds apart to reduce sharp variations in $\partial T/\partial r$. An alternative approach would be to use an algorithm which chooses an optimum spacing for the nodes — variable nodes instead of fixed nodes. Tests need to be carried out to investigate if in our case of uniform interval data points representing a smooth continuous $\dot{R}$ function, the non-linear algorithm of variable nodes will give us an advantage, particularly for the case when the $\partial T/\partial r$ values are magnified more than 2 times the $\ddot{R}$ values.

The choice of low degree reference field represented by (12, 12) potential coefficients out of GEM-7 appears to be very suitable for computing $\dot{R}$. As these coefficients are well determined, the residual range-rate $\dot{R}$ does not have any significant bias due to errors in potential coefficients. Secondly, a degree 12 field is adequate at GEOS-3 altitude to make the covariance function of $\partial T/\partial r$ negligibly small beyond 7°.5 thereby allowing a relatively few number of points at 30 seconds data interval (Table 4.15) to recover the anomalies.

The improvement in the recovery of anomalies as data from additional revolutions is added (Table 4.14) indicates that we should have data from at least one ascending and one descending revolution over each anomaly. As we have found that initial state vectors may be obtained by integration from converged elements at epochs 4 to 6 days apart, it is comparatively easy to reduce data from more revolutions to achieve the required density.

The $\partial T/\partial r$ data should, however, be first examined for each revolution separately by predicting a few anomalies in common to determine if there is a system bias in the range-rate sum observations in any revolution. We found two such revolutions (232 and 268) in the present investigations.

The selected revolutions would still have a small linear bias in $\partial T/\partial r$ values due to modeling errors caused by residual errors in the initial state vectors. We need to determine two unknowns for a zero offset and a slope coefficient in each revolution to adjust the $\partial T/\partial r$ values to have a minimum variance discrepancy at crossover points between ascending and descending revolutions. The problem becomes 'over-determined' for more than four ascending and four descending revolutions. As we did not have a sufficient number of revolutions reduced for the present study, the adjustment for the cross-over constraints was not attempted.

With the unadjusted values of $\partial T/\partial r$ values, we found that the solutions for the predicted anomalies were unstable for assumed standard deviations of $\partial T/\partial r$ less than 1.5 mgals. It is likely that this may be reduced with adjusted $\partial T/\partial r$ values. This would then result in better agreement of predicted anomalies with the expected values in terms of RMS values, and also reduced standard deviations of the predicted anomalies.

The final solution for eight 5° anomalies, using range rate sum observations in five revolutions shown in Figure 4.9, is given at Table 4.15.

References

Agajelu, S. I., The Influence of the Short Wavelength Features of the Earth's Gravity Field on Low Orbiting Satellites, Department of Geodetic Science Report No. 246, The Ohio State University, Columbus, October, 1976.

Agajelu, S. I., On the Use of Least Squares Collocation to Estimate Gravity Anomalies Using Satellite to Satellite Tracking Data, internal report, Department of Geodetic Science, The Ohio State University, Columbus, March, 1977.

Ahlberg, J. H., E. N. Nilson and J. L. Walsh, The Theory of Splines and Their Applications, Academic Press, New York, 1967.

Bryan, J. W., J. J. Lynn and A. O. Hinely, A User's Guide for Satellite to Satellite System Observations and Data Formats, Goddard Space Flight Center, Greenbelt, Maryland, March, 1975.

De Boor, C., Package for Calculating with B-Splines, SIAM Journal on Numerical Analysis, Vol. 14, No. 3, June, 1977, pages 441-472.

Eddy, W. and R. Sutermeister, Satellite to Satellite Measurements, Wolf Research and Development Group, Riverdale, Maryland, August, 1975.

GEODYN System Description, Vol. I, Parts 1 and 2, Wolf Research and Development Group, Riverdale, Maryland, August, 1976.

GEODYN Operations Description, Vol. III, Wolf Research and Development Corporation, Riverdale, Maryland, April, 1975.

Hajela, D. P., Direct Recovery of Mean Gravity Anomalies from Satellite to Satellite Tracking, Department of Geodetic Science Report No. 218, The Ohio State University, Columbus, December, 1974.

Kaula, W. M., Error Analysis of Earth Physics Satellite Systems, Final Report, Part I, University of California, Los Angeles, October, 1972.

Kaula, W. M., M. E. Parmenter, N. Burkhard and D. D. Jackson, Application of Inversion Theory to New Satellite Systems for Determination of the Gravity Field, University of California, Los Angeles, August, 1975.

Lawson, C. H. and R. J. Hanson, Solving Least Squares Problems, Prentice-Hall, Inc., New Jersey, 1974.

Marsh, J. G., Private Communication (Initial State Vectors for ATS-6/GEOS-3 Revolutions 154, 268, 439, 453, 467), Goddard Space Flight Center, NASA, November, 1976.

Marsh, J. G., Private Communication (Initial State Vectors for ATS-6/GEOS-3 Revolutions 175, 232, 246), Goddard Space Flight Center, NASA, June, 1977.

Martin, C. F., Geodyn Modifications for Satellite to Satellite Tracking and Surface Density Layer Estimation, Wolf Research and Development Corporation, Riverdale, Maryland, February, 1972.

Martin, T. V., Private Communication (ATS-R Preprocessor Program), Wolf Research and Development Group, Riverdale, Maryland, September, 1975.

Moritz, H., Least Squares Collocation as a Gravitational Inverse Problem, Department of Geodetic Science Report No. 249, The Ohio State University, Columbus, November, 1976.

Muller, P. M. and W. L. Sjogren, Mascons: Lunar Mass Concentrations, Science, Vol. 161, 16 August, 1968, pages 680-684.

NASA, ATS-6/GEOS-3 SSE Tracking Data Supplement for 4/9/75 - 6/28/75, April, 1976.

Rapp, R. H., Potential Coefficient Determinations from 5° Terrestrial Gravity Data, Department of Geodetic Science Report No. 251, The Ohio State University, Columbus, January, 1977.

Rice, J. R., The Approximation of Functions, Vol. 2, Non-linear and Multivariate Theory, Addison Wesley Publishing Co., Massachusetts, 1969.

Rummel, R., Downward Continuation of Gravity Information from Satellite to Satellite Tracking or Satellite Gradiometry in Local Areas, Department of Geodetic Science Report No. 221, The Ohio State University, Columbus, April, 1975.

Rummel, R., D. P. Hajela and R. H. Rapp, Recovery of Mean Gravity Anomalies from Satellite-Satellite Range-Rate Data Using Least Squares Collocation, Department of Geodetic Science Report No. 248, The Ohio State University, Columbus, September, 1976.

Schwarz, C. R., Gravity Field Refinement by Satellite to Satellite Doppler Tracking, Department of Geodetic Science Report No. 147, The Ohio State University, Columbus, December, 1970.

Schulz, M. H., Spline Analysis, Prentice-Hall, Inc., New Jersey, 1973.

Sjogren, W. L., P. A. Laing, A. S. Liu and R. N. Wimberley, GEOS-3 Experiment Final Report: Analysis of SST Doppler Data for the Determination of Earth Gravity Field Variations, Jet Propulsion Laboratory, May, 1976.

Spath, H., Spline Algorithms for Curves and Surfaces (Translated from the German by W. D. Hoskins and H. W. Sager), Utilitas Mathematica Publishing, Inc., Winnipeg, 1974.

Tscherning, C. C., Covariance Expressions for Second and Lower Order Derivatives of the Anomalous Potential, Department of Geodetic Science Report No. 225, The Ohio State University, Columbus, January, 1976.

Tscherning, C. C. and R. H. Rapp, Closed Covariance Expressions for Gravity Anomalies, Geoid Undulations, and Deflections of the Vertical Implied by Anomaly Degree Variance Models, Department of Geodetic Science Report No. 208, The Ohio State University, Columbus, May, 1974.

Vonbun, F. O., W. D. Kahn, W. T. Wells and T. D. Conrad, Apollo-Soyuz Gravity Anomaly Determination, Presented at the American Geophysical Union Meeting, Washington, D. C., June, 1977.

Wagner, C. A., F. J. Lerch, J. E. Brownd and J. A. Richardson, Improvement in the Geopotential Derived from Satellite and Surface Data (GEM 7 and 8), Goddard Space Flight Center, NASA, January, 1976.